NASA TECHNICAL MEMORANDUM

NASA TM X-2600

NASA TM X-2600

WIND-TUNNEL INVESTIGATION OF A LARGE-SCALE 35° SWEPT-WING JET TRANSPORT MODEL WITH AN EXTERNAL BLOWING TRIPLE-SLOTTED FLAP

by Kiyoshi Aoyagi, Leo P. Hall, and Michael D. Falarski

Ames Research Center
and
U.S. Army Air Mobility R&D Laboratory
Moffett Field, Calif. 94035

NATIONAL AERONAUTICS AND SPACE ADMINISTRATION • WASHINGTON, D. C. • JULY 1972

1. Report No.	2. Government Accession No.	3. Recipient's Catalog No.
NASA TM X-2600		

4. Title and Subtitle	5. Report Date
WIND–TUNNEL INVESTIGATION OF A LARGE–SCALE 35° SWEPT–WING JET TRANSPORT MODEL WITH AN EXTERNAL BLOWING TRIPLE–SLOTTED FLAP	July 1972
	6. Performing Organization Code

7. Author(s)	8. Performing Organization Report No.
Kiyoshi Aoyagi, Leo P. Hall, and Michael D. Falarski	A–3753
	10. Work Unit No. 721–52–11–01–00–21
9. Performing Organization Name and Address NASA Ames Research Center and U.S. Army Air Mobility R&D Laboratory Moffett Field, Calif., 94035	11. Contract or Grant No.
	13. Type of Report and Period Covered Technical Memorandum
12. Sponsoring Agency Name and Address National Aeronautics and Space Administration Washington, D. C. 20546	14. Sponsoring Agency Code

15. Supplementary Notes

Edited by NASA Ames Research Center

16. Abstract

An investigation has been conducted to determine the aerodynamic characteristics of a large-scale subsonic jet transport model with an externally jet-augmented flap system that would augment lift and provide direct-lift control. The model had a 35° swept wing of aspect ratio 7.82 and two side-by-side engines mounted on a single pylon under each wing close to the fuselage. The lift of the flap system was augmented by jet engine exhaust impingement on the triple-slotted flap surfaces. The rearmost flap provided direct lift control. Results were obtained for several combinations of flap deflections at gross thrust coefficients from 0 to 2.0. Three-component longitudinal data are presented with four engines operating. Limited longitudinal and lateral data are presented for asymmetric and symmetric thrust conditions with three engines operating.

For the same overall flap deflection, lift coefficient and maximum lift coefficient were improved 13 and 7 percent compared to coefficients obtained with a double-slotted flap configuration. A maximum lift coefficient of 6.3 was obtained at a gross thrust coefficient of 2.0.

At the same flap deflection lateral and directional trim moment requirements with an engine inoperative were reduced 55 and 33 percent, respectively, compared to those with the engines located farther outboard on the wing. Trim moment requirements in pitch were also reduced significantly. However, pitching-moment instability occurred and increased with gross thrust coefficient.

The agreement between theoretical jet flap lift increment and measured values was fair with the aft flap undeflected and poor with the aft flap deflected.

17. Key Words (Suggested by Author(s))	18. Distribution Statement
External-flow jet flap High lift STOL	UNCLASSIFIED – UNLIMITED

19. Security Classif. (of this report)	20. Security Classif. (of this page)	21. No. of Pages	22. Price*
Unclassified	Unclassified	74	$3.00

* For sale by the National Technical Information Service, Springfield, Virginia 22151

SYMBOLS

b wing span, m (ft)

c wing chord measured parallel to the plane of symmetry, m (ft)

c_t horizontal tail chord measured parallel to the plane of symmetry, m (ft)

c_v vertical tail chord, m (ft)

$\bar{c}$ mean aerodynamic chord of wing, $\frac{2}{S}\int_0^{b/2} c^2\, dy$, m (ft)

C_D drag coefficient, $\frac{drag}{q_\infty S}$

C_L lift coefficient, $\frac{lift}{q_\infty S}$

C_{L_Γ} jet-induced lift coefficient

C_l rolling-moment coefficient about stability axis, $\frac{rolling\ moment}{q_\infty Sb}$

C_m pitching-moment coefficient about 0.25 $\bar{c}$, $\frac{pitching\ moment}{q_\infty S\bar{c}}$

C_n yawing-moment coefficient about stability axis, $\frac{yawing\ moment}{q_\infty Sb}$

C_T engine gross thrust coefficient, $\frac{F_g}{q_\infty S}$

$C_{t_{net}}$ engine net thrust coefficient, $\frac{T}{q_\infty S}$

C_y side-force coefficient about stability axis, $\frac{side\ force}{q_\infty S}$

F_A static (wind off) incremental axial force due to flap deflection with power on, N (lb)

F_g gross thrust with flaps undeflected and $\delta_d = 0°$, N (lb) (obtained statically)

F_N static (wind off) incremental normal force due to flap deflection with power on, N (lb)

F_R resultant force $\sqrt{F_A{}^2 + F_N{}^2}$, N (lb)

IB	inboard
ID	internal diameter
i_t	horizontal tail incidence, deg
LH	left hand
OB	outboard
q_∞	free-stream dynamic pressure, N/m^2 (lb/sq ft)
RH	right hand
S	wing area, m^2 (sq ft)
T	gross thrust minus nacelle inlet ram drag, N (lb)
WCP	wing chord plane
y	spanwise distance perpendicular to the plane of symmetry, m (ft)
a	angle of attack of fuselage, deg
δ_a	aileron deflection, deg
δ_d	jet exhaust deflection angle, deg (see fig. 2(d))
δ_e	horizontal tail elevator deflection, deg
δ_{f_1}	trailing-edge forward flap deflection measured normal to its hinge line, deg (see fig. 2(d))
δ_{f_2}	trailing-edge midflap deflection measured normal to its hinge line, deg (see fig. 2(d))
δ_{f_3}	trailing-edge aft flap deflection measured normal to its hinge line, deg (see fig. 2(d))
$\delta_{f_{total}}$	total trailing-edge flap deflection, $\delta_{f_1} + \delta_{f_2} + \delta_{f_3}$, deg
δ_j	jet exhaust deflection angle, $\tan^{-1} \frac{F_A}{F_N}$, deg
δ_r	rudder deflection, deg
δ_s	slat deflection, measured perpendicular to the leading edge, deg

η wing semispan station, $\frac{y}{b/2}$

η_f flap system static turning efficiency, $\frac{F_R}{F_g}$

$()_u$ uncorrected

WIND–TUNNEL INVESTIGATION OF A LARGE–SCALE 35° SWEPT–WING JET TRANSPORT MODEL WITH AN EXTERNAL BLOWING TRIPLE–SLOTTED FLAP

Kiyoshi Aoyagi, Leo P. Hall, and Michael D. Falarski

Ames Research Center
and
U.S. Army Air Mobility R&D Laboratory

SUMMARY

An investigation has been conducted to determine the aerodynamic characteristics of a large-scale subsonic jet transport model with an externally jet-augmented flap system that would augment lift and provide direct-lift control. The model had a 35° swept wing of aspect ratio 7.82 and two side-by-side engines mounted on a single pylon under each wing close to the fuselage. The lift of the flap system was augmented by jet engine exhaust impingement on the triple-slotted flap surfaces. The rearmost flap provided direct lift control. Results were obtained for several combinations of flap deflections at gross thrust coefficients from 0 to 2.0. Three-component longitudinal data are presented with four engines operating. Limited longitudinal and lateral data are presented for asymmetric and symmetric thrust conditions with three engines operating.

For the same overall flap deflection, lift coefficient and maximum lift coefficient were improved 13 and 7 percent compared to coefficients obtained with a double-slotted flap configuration. A maximum lift coefficient of 6.3 was obtained at a gross thrust coefficient of 2.0.

At the same flap deflection lateral and directional trim moment requirements with an engine inoperative were reduced 55 and 33 percent, respectively, compared to those with the engines located farther outboard on the wing. Trim moment requirements in pitch were also reduced significantly. However, pitching-moment instability occurred and increased with gross thrust coefficient.

The agreement between theoretical jet flap lift increment and measured values was fair with the aft flap undeflected and poor with the aft flap deflected.

INTRODUCTION

A previous investigation of the same model (35° swept wing) with four pod-mounted jet engines and an externally augmented double-slotted jet flap has been reported in reference 1. Data from reference 1 indicated that pitching moments for trim and lateral and directional trim moment from an engine-out condition were too large. For the tests described here the engines were relocated farther inboard on a single pylon close to the fuselage to reduce these moments. The double-slotted

flap was replaced with a triple-slotted flap in an attempt to improve performance. The flap consisted of a 15 percent chord forward flap, a 12 percent chord midflap, and a10 percent chord aft flap.

The purpose of the investigation was to determine the aerodynamic characteristics of the model with this flap system and engine arrangement. Results were obtained with several combinations of forward flap, midflap, and aft flap deflections. Limited data were obtained with the operation of three engines for asymmetric and symmetric thrust conditions. All the data were obtained at Reynolds numbers from 2.0×10^6 to 2.9×10^6, based on a mean aerodynamic chord of 1.59 m (5.22 ft) and a dynamic pressure of 215 to 479 N/m^2 (4.5 to 10.0 psf).

MODEL AND APPARATUS

Figure 1 is a photograph of the model in the 12.2– by 24.2 m (40– by 80–foot) wind tunnel. Pertinent dimensions of the model are given in figure 2(a). The model was equipped with four T–58–6A engines modified to operate as conventional jet engines.

Wing

The wing had a quarter chord sweep of 35°, an aspect ratio of 7.82, a dihedral of 6°, and an incidence of 2°. The airfoil section had an NACA 65–012 thickness distribution at the root tapering linearly to an NACA 65–009 thickness distribution at the tip with a 230 mean line at these sections.

Leading-Edge Slats

Leading-edge slats were used to delay wing leading-edge flow separation. A 0.15 c slat extended from $\eta = 0.11$ to 0.48, and a 0.20 c slat extended from $\eta = 0.48$ to 1.0. Both slats were deflected 35° (optimum setting) with respect to the wing chord plane as shown in figure 2(b) when the flaps were deflected. The slats were deflected 45° when the flaps were undeflected. The slats were attached to the wing leading edge throughout the investigation.

Trailing-Edge Flap System

Flap details– The flap system had three segments with fixed pivots as shown in figure 2(c). Each flap segment extended from 0.11 to 0.68 η with a break at 0.37 η and could be deflected 0° to 40° normal to their respective pivot lines. The total flap chord was 0.30 of the wing chord; the forward flap, midflap, and aft flap chords were, respectively, 0.500, 0.413, and 0.333 of the total flap chord. The pivots of the forward and aft flaps are located the same as those of the double-slotted flap of reference 1. Flap gaps are tabulated on figure 2(d). Each flap segment was deflected over the full spanwise extent (0.11 to 0.68 η) throughout the investigation.

Aileron

A plain 0.3 c aileron extended from $\eta = 0.68$ to 1.0 on the wing and could be deflected 20° differentially or 30° symmetrically.

Fuselage

The fuselage had a constant 1.2-m diameter (4-ft diam.) except at the nose and tail. The nose section had elliptical outlines with circular cross sections that decreased from 4 ft to smaller diameters. The tail section tapered from a 1.2-m diameter (4-ft) circular section to a small elliptical section.

Tail

The geometry of the horizontal and vertical tails is described in figure 2(a). An inverted leading-edge slat, which tapered linearly from 0.15 c_t at the root to 0.20 c_t at the tip, was mounted along the full extent of the horizontal tail and was deflected −35°. The horizontal-tail incidence and elevator deflections were set at 0° throughout the investigation. The vertical tail rudder tapered linearly from 0.31 c_v at the base to 0.47 c_v at 0.93 of the tail span and could be deflected −30°, 0°, and 30°. Both tails were on the model throughout the investigation.

Engines

T−58−6A engines, modified to operate as conventional jet engines, were located at 0.23 and 0.33 of the wing semispan and mounted on a single pylon. The engine centerline was pitched 4.5° nose down to provide better jet exhaust impingement on the flap surface. A jet exhaust nozzle composed of seven 0.033-m ID (0.11-ft) and twenty-four 0.027-m ID (0.09-ft) tubes that were mounted to a 0.30-m (0.98-ft) end plate was installed on each engine to increase the diameter of the jet exhaust efflux over that of a conventional tail-pipe of 0.16-m ID (0.52 ft) (ref. 1). Behind the multitubed nozzle of each engine was a 0.43-m (1.42-ft) diameter ejector, 0.72 m (2.36 ft) long, with a faired leading-edge radius of 0.037 m (0.12 ft) (see fig. 2(d)). Its purpose was to simulate the exhaust wake of a turbofan jet engine. The combined ejector and jet exhaust flow provided external jet augmentation on the trailing-edge flap surface. A jet exhaust deflector behind the ejector pivoted about the ejector centerline (fig. 2(d)). The deflector had a constant chord of 0.36 m (1.17 ft) and extended the ejector diameter. A deflection of 15° from the engine centerline was used when the flaps were deflected, and a deflection of 0° was used when the flaps were undeflected.

TESTING AND PROCEDURE

In most cases, forces and moments were measured through an angle-of-attack range of −4° to 22°. Tests were conducted at Reynolds numbers from 2.0×10^6 to 2.9×10^6, based on a mean aerodynamic chord of 1.59 m (5.22 ft) and dynamic pressures of 215 to 479 N/m^2 (4.5 and 10.0 psf), respectively.

Tests With Constant C_T and Varying Angle of Attack

Four engines operating– A constant C_T was maintained as angle of attack was varied for each flap configuration tested. The nominal C_T values used in most cases during the investigation are shown below:

C_T (4 engines)	q_u, N/m^2	psf
0	479	10.0
.25	479	10.0
.50	479	10.0
1.0	431	9.0
1.4	302	6.3
2.0	215	4.5

The C_T values were based on the calibration of engine static thrust variation with engine tailpipe exhaust pressure with both the flaps and jet exhaust deflector at 0°. Forward flap deflections ranging from 0° to 40° were tested with several combinations of midflap and aft flap deflections. The midflap deflections ranged from 0° to 30°, and the aft flap deflections ranged from 0° to 40°.

Three engines operating– Data were obtained with equal thrust per engine and equal thrust per wing panel for two flap configurations with and without the horizontal tail. The left-hand outboard engine was inoperative when the tail was on, and the right-hand outboard engine was inoperative when the tail was off. In addition, a flap configuration was tested for an asymmetric thrust condition with the left-hand inboard engine inoperative and with the horizontal tail.

Test With Constant C_T and Varying Angle of Sideslip

A constant C_T was maintained at 0° angle of attack as sideslip was varied from 4° to −16°. The effects of differential auxiliary flap deflection (0° left, 20° right), aileron deflections (±20°), and rudder deflection (0°, 30°) were investigated for an asymmetric thrust condition with three engines operating.

CORRECTIONS

The data were corrected for strut tares and wind tunnel wall effects. The tunnel wall corrections were as follows:

$$\alpha = \alpha_u + 0.375\, C_L$$

$$C_D = C_{D_u} + 0.0065\, C_L{}^2$$

$$C_m = C_{m_u} + 0.0122\, C_L$$

RESULT AND DISCUSSION

The data are presented for specified gross thrust coefficients C_T. The estimated relationship between $C_{T_{net}}$ and C_T is shown in figure 3.

The basic force data with four engines operating are presented in figures 4 and 5 with the flaps undeflected and in figures 6 through 18 with the flaps deflected. The basic force data with three engines operating are presented in figures 19 through 28. A comparison of measured and theoretical flap lift increments is shown in figure 29.

Longitudinal Characteristics of the Model With Plain Wing

The longitudinal characteristics of the model with the leading-edge slats extended, and with and without power are shown in figure 4. Power increased lift-curve slope, $C_{L_{max}}$ values, and nose-up pitching moments because of the low engine position. Power also caused a static margin shift ($dC_m/dC_L = -0.12$ at $C_T = 0$ to 0 at $C_T = 1.0$) and a slight static instability at $C_T = 2.0$.

The effect of nacelle spanwise location and arrangement on the longitudinal characteristics of the model as used in the present investigation and as used in reference 1 is shown in figure 5. In the present investigation the inboard and outboard nacelles were located at $\eta = 0.23$ and 0.33, respectively, and in reference 1 at $\eta = 0.28$ and 0.49. These will be referred to as clustered and spread engine arrangements, respectively. With power off, the clustered arrangement had higher drag coefficients and a lower static margin as shown in figure 5(a). Pitch-up instability occurred at $\alpha = 8°$ for the clustered, and at $\alpha = 12°$ for the spread configuration. These differences are probably due to the twin nacelle locations and the downwash field difference at the same horizontal-tail location. With power on, the clustered arrangement had higher lift and drag coefficients and a decreased static margin. The large reduction in static margin with increasing power compared to nearly no change for the configuration of reference 1 indicates that the clustered-engine jet exhaust flow increased the downwash at the tail. Similar results were also reported in reference 2.

Longitudinal Characteristics of the Model With Flap Deflection and Four Engines Operating

Effect of angle of attack– The longitudinal characteristics of the model with $\delta_{f_1} = 20°$, 30°, and 40° at several midflap and aft flap deflections are shown in figures 6 through 11. As shown, the angle of attack for the upper limit of the linear lift-curve slope and for $C_{L_{max}}$ was extended approximately 6° when C_T increased from 0 to 2.0. Lift varied with thrust coefficient and flap deflection as summarized in figure 12. An untrimmed $C_{L_{max}}$ of 6.3 was obtained at a flap deflection of $\delta_{f_1}/\delta_{f_2}/\delta_{f_3} = 40/20/40$ with $C_T = 2.0$. Deflection of the aft flap increased lift up to $\delta_{f_3} = 30°$ when the forward and middle flaps were deflected 20° but only up to $\delta_{f_3} = 20°$ at the higher forward flap deflection (see fig. 12).

The model with flaps deflected was longitudinally stable nearly to the stall angle when $C_T = 0$ (figs. 6 through 11). However, instability occurred below the stall angle with jet-augmentation (C_T values), which was not the case in a previous investigation of the same model with different nacelle spanwise locations (ref. 1). The effect of operating the engines located farther inboard than those of reference 1 was to decrease the tail contribution to stability. This reduction was probably due to the higher rate of downwash angle change with angle of attack similar to that reported in reference 2. Reference 3 reported that the longitudinal stability of a model with a similar problem was improved by relocation of the horizontal tail. This may be one possible method of improving the longitudinal stability of the present model. In most cases, static margin was reduced from −0.20 at $C_T = 0$ to neutral at $C_T = 1.4$. In general, the effect of jet augmentation and flap deflection was to increase nose-down pitching moment as shown in figure 13.

To determine the effect of crossflow under the fuselage from the jet exhaust impingement on the flap surface, an end plate 0.46X0.82 m (1.5 X 2.7 ft) was added at each end of the flap root section. Figure 9(c) compares the longitudinal characteristics with and without end plates. As shown, no significant effect was found.

Comparison between triple-slotted and double-slotted flap– Figure 14 shows a comparison of C_L, C_D, and C_m based on the same total flap deflections ($\delta_{f_1} + \delta_{f_2} + \delta_{f_3}$) and nacelle arrangement between the two flap configurations. With the forward flap deflected 20°, C_L, C_D, and C_m values were nearly the same with either the triple- or double-slotted flap configuration. With the forward flap deflected 40°, higher C_L and C_D values and greater nose-down C_m values were obtained with the triple-slotted flap configuration ($\delta_{f_1}/\delta_{f_2}/\delta_{f_3} = 40°/20°/20°$). With the latter configurations, C_L and $C_{L_{max}}$ values increased 13 and 7 percent, respectively, compared to those obtained with the double-slotted flap configuration ($\delta_{f_1}/\delta_{f_2}/\delta_{f_3} = 40°/0°/40°$) at $C_T = 2.0$.

Effect of nacelle spanwise locations– Figure 15 shows the longitudinal characteristics of the model with the clustered nacelle arrangement and with the spread nacelle arrangement of reference 1. Lift and drag coefficients were nearly the same for either location as shown in the figure. However, pitching-moment coefficients were significantly reduced with the nacelles located closer to the fuselage. At $\delta_{f_1}/\delta_{f_2}/\delta_{f_3} = 40°/0°/40°$ and $C_T = 2.0$, trim moment requirements in pitch were 20 percent of that required with the engines operating farther outboard on the wing.

Analysis of lift with jet augmentation at 0° angle of attack – The lift components for a fixed flap chord and deflection are due to lift without jet augmentation, direct jet reaction, and jet-induced effect. The lift due to jet reaction depends on the effectiveness of the flap system in turning the jet. Figure 16 shows the variation of static (wind off) jet turning angle and turning efficiency with total geometric flap deflection ($\delta_{f_1} + \delta_{f_2} + \delta_{f_3}$). With $\delta_{f_3} = 0°$, the jet turning angle was less than the total geometric flap angle, ranging from 77 percent of 30° total to 90 percent of 60° total. With $\delta_{f_3} = 30°$, the jet turning angle increased an additional 30° at $\delta_{f_1}/\delta_{f_2} = 20°/10°$ and 19° at $\delta_{f_1}/\delta_{f_2} = 40°/20°$. The static force due to the jet decreased with increasing total flap deflection because of the turning losses. The static turning efficiency (η_f) ranged from 84 percent at $\delta_{f_1}/\delta_{f_2}/\delta_{f_3} = 20°/10°/0°$ to 67 percent at $\delta_{f_1}/\delta_{f_2}/\delta_{f_3} = 40°/20°/30°$.

For the same double-slotted flap deflection, figure 17 compares the static jet turning angle and turning efficiency between the clustered nacelle arrangement and the spread nacelle arrangement of reference 1. Improvements of 6 percent in jet turning angle and 5 percent or higher in jet turning efficiency were obtained with the clustered arrangement as shown in the figure, probably because of the larger flap chord behind the jet exhaust efflux.

The lift components at $\delta_{f_1}/\delta_{f_2} = 20°/10°$ and $40°/20°$ for several aft flap deflections are shown in figures 18(a) and (b), respectively. The lift due to jet reaction is based on the static jet turning angle and turning efficiency shown in figure 16. At the lower flap deflections the lift increment due to jet-induced effect accounted for 32 to 36 percent of the total lift, and at the higher flap deflections, 38 to 44 percent.

Longitudinal and Lateral Characteristics of the Model With Three-Engine Operation

Effect of equal thrust per engine– The longitudinal and lateral characteristics of the model with three engines operating (*LH OB* engine inoperative) are limited to flap deflections of $\delta_{f_1}/\delta_{f_2}/\delta_{f_3} = 20°/20°/10°$ and $40°/20°/20°$ and are shown in figures 19 and 20, respectively. The lift and drag coefficients were the same as obtained with four engines operating at equal thrust for the same C_T value, as summarized in figure 21. Pitching-moment coefficients were less than those with four engines operating (30 percent reduction at $C_T = 1.4$ with $\delta_{f_1}/\delta_{f_2}/\delta_{f_3} = 40°/20°/20°$).

For a constant C_T, yawing-moment coefficients were constant with angle of attack (fig. 19(b)) at $\delta_{f_1}/\delta_{f_2}/\delta_{f_3} = 20°/20°/10°$ with $C_n = -0.045$ at $C_T = 1.5$, but they varied slightly with angle of attack (fig. 20(b)) at $\delta_{f_1}/\delta_{f_2}/\delta_{f_3} = 40°/20°/20°$ with maximum $C_n = -0.025$ at $C_T = 1.5$. Out of trim rolling-moment coefficient caused by asymmetric engine thrust increased with angle of attack up to the stall angle and with C_T at either flap deflection. A maximum C_l of -0.15 at the stall angle was measured at $C_T = 1.5$ at either flap deflection.

As mentioned previously, one reason for relocating the engine nacelles farther inboard than those of reference 1 was to reduce trim directional and lateral moments. Figure 22 shows the values of C_n and C_l were reduced 33 and 56 percent, respectively, at $C_T = 1.5$.

The variation of C_y, C_n, and C_l with sideslip is shown in figures 23 and 24 for $\delta_{f_1}/\delta_{f_2}/\delta_{f_3} = 20°/20°/10°$ and $40°/20°/20°$, respectively. In each case, the dihedral effect and rudder-fixed static directional stability were stable over the sideslip range investigated (4° to −16°). The variation of C_n with sideslip was linear and nearly the same for asymmetric and symmetric condition (four engines operating) as shown in the figures. Figure 23 also shows the effect of differential aft flap deflection (left hand 0°, right hand 20°) and aileron deflection of ±20°. A control power of $\Delta C_l = 0.095$ was developed with the combined use of the two control devices over the sideslip range investigated. Approximately 42 percent was due to the differential auxiliary flap deflection, which also added a ΔC_n increase of 0.03. A rudder deflection of −30° developed a ΔC_n value of 0.07 and 0.05 at $C_T = 1.05$ and 0.75, respectively, over the sideslip range investigated as shown in figure 24. This value is sufficient to trim the model at an angle of sideslip that compensates for the rolling moment caused by the loss of an engine.

Effect of equal thrust per wing panel– The longitudinal and lateral characteristics of the model with three engines operating to provide symmetric thrust are shown in figures 25 and 26 for $\delta_{f_1}/\delta_{f_2}/\delta_{f_3} = 20°/20°/10°$ and $40°/20°/20°$, respectively. For a constant C_T value, the longitudinal characteristics of the model were the same as those obtained with asymmetric thrust (three engines operating), or all four engines operating as summarized in figures 27 and 28. For the C_T values investigated, C_n values were close to zero with angle of attack up to the stall angle for $\delta_{f_1}/\delta_{f_2}/\delta_{f_3} = 20°/20°/10°$ and $40°/20°/20°$ as shown in figures 25(b) and 26(b). Values of C_l were nearly constant with angle of attack up to the stall angle for $\delta_{f_1}/\delta_{f_2}/\delta_{f_3} = 20°/20°/10°$, but increased with angle of attack for $\delta_{f_1}/\delta_{f_2}/\delta_{f_3} = 40°/20°/20°$. A maximum C_l of -0.05 at $C_T = 1.0$ was measured at the stall angle for either flap deflection, which was one-third of that obtained with asymmetric thrust (three engines operating). Thus, the rolling moment required to trim after an initial engine loss could be reduced significantly if the remaining three engines were throttled back to provide a symmetric thrust condition, but probably at the cost of reducing lift.

Comparison of Flap Lift Increment With Theory

Theoretical jet-flap-induced lift increments were calculated assuming that the jet efflux spreads over the entire span of the flap. The measured effective jet angle and resultant force were used with the method of reference 4 to calculate the theoretical curves shown in figure 29. For the flap deflections examined, the measured values were less than those obtained theoretically. The largest discrepancy occurred at $C_T = 0$ when the airflow over the flap was separated, and decreased as the engine airflow provided attached flow. When $\delta_{f_3} = 0°$, the agreement between measured and theoretical values was fair to good with $\delta_{f_1}/\delta_{f_2} = 20°/10°$ and $40°/20°$. When δ_{f_3} was deflected, the agreement was poor. Similar comparisons between measured and theoretical results were obtained with the double-slotted flap configurations of reference 1.

SUMMARY OF RESULTS

A large-scale model with an externally blown triple-slotted flap has been investigated to determine its aerodynamic characteristics. Significant results are summarized below.

With the plain wing and power on, C_L and $C_{L_{max}}$ values increased with the clustered engine arrangement compared to those obtained with the spread engine arrangement. With the flaps deflected, C_L values were essentially the same with either engine arrangement, but C_m values were significantly reduced with the clustered engine arrangement.

At the higher flap deflection an externally jet-augmented triple-slotted flap increased C_L and $C_{L_{max}}$ 13 and 7 percent, respectively, compared to a double-slotted flap. A maximum untrimmed $C_{L_{max}}$ of 6.3 was obtained with $\delta_{f_1}/\delta_{f_2}/\delta_{f_3} = 40°/20°/40°$ at $C_T = 2.0$.

Lateral and directional trim moment requirements with an engine inoperative were reduced substantially by moving the inboard and outboard engines to 0.23 and 0.33 from 0.28 and 0.49 of

the wing semispan, respectively. For the same flap deflection, these moments were reduced 55 and 33 percent, respectively. Trim moment requirements in pitch were also reduced significantly; however, the operation of the engines located closer to the fuselage resulted in longitudinal instability for the tail location investigated.

The agreement between theoretical and measured jet-flap-induced lift was fair with the aft flap undeflected and poor with the aft flap deflected.

Ames Research Center
National Aeronautics and Space Administration
and
U.S. Army Air Mobility R&D Laboratory
Moffett Field, Calif., 94035, April 17, 1972

REFERENCES

1. Aoyagi, Kiyoshi; and Hall, Leo P.: Wind-Tunnel Investigation of a Large 35° Swept Wing Jet Transport Model With an External-Flow Jet-Augmented Double-Slotted Flap. NASA TN D-6482, 1971.

2. Parlett, Lysle, P.; and Shivers, James P.: Wind-Tunnel Investigation of an STOL Aircraft Configuration Equipped With an External-Flow Jet Flap. NASA TN D–5364, 1969.

3. Parlett, Lysle, P.; Freeman, Delma C., Jr.; and Smith, Charles C., Jr.: Wind-Tunnel Investigation of a High Thrust-Weight Ratio Jet Transport Aircraft Configuration With an External-Flow Jet Flap. NASA TN D–6058, 1970.

4. Williams, J.; Butler, S. F. J.; and Wood, M. N.: The Aerodynamics of Jet Flaps. RAE Rep. Aero. 2646, 1961.

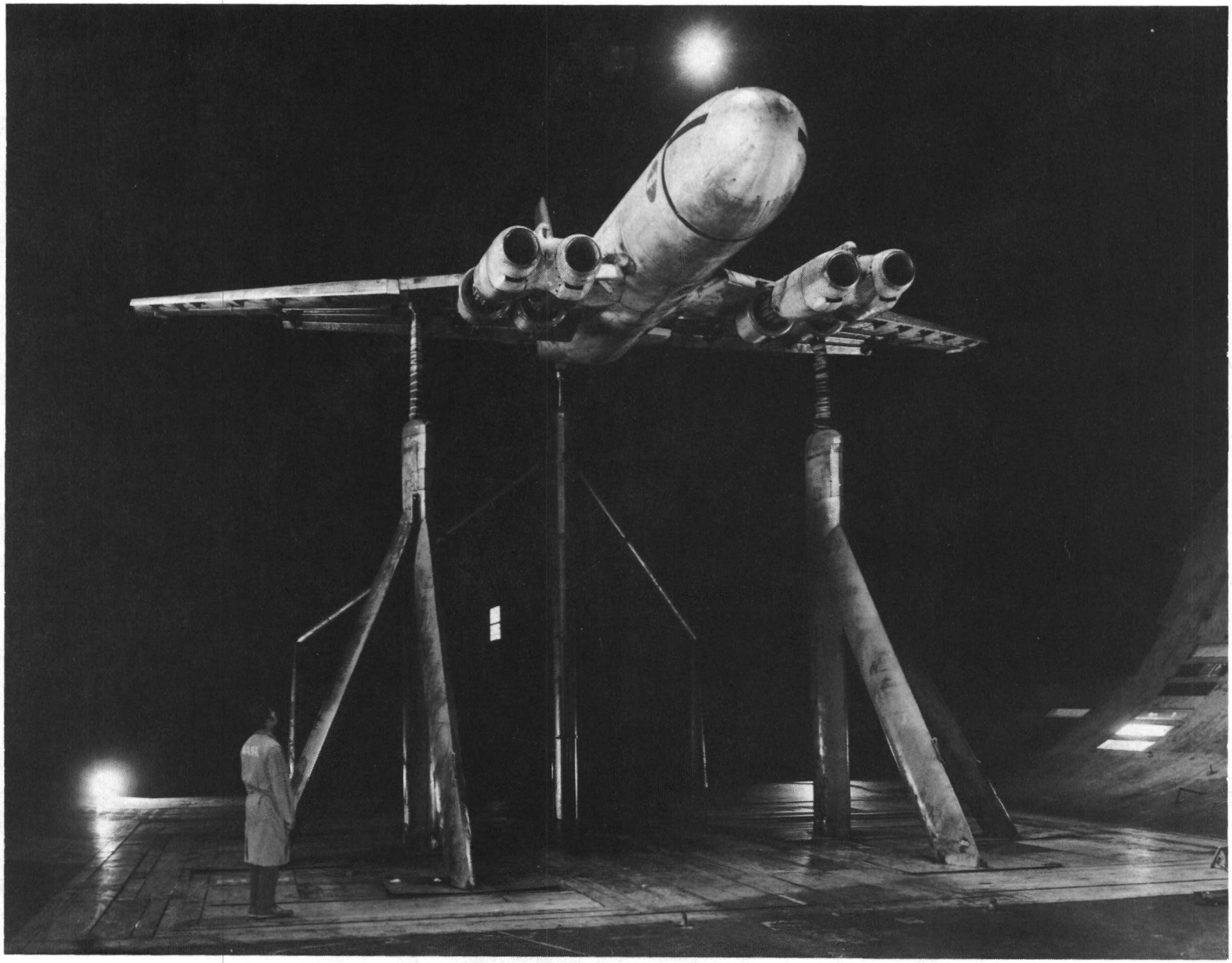

Figure 1.– Photograph of the model as mounted in the Ames 40– by 80–Foot Wind Tunnel.

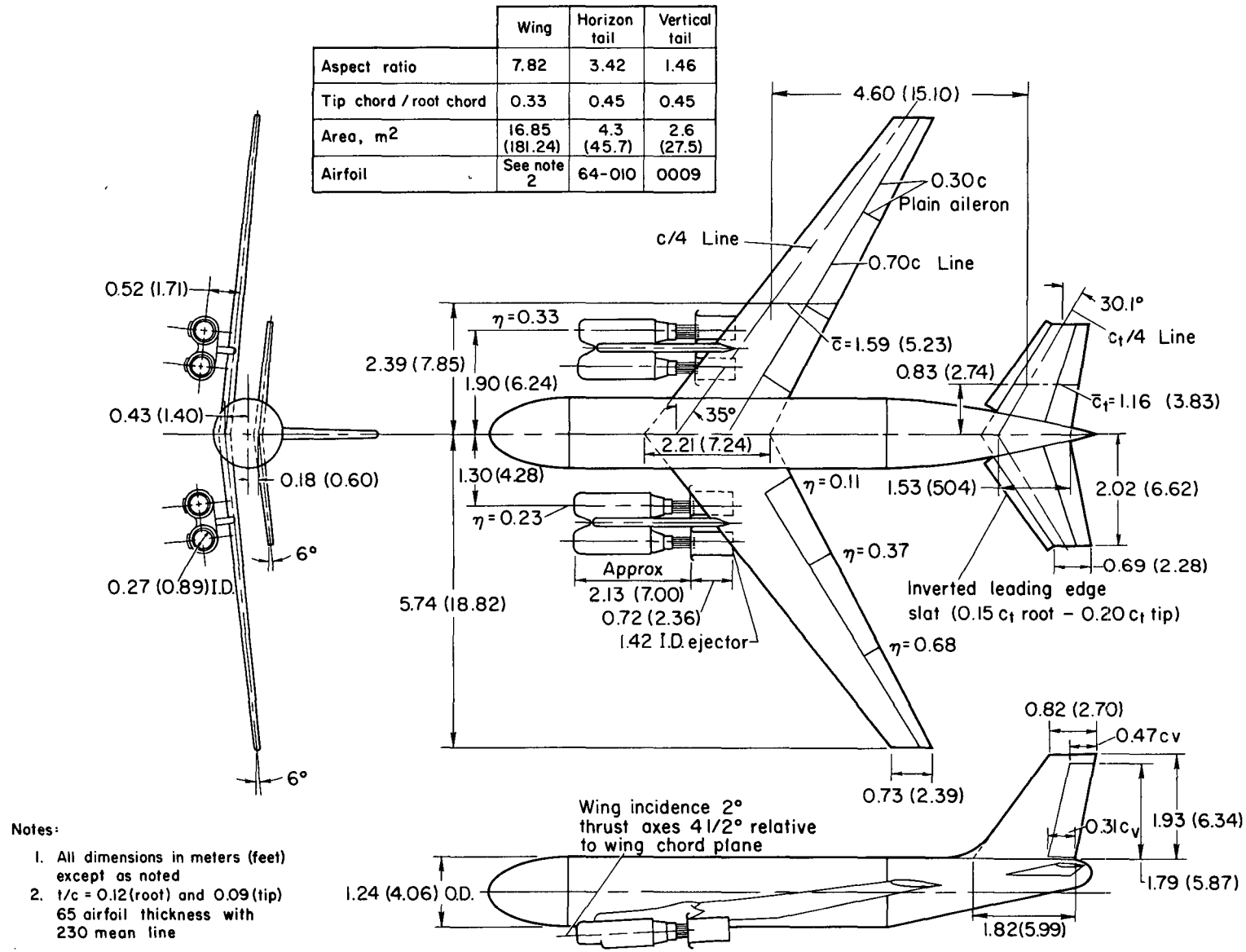

(a) General arrangement of the model.

Figure 2.– Geometric details of the model.

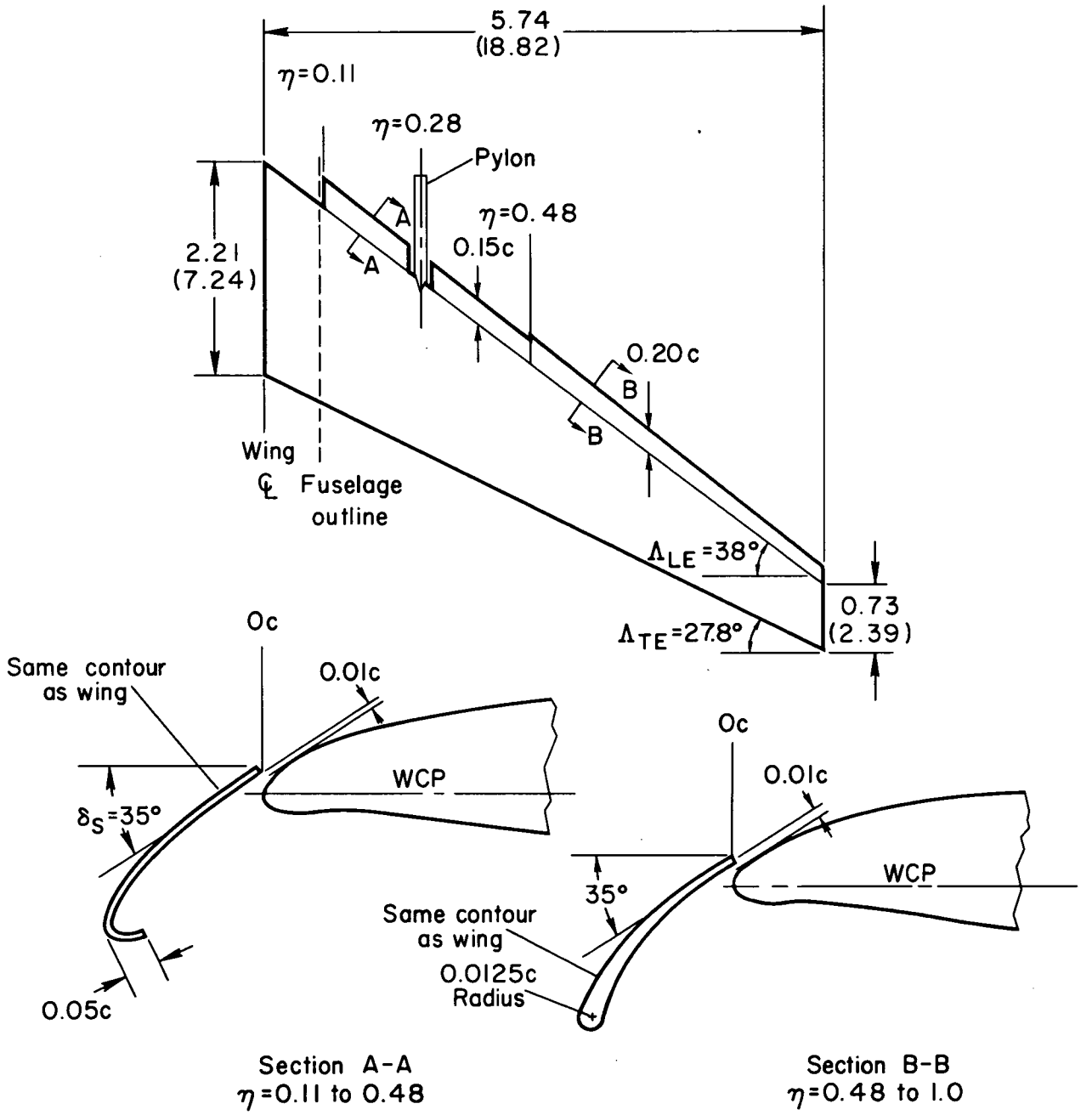

Note:

1. All dimensions in meters (feet) unless otherwise noted.

(b) Leading-edge slat.

Figure 2.– Continued.

Streamwise direction

Forward flap ordinates			Midflap ordinates			Aft flap ordinates		
X, % c	y_u, % c	y_l, % c	X, % c	y_u, % c	y_l, % c	X, % c	y'_u, % c	y'_l, % c
0	-1.274	-1.274	10.000	-0.872	-0.872	20.000	-0.348	-0.348
0.448	-0.314	-2.018	10.415	-0.041	-1.376	20.274	0.049	-0.679
0.814	0.041	-2.166	11.070	0.572	-1.536	20.502	0.251	-0.743
2.269	1.023	-2.550	11.537	0.857	-1.576	20.731	0.396	-0.792
3.003	1.377	-2.548	12.983	1.435	-1.622	20.960	0.509	-0.808
5.888	2.252	-2.342	14.330	1.695	-1.494	21.416	0.686	-0.823
7.333	2.519	-2.207	15.812	1.755	-1.380	21.872	0.799	-0.807
8.755	2.564	—	16.551	1.744	-1.279	22.328	0.871	—
9.337	—	-0.999	16.836	—	-1.250	22.783	0.903	—
10.181	2.511	—	17.823	—	-0.997	23.238	0.902	—
10.696	—	0.694	18.743	—	-0.502	23.692	0.870	—
11.612	2.392	-1.764	19.660	—	0.073	26.308	0.538	-0.401
12.237	—	1.513	20.585	—	0.525	30.000	0.058	-0.062
12.657	2.202	—	21.498	—	0.823			
13.680	—	1.825	22.410	1.097	0.968			
15.025	1.960	1.822						

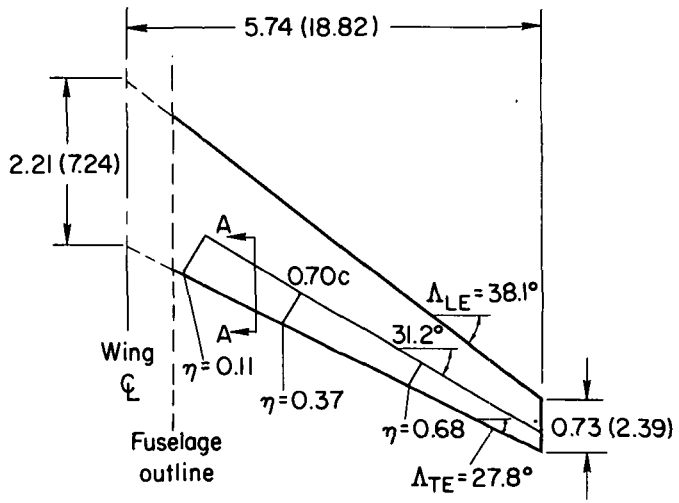

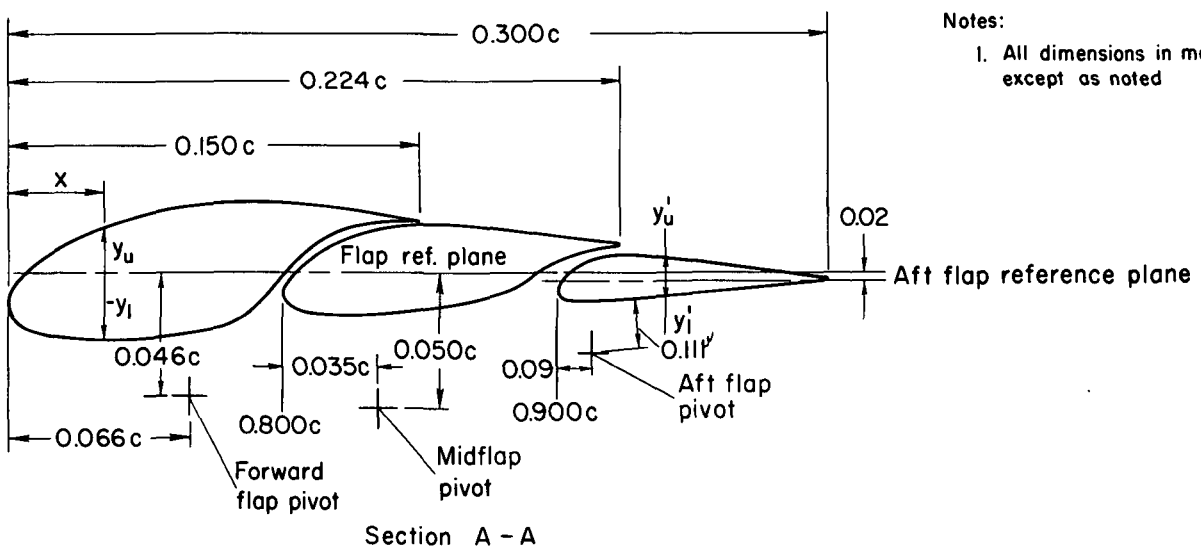

Notes:

1. All dimensions in meters (feet) except as noted

(c) Trailing-edge flap.

Figure 2.– Continued.

Averaged flap gaps

δ_f, deg	X_1, %c	y_1, %c	δ_{f_2}, deg	X_2, %c	y_2, %c	δ_{f_3}, deg	X_3, %c	y_3, %c
10	0.038	0.006	10	0.036	0.003	10	0.015	0.006
20	0.032	0.009	20	0.028	0.005	20	0.010	0.007
30	0.025	0.010	30	0.019	0.006	30	0.005	0.009
40	0.020	0.011	—	—	—	40	0.005	0.010

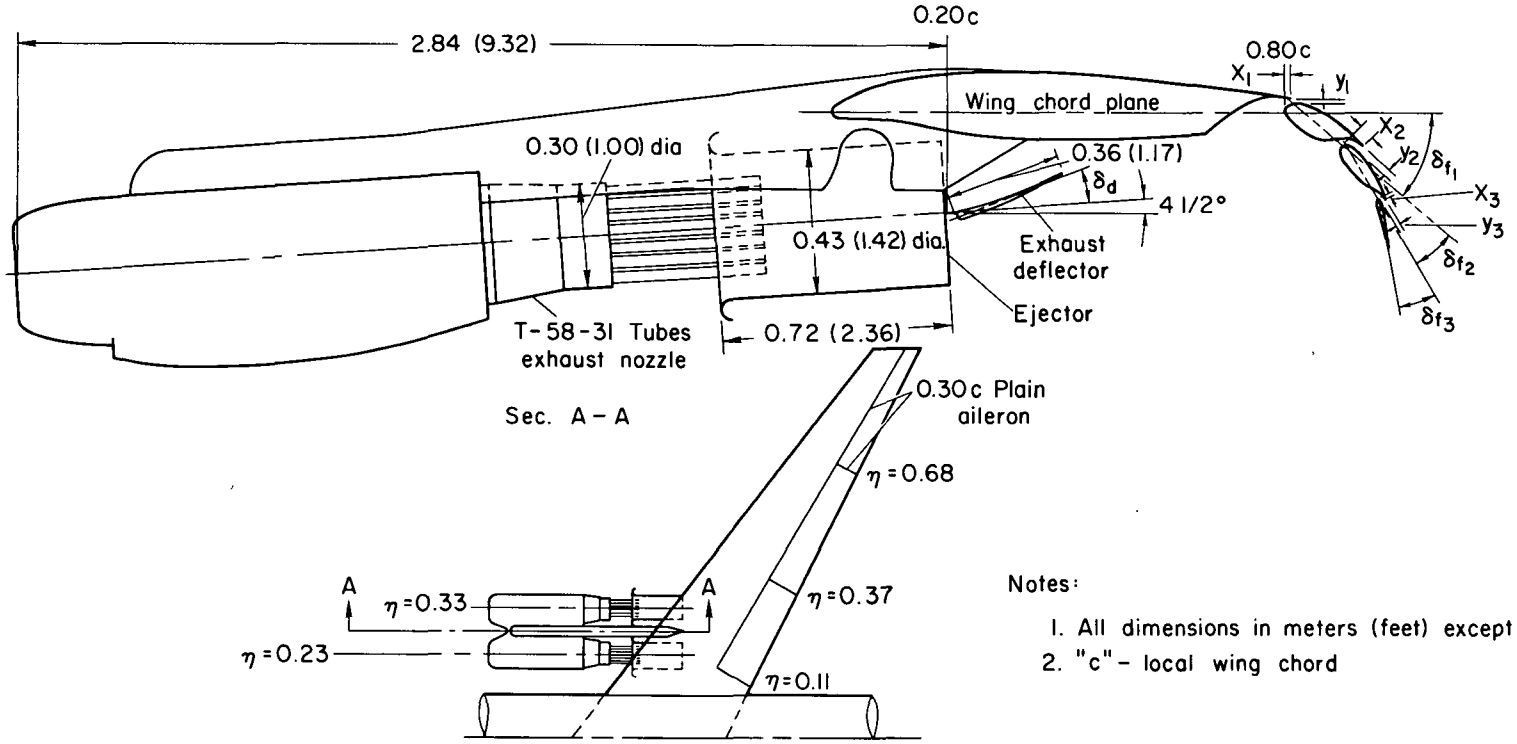

Notes:

1. All dimensions in meters (feet) except as noted
2. "c" – local wing chord

(d) Jet-augmented flap arrangement.

Figure 2.– Concluded.

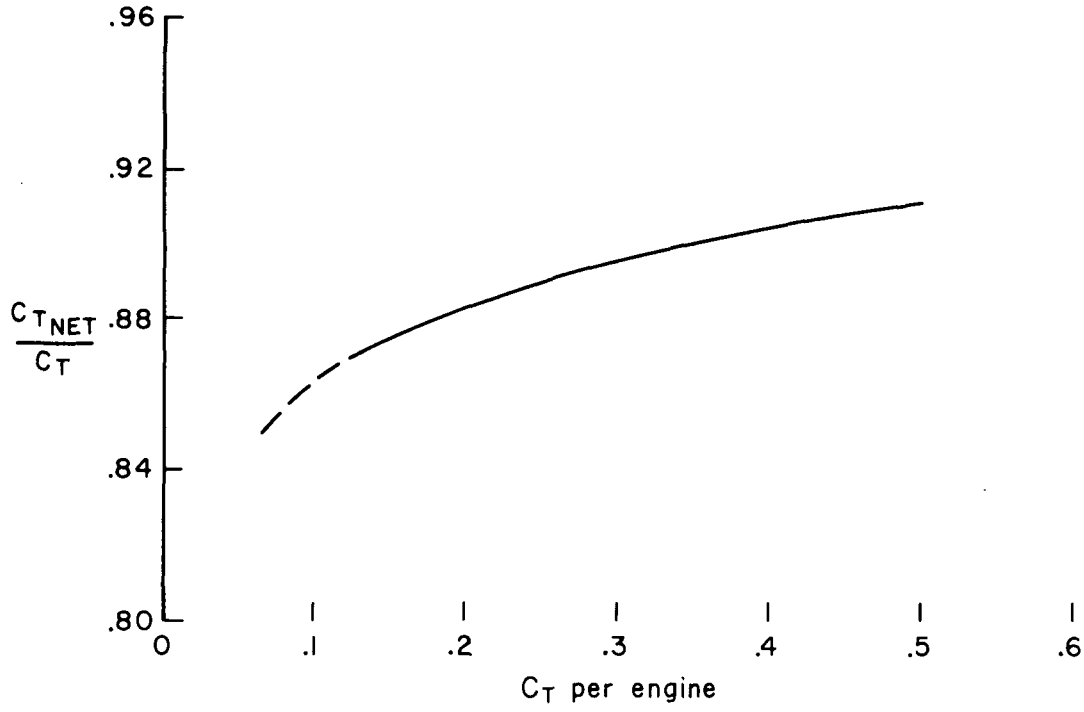

Figure 3.– Estimated relationship between C_T and $C_{T_{NET}}$ for engines used during the investigation.

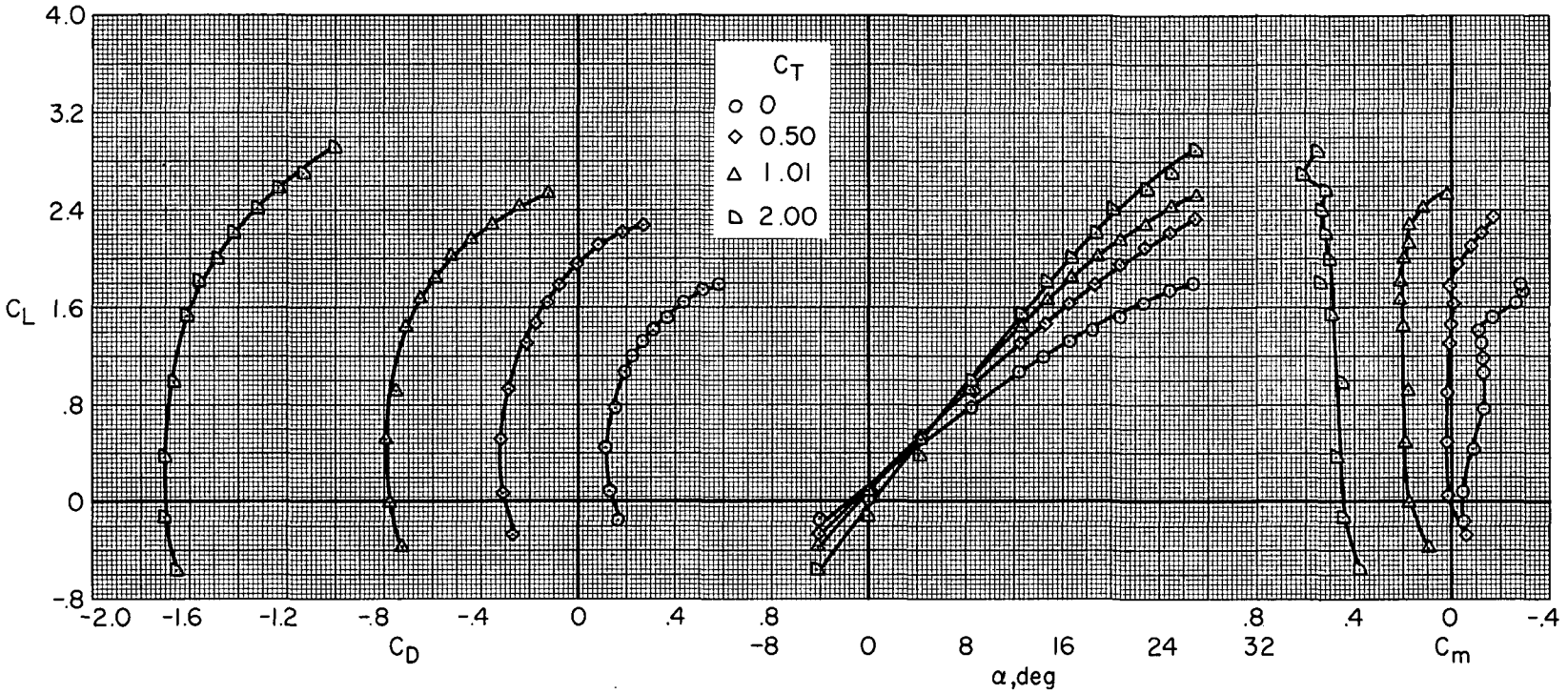

Figure 4.– Longitudinal characteristics of the model with plain wing.

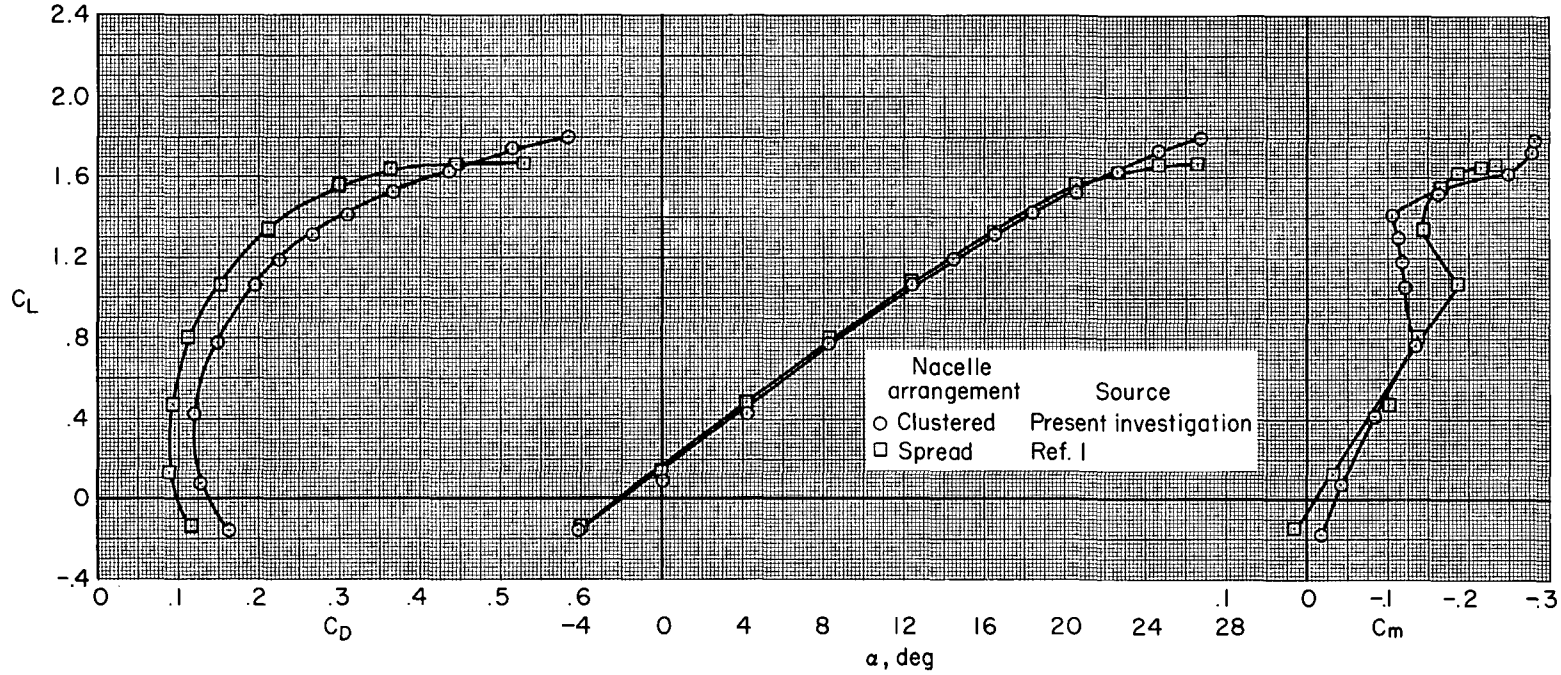

(a) $C_T = 0$

Figure 5.– Longitudinal characteristics of model with plain wing with spread and clustered nacelle arrangements.

A–3753

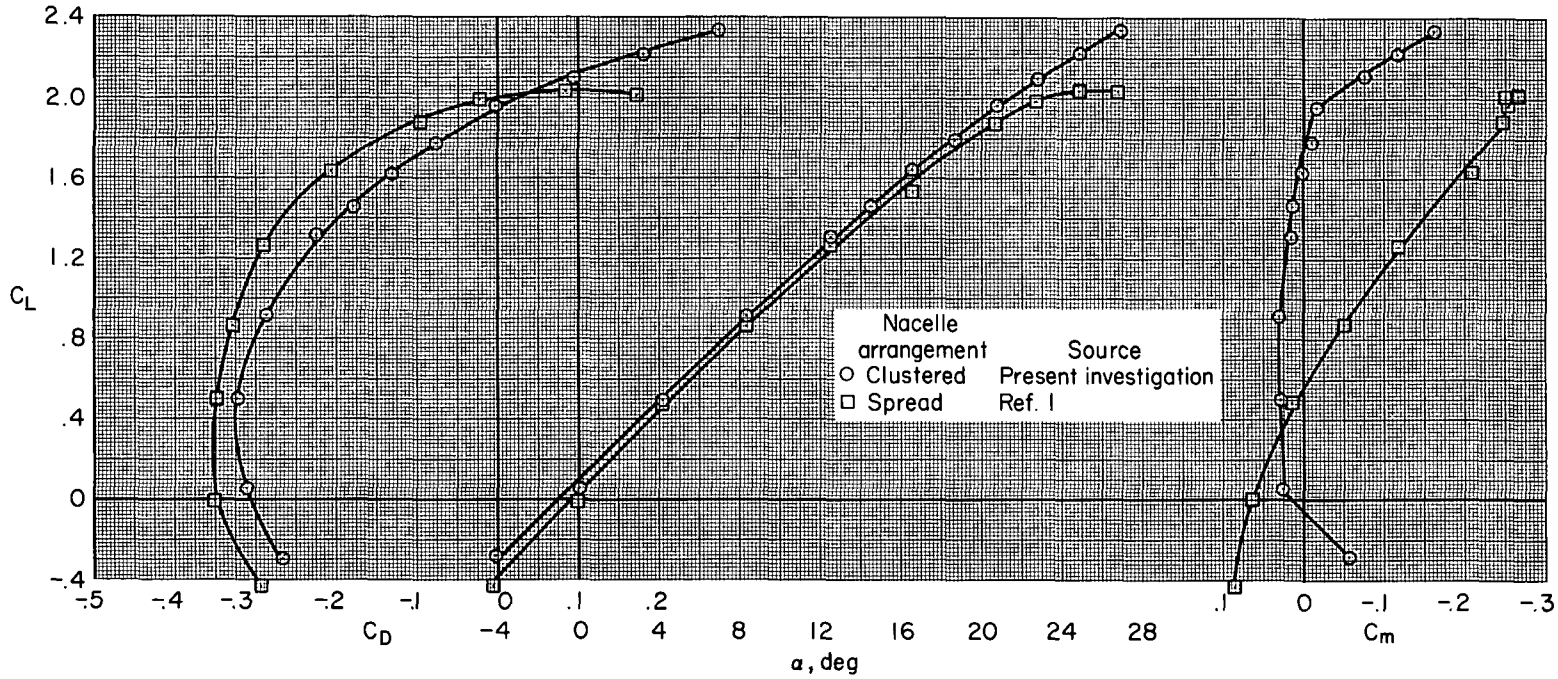

(b) $C_T = 0.50$

Figure 5.– Continued.

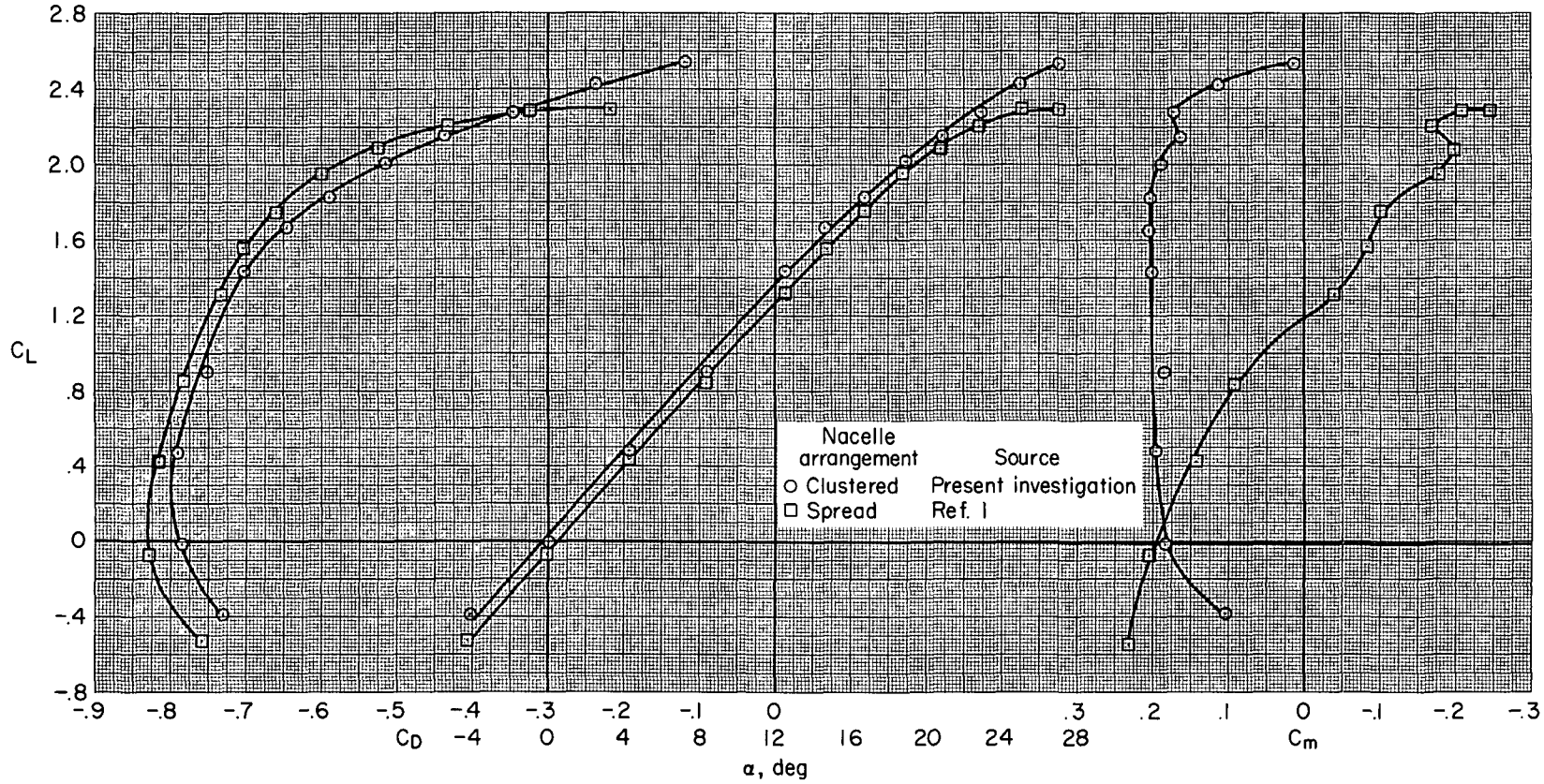

(c) $C_T = 1.0$

Figure 5.– Concluded.

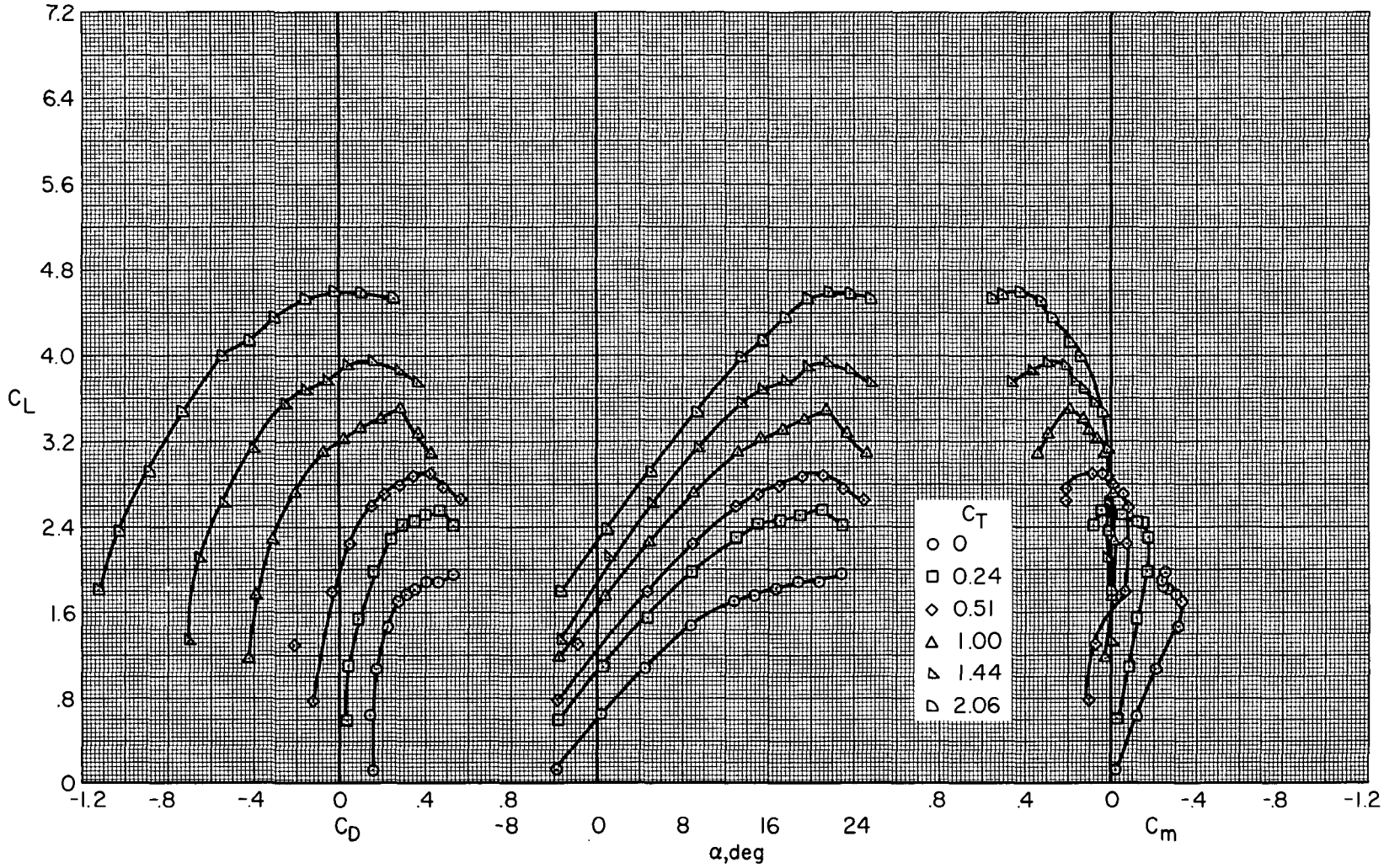

Figure 6.– Longitudinal characteristics of the model with the flaps deflected; $\delta_{f_1}/\delta_{f_2}/\delta_{f_3} = 20°/0°/20°$.

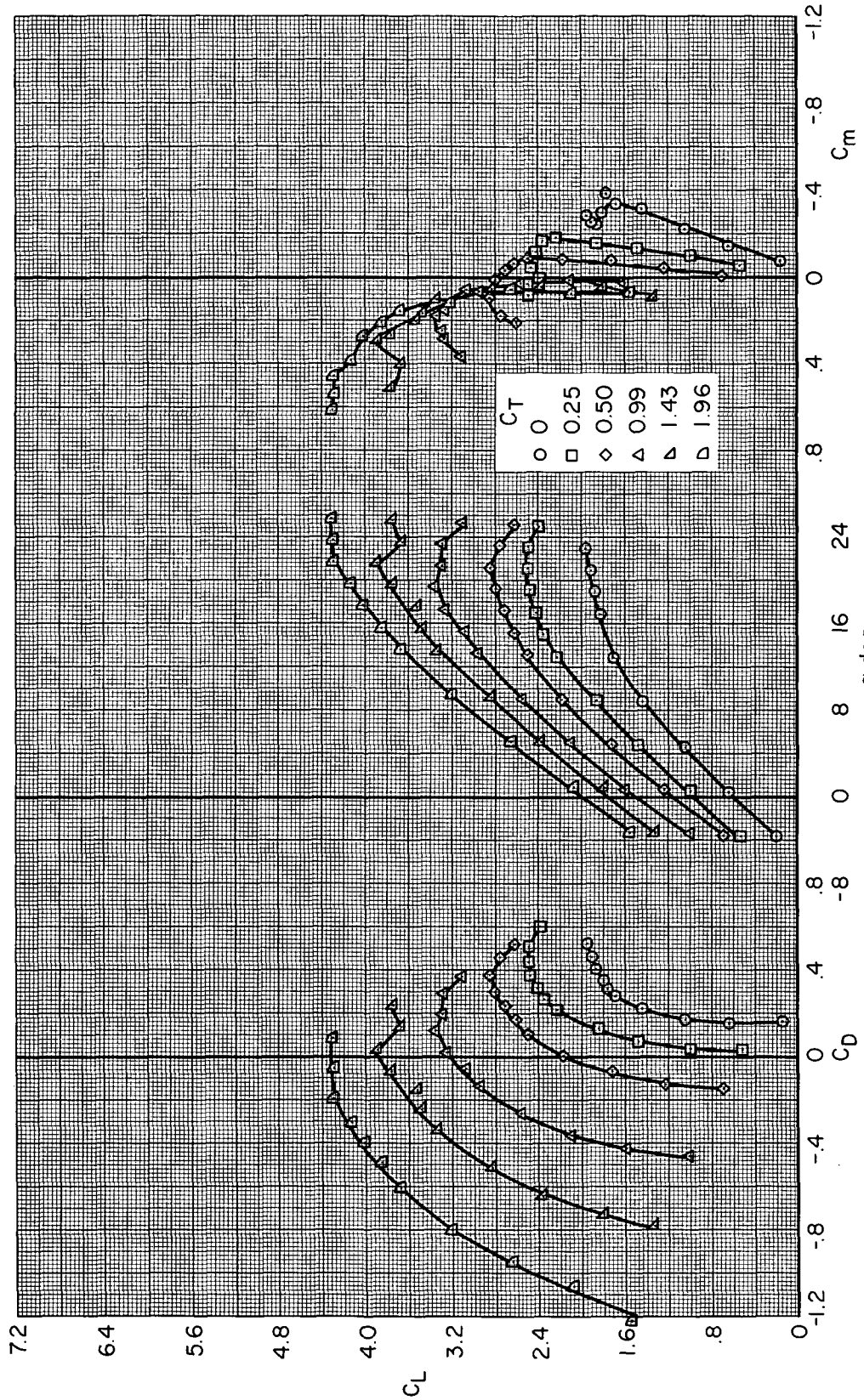

(a) $\delta_{f_3} = 0°$

Figure 7.– Longitudinal characteristics of the model with the flaps deflected; $\delta_{f_1}/\delta_{f_2} = 20°/10°$.

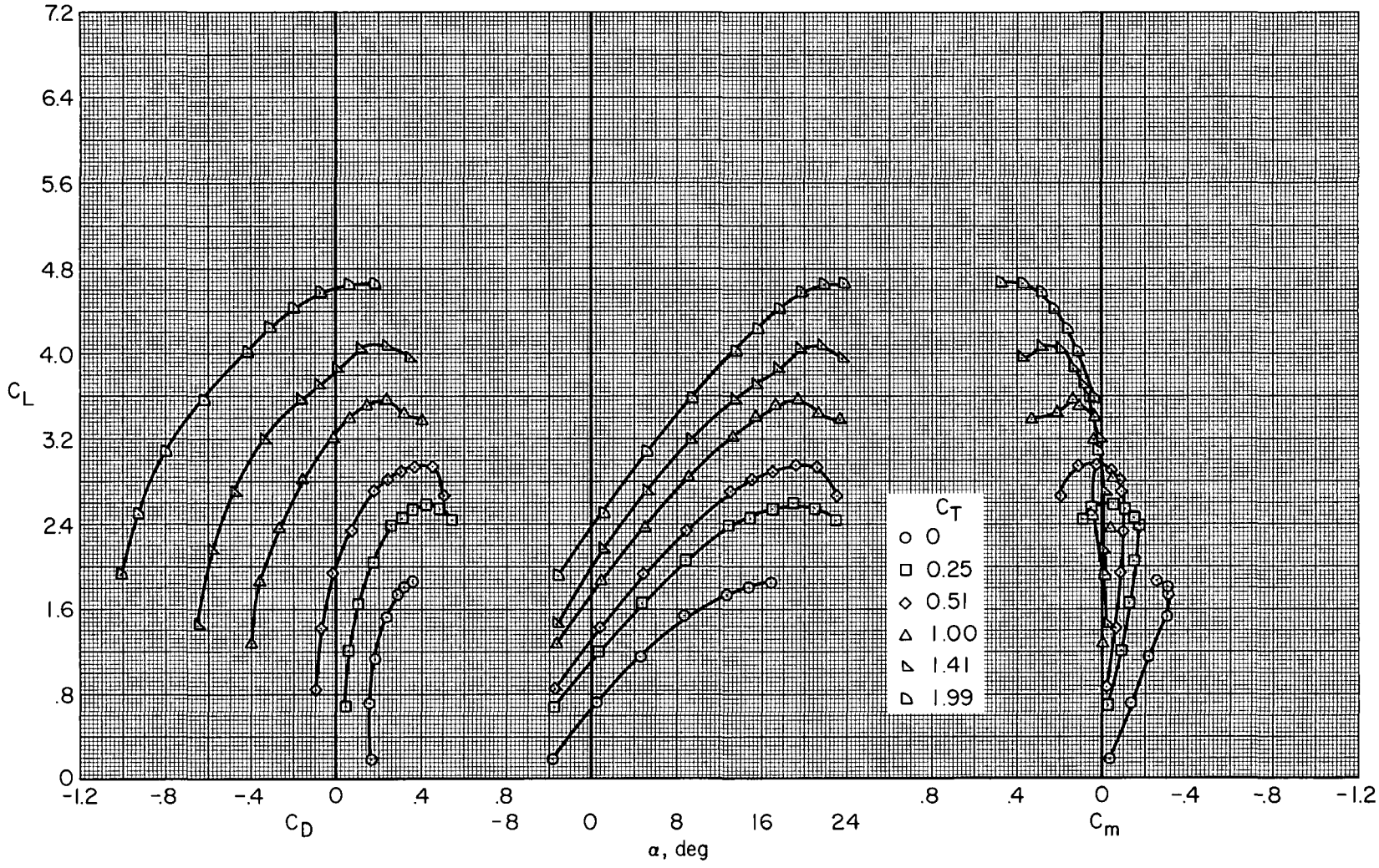

(b) $\delta_{f_3} = 10°$

Figure 7.– Continued.

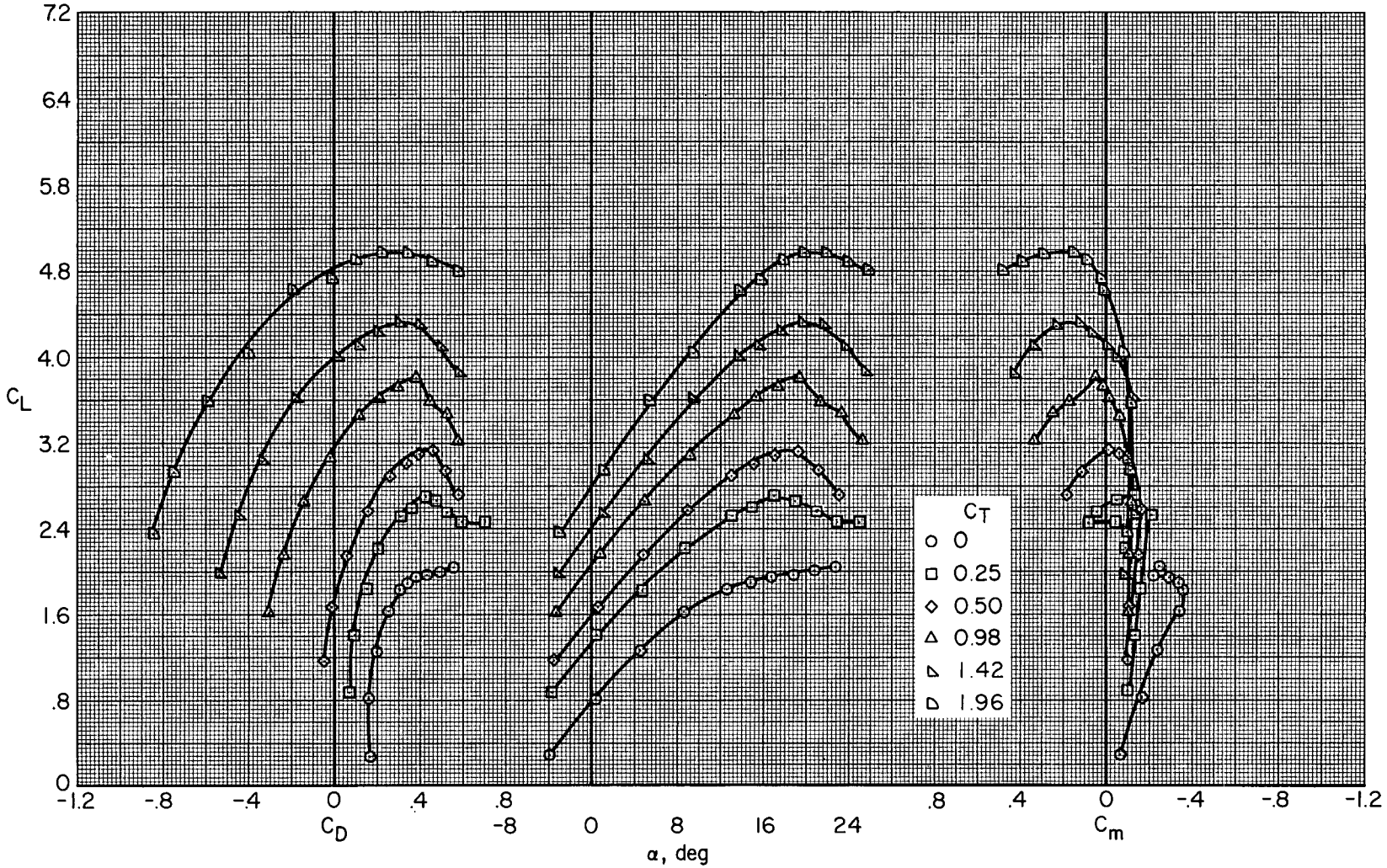

(c) $\delta_{f_3} = 20°$

Figure 7.– Concluded.

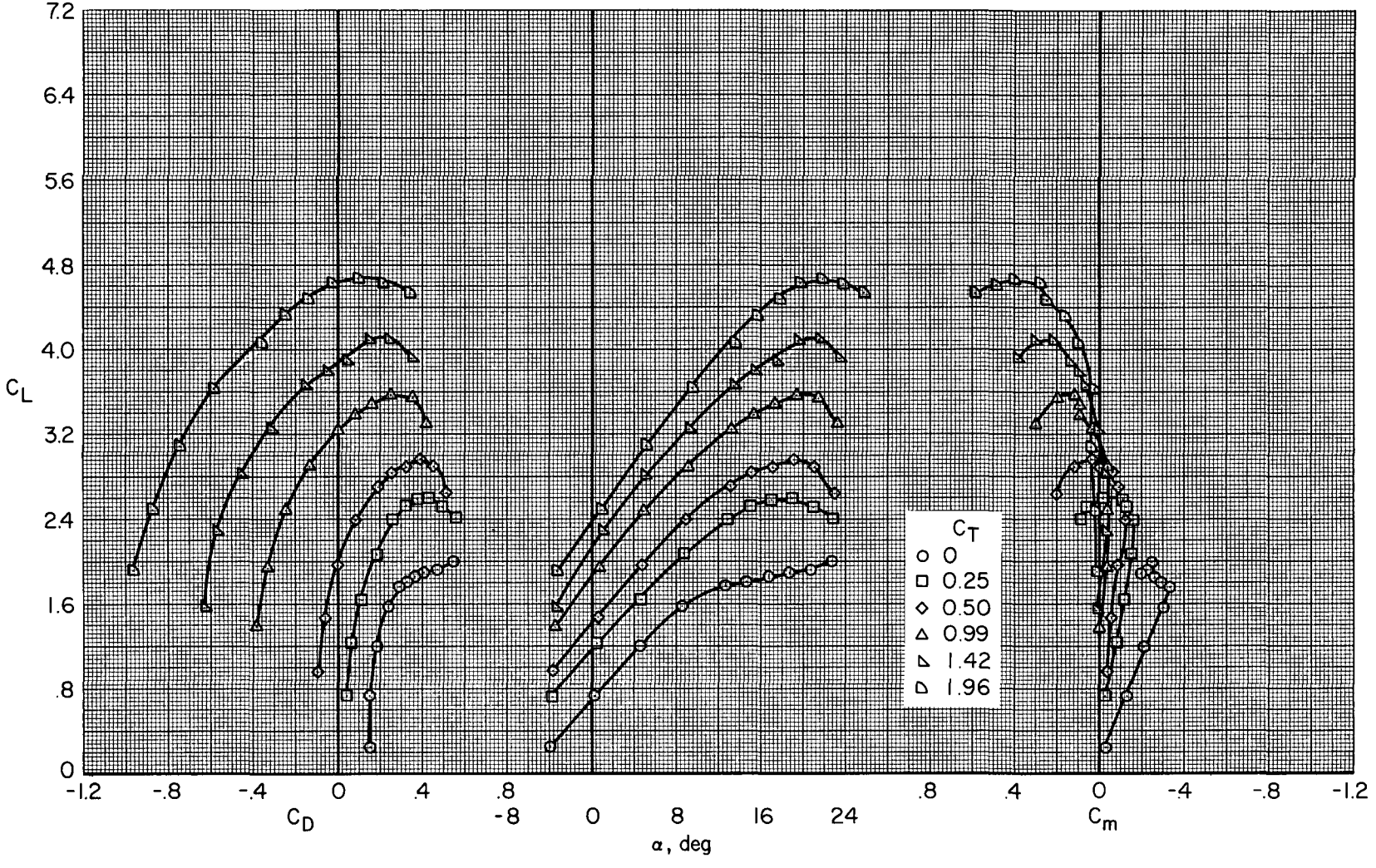

(a) $\delta_{f_3} = 0°$

Figure 8.– Longitudinal characteristics of the model with the flaps deflected; $\delta_{f_1}/\delta_{f_2} = 20°/20°$.

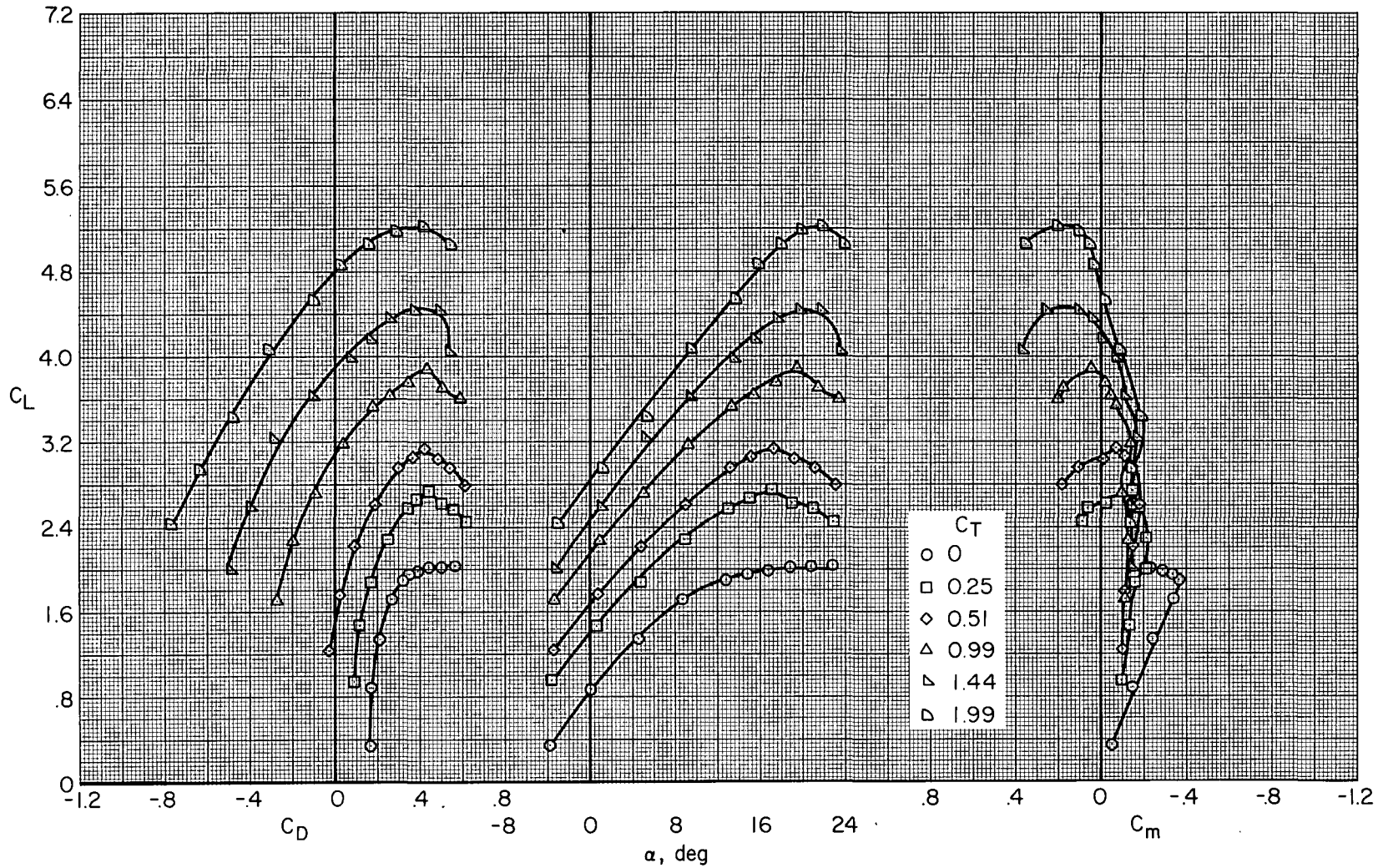

(b) $\delta f_3 = 10°$

Figure 8.– Continued.

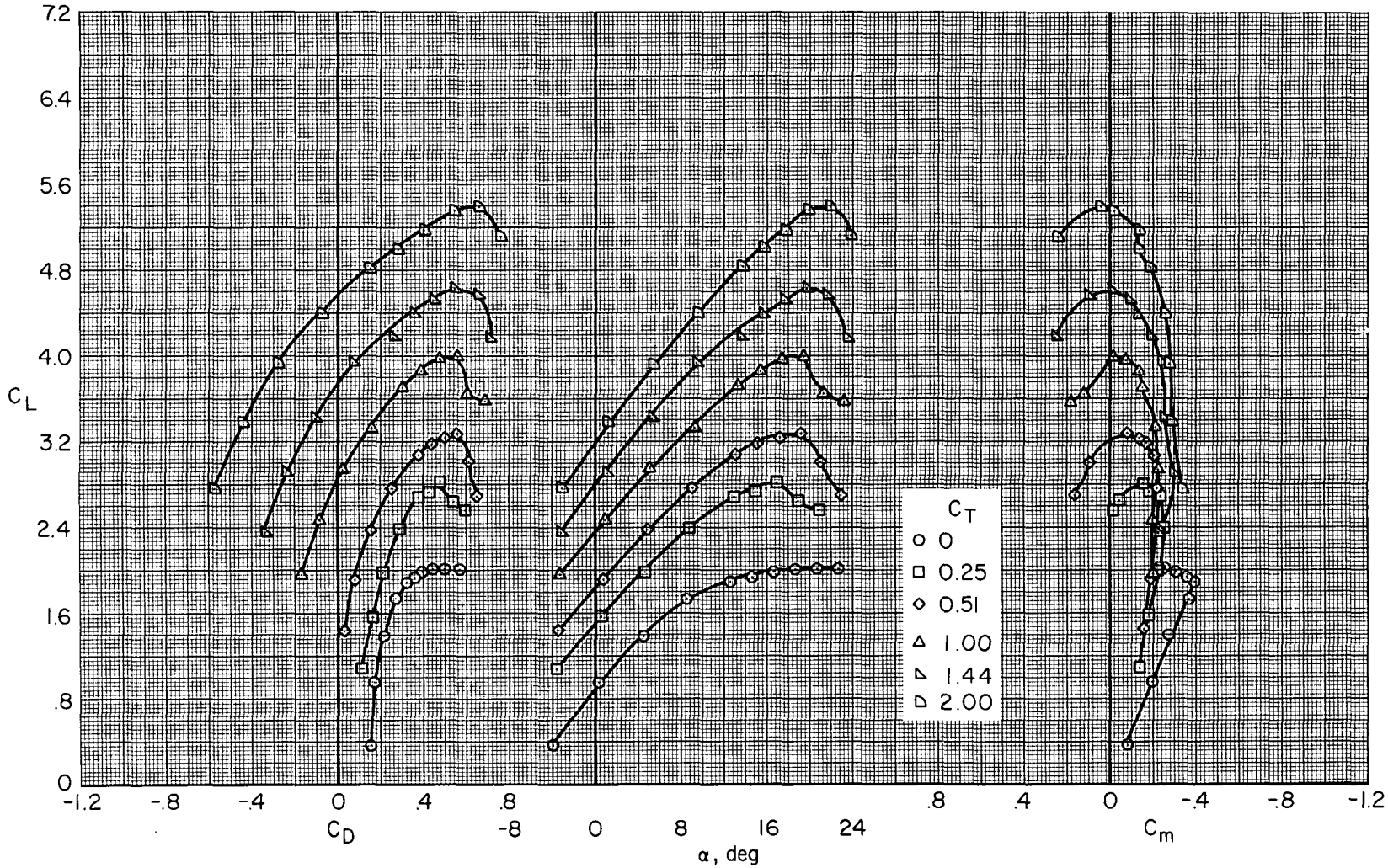

(c) $\delta_{f_3} = 20°$

Figure 8.– Continued.

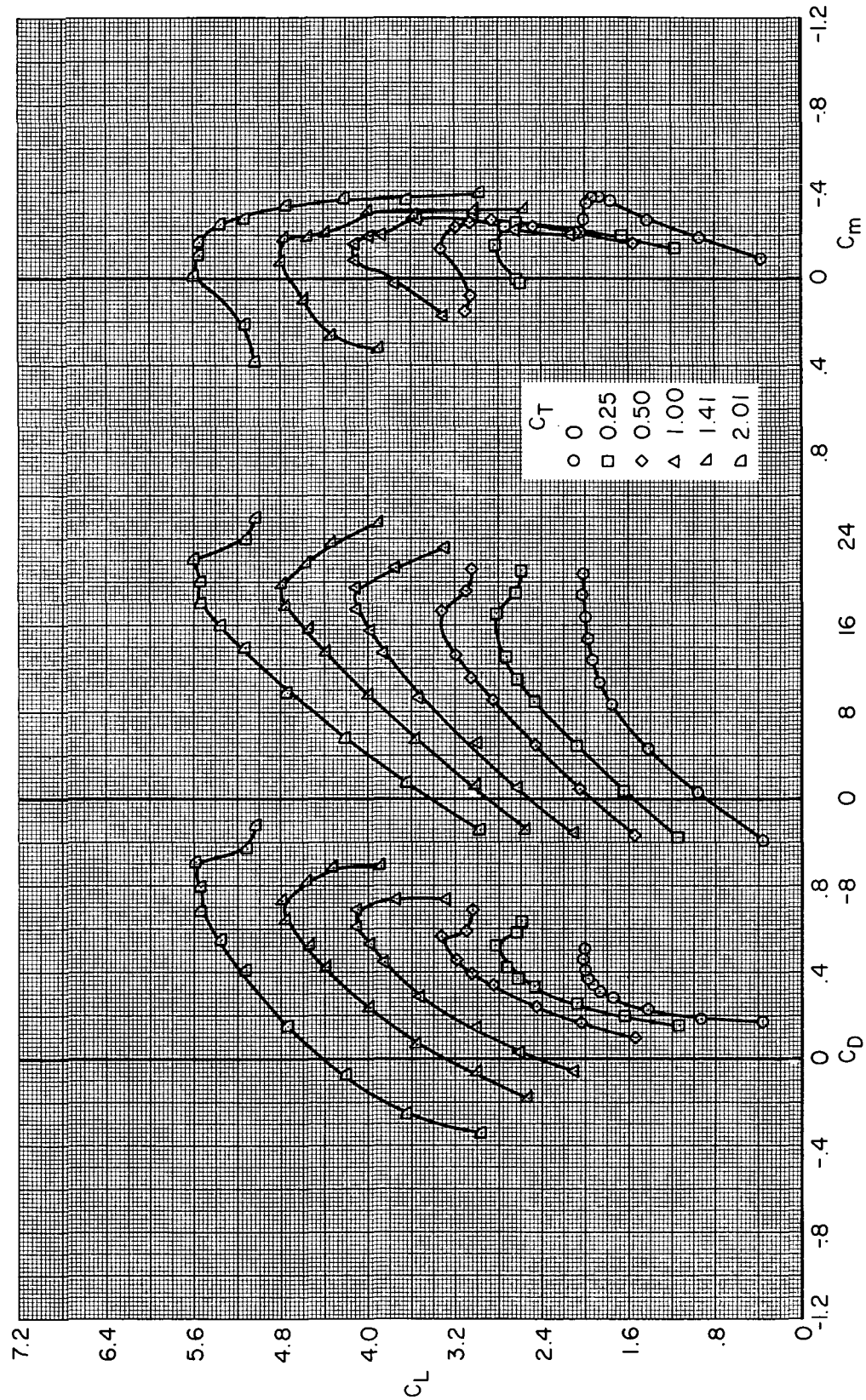

(d) $\delta_{f_3} = 30°$

Figure 8.– Continued.

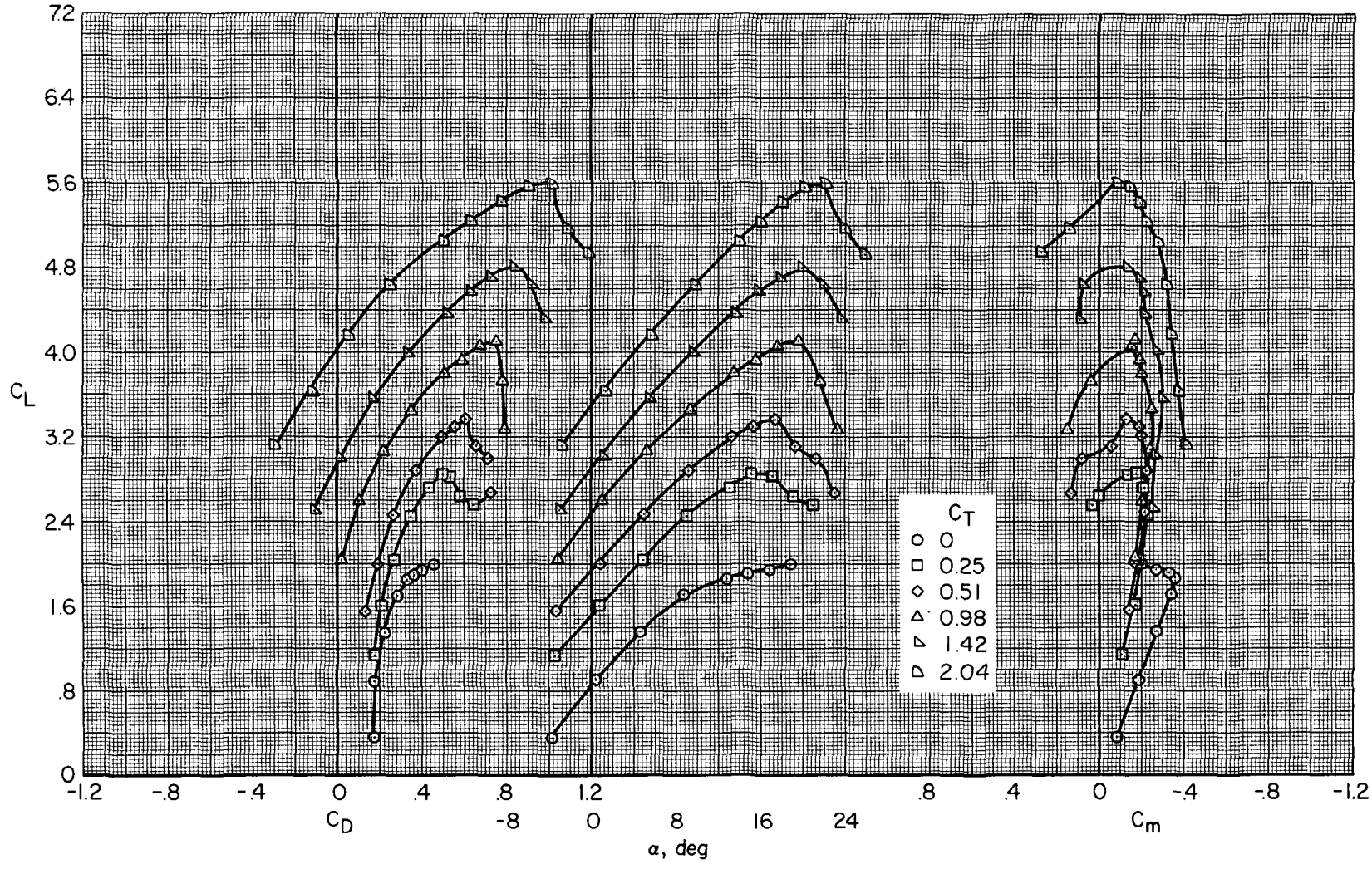

(e) $\delta_{f_3} = 40°$

Figure 8.– Concluded.

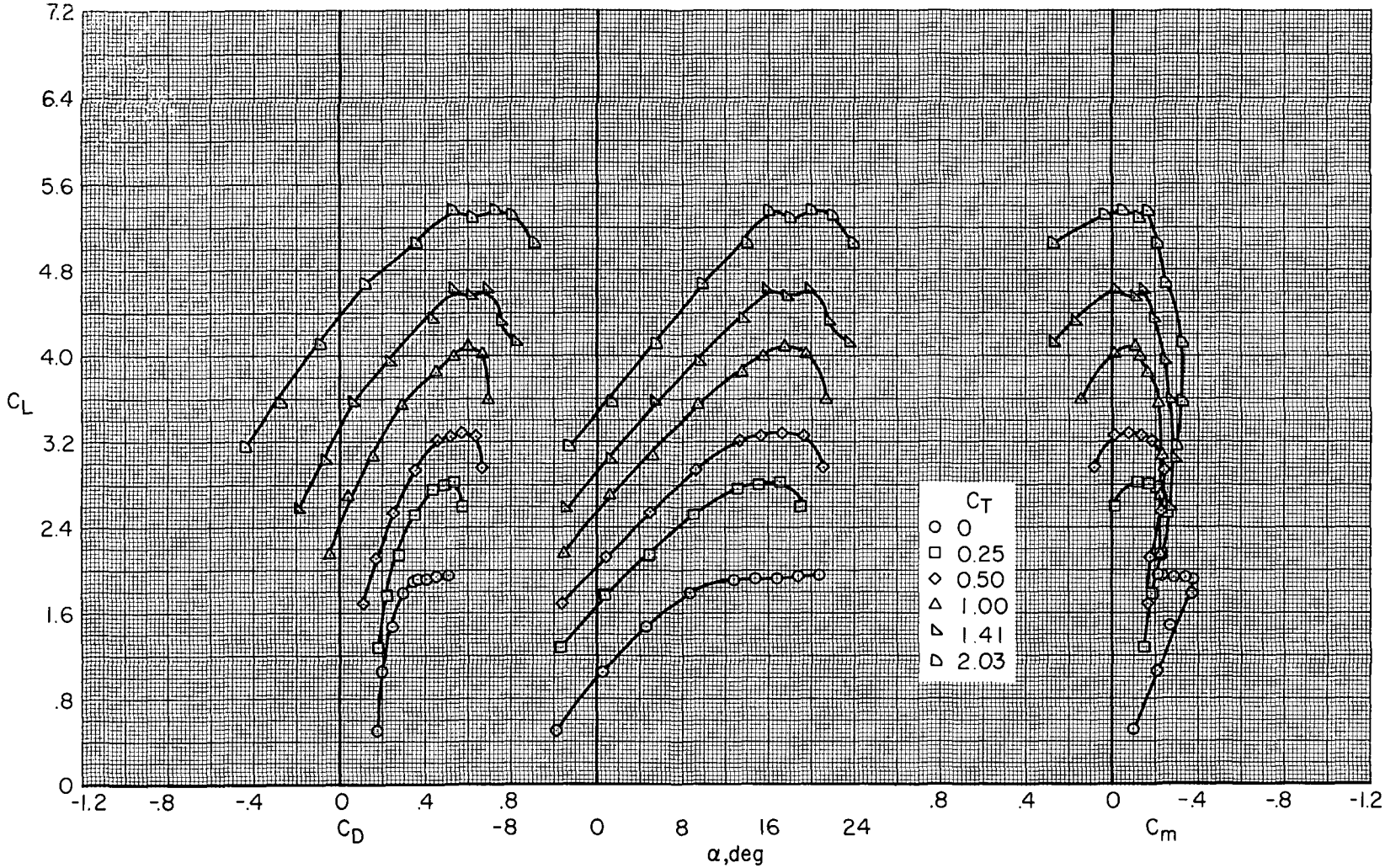

(a) $\delta_{f_3} = 0°$

Figure 9.– Longitudinal characteristics of the model with the flaps deflected; $\delta_{f_1}/\delta_{f_2} = 30°/30°$.

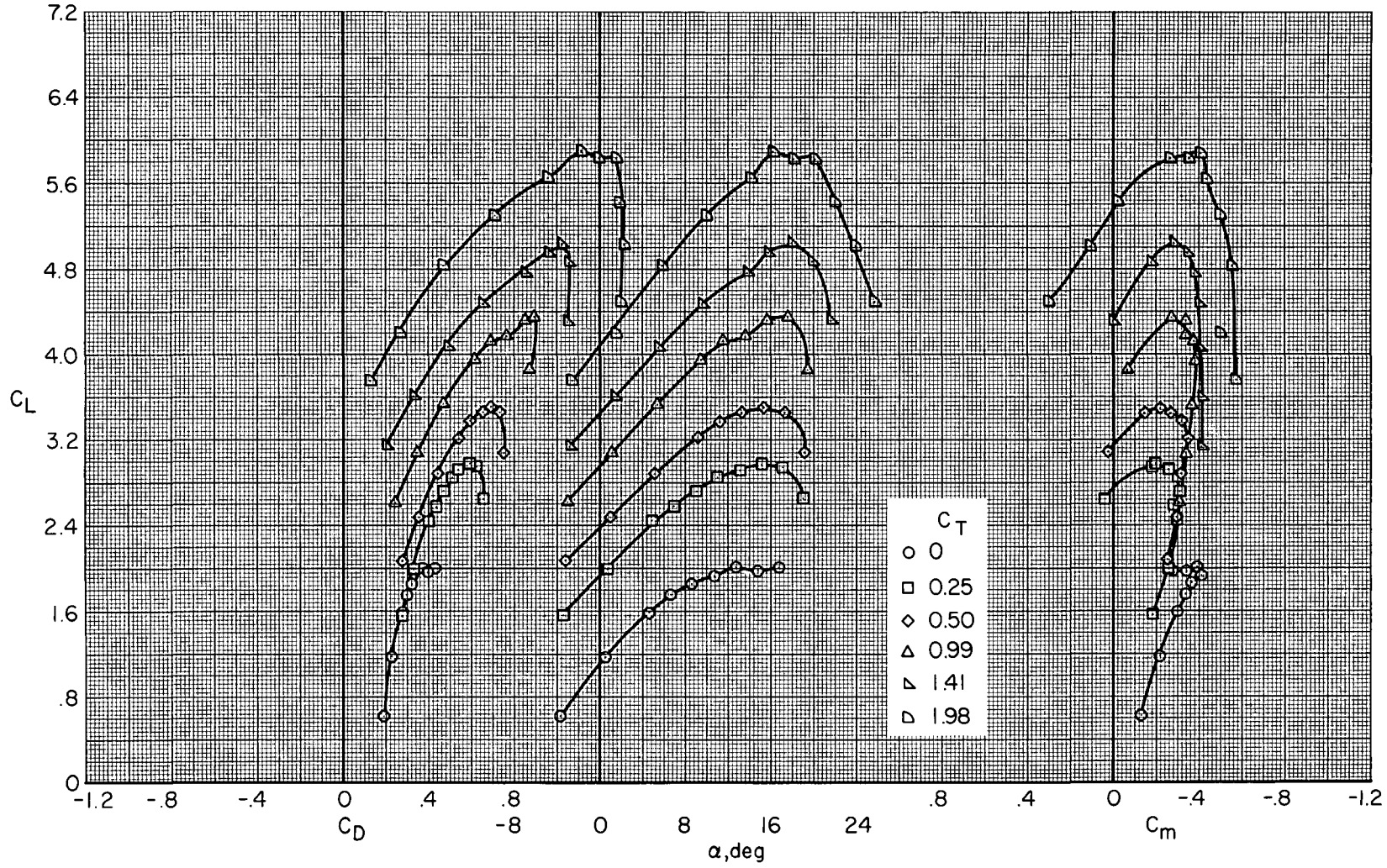

(b) $\delta_{f_3} = 20°$

Figure 9.– Continued.

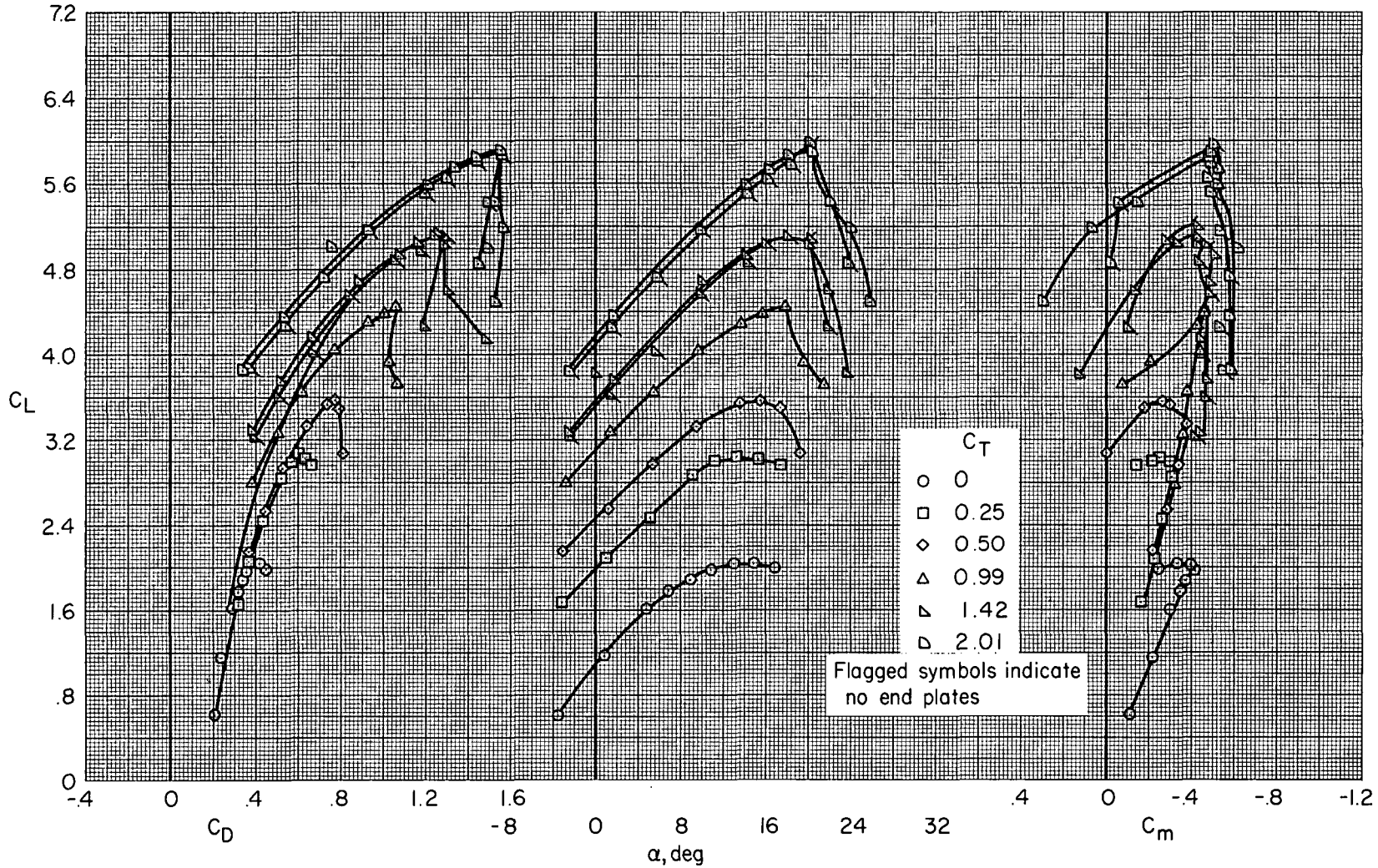

(c) $\delta_{f_3} = 30°$ (0.46X0.82 m (1.5X2.7 ft) end plates at each end of flap root).

Figure 9.– Concluded.

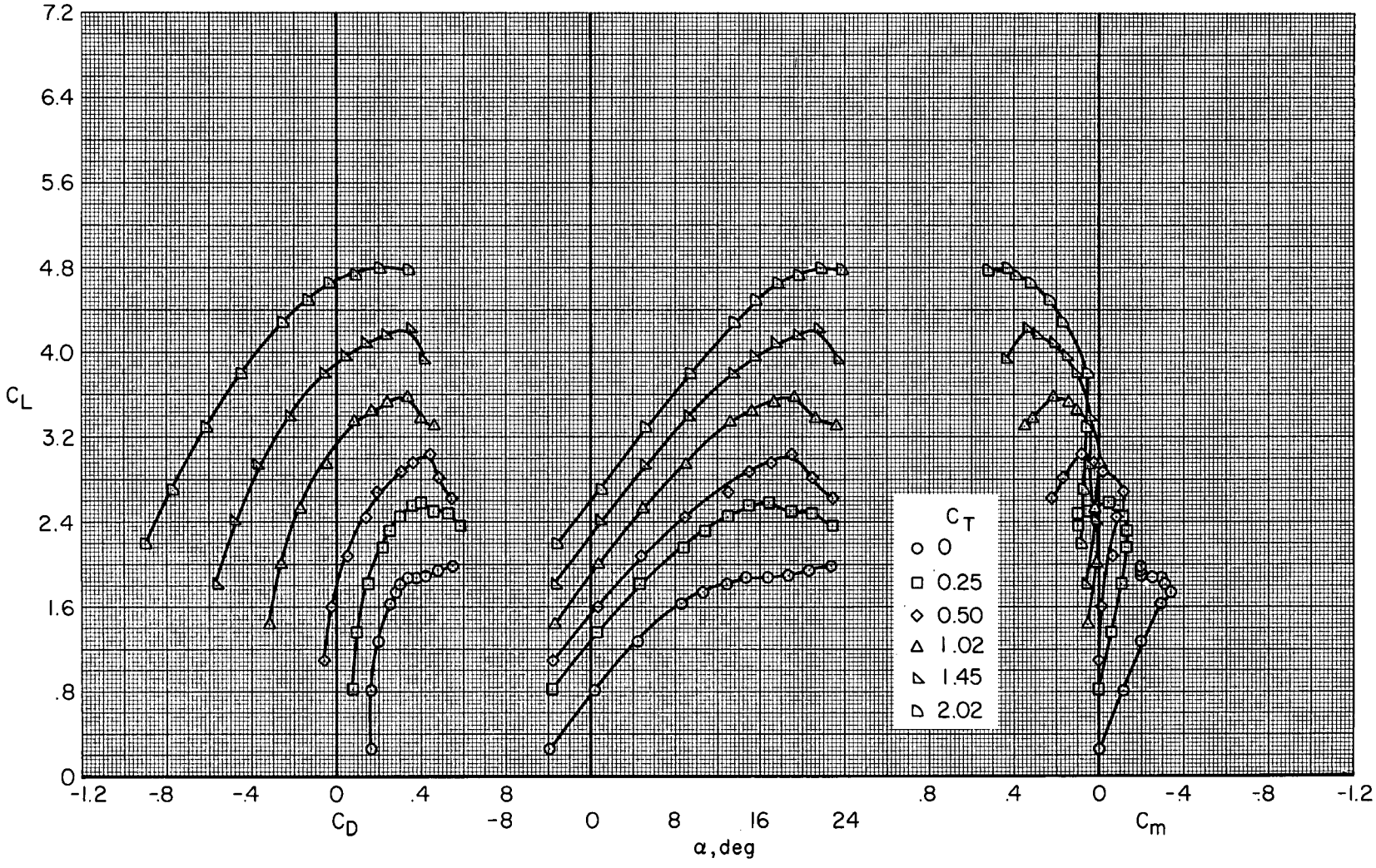

(a) $\delta_{f_3} = 0°$

Figure 10.– Longitudinal characteristics of the model with the flaps deflected; $\delta_{f_1}/\delta_{f_2} = 40°/0°$.

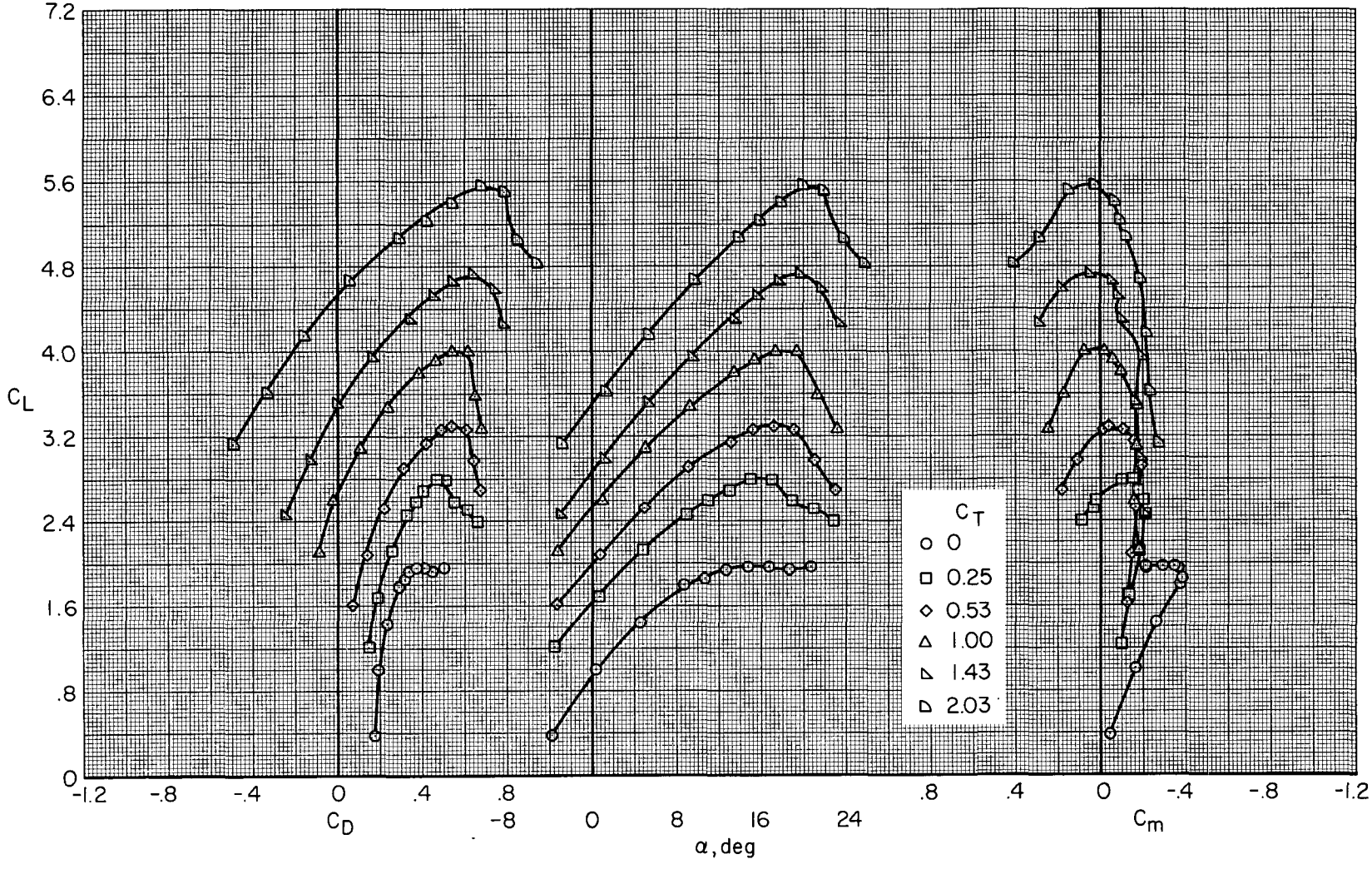

(b) $\delta_{f_3} = 20°$

Figure 10.– Continued.

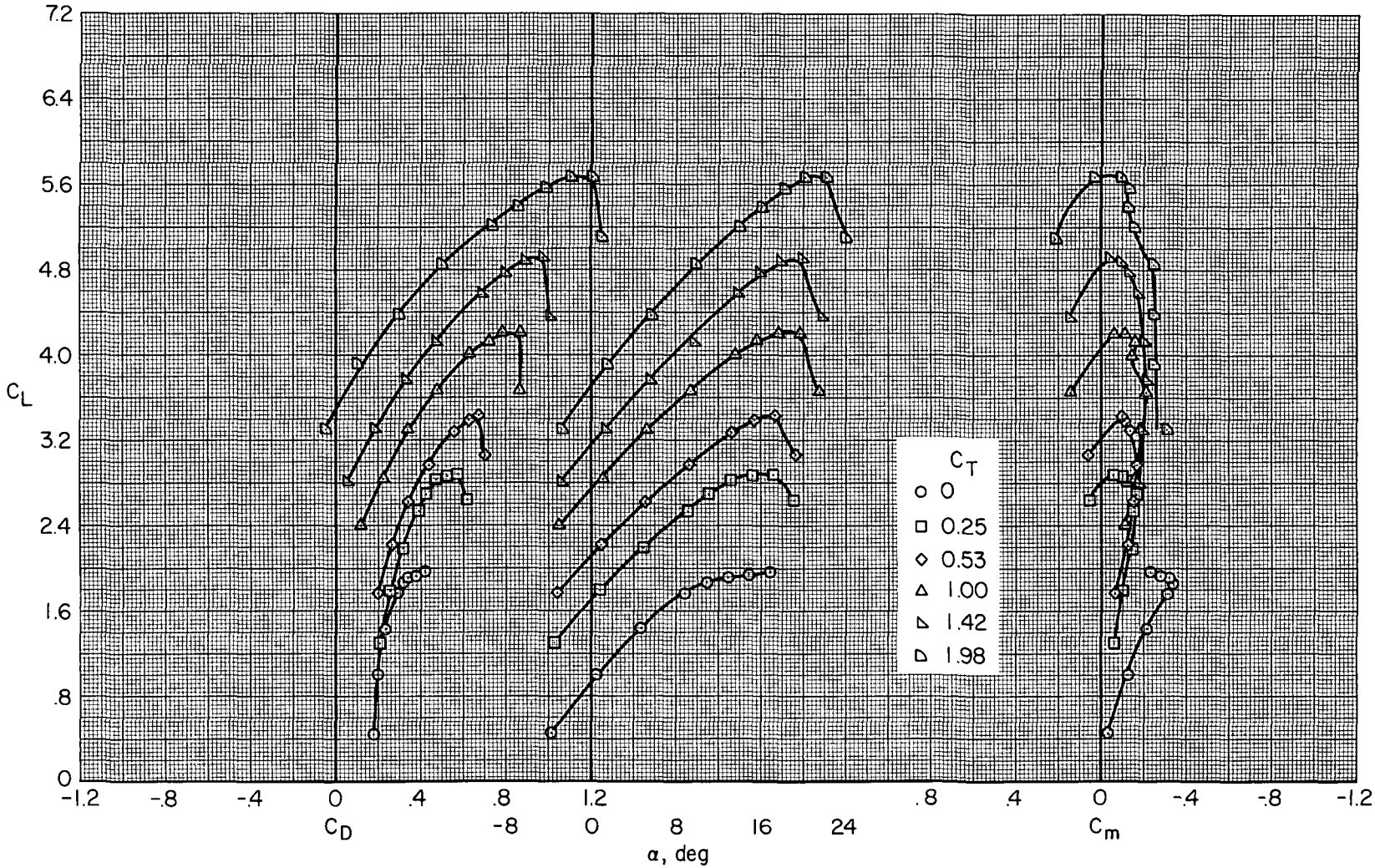

(c) $\delta_{f_3} = 40°$

Figure 10.– Concluded.

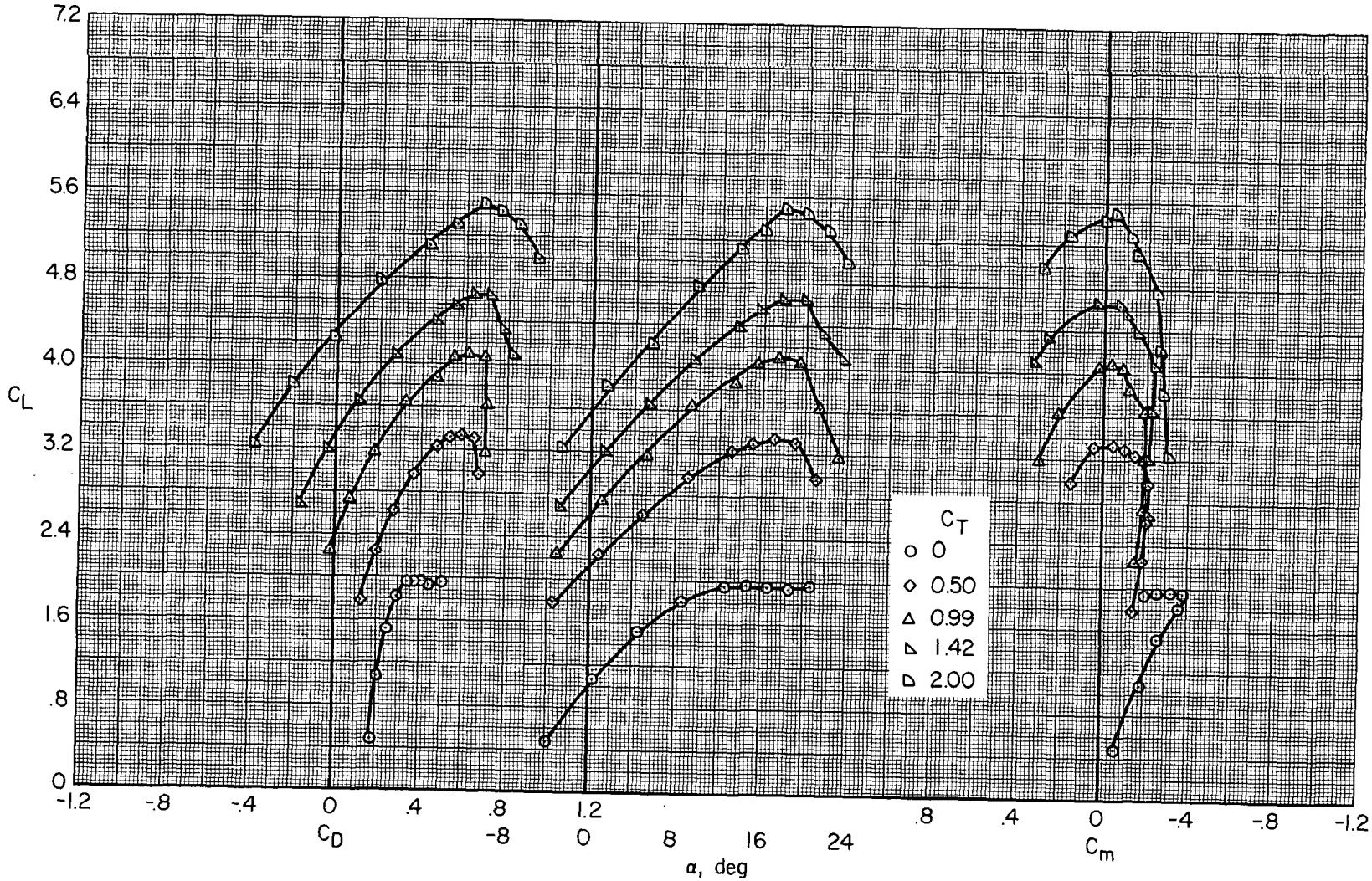

(a) $\delta_{f_3} = 0°$

Figure 11.– Longitudinal characteristics of the model with the flaps deflected; $\delta_{f_1}/\delta_{f_2} = 40°/20°$.

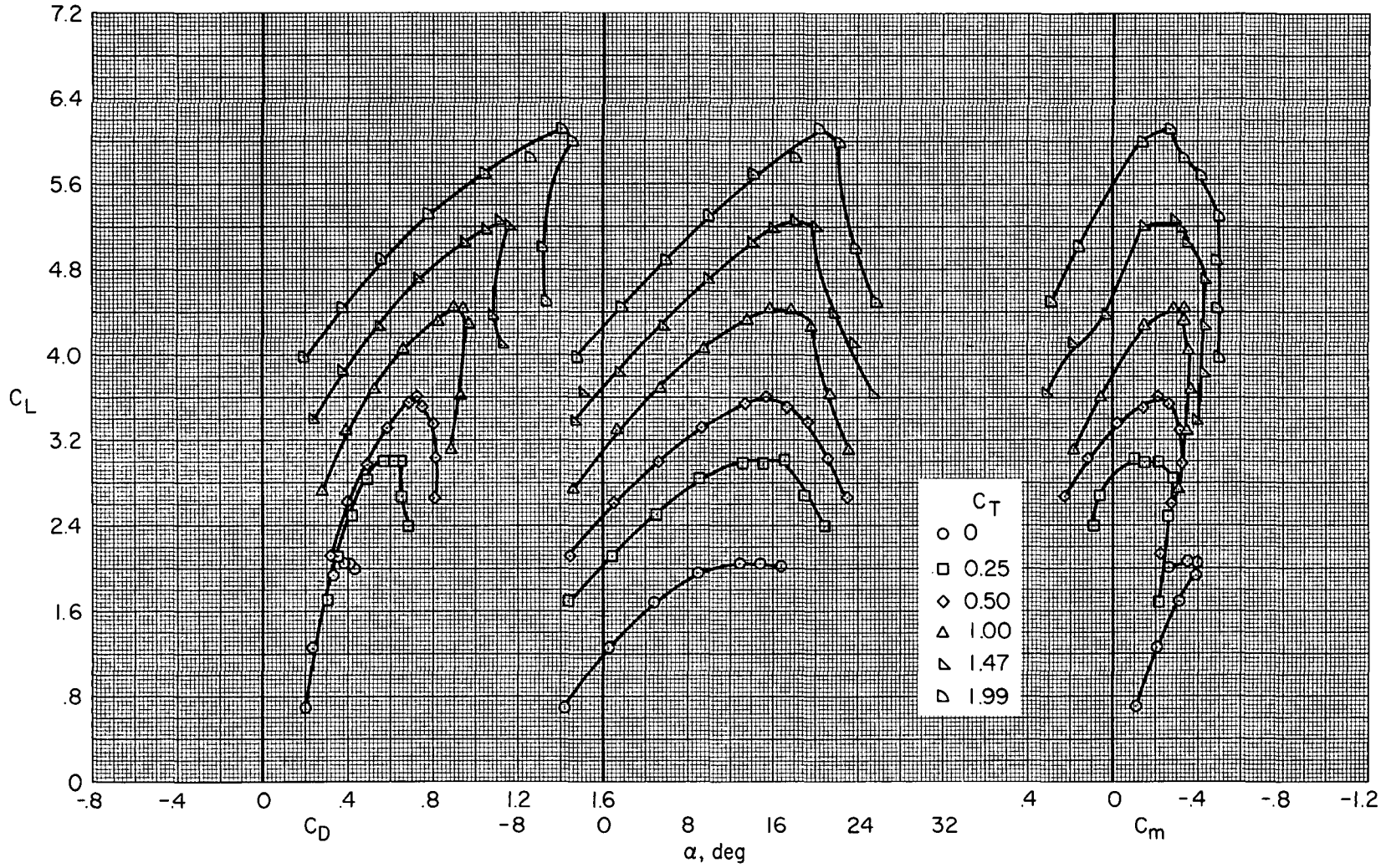

(b) $\delta_{f_3} = 20°$

Figure 11.– Continued.

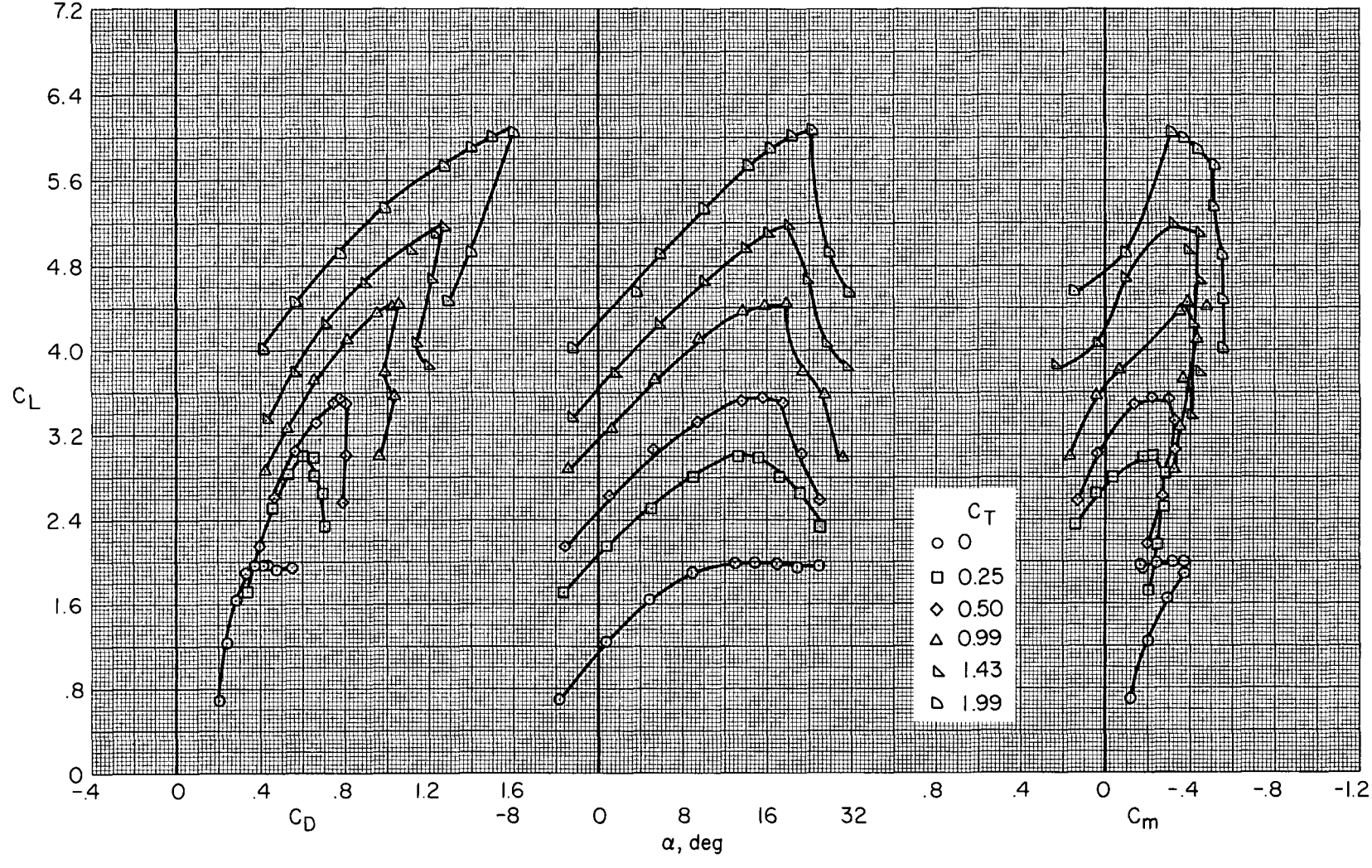

(c) $\delta_{f_3} = 30°$

Figure 11.– Concluded.

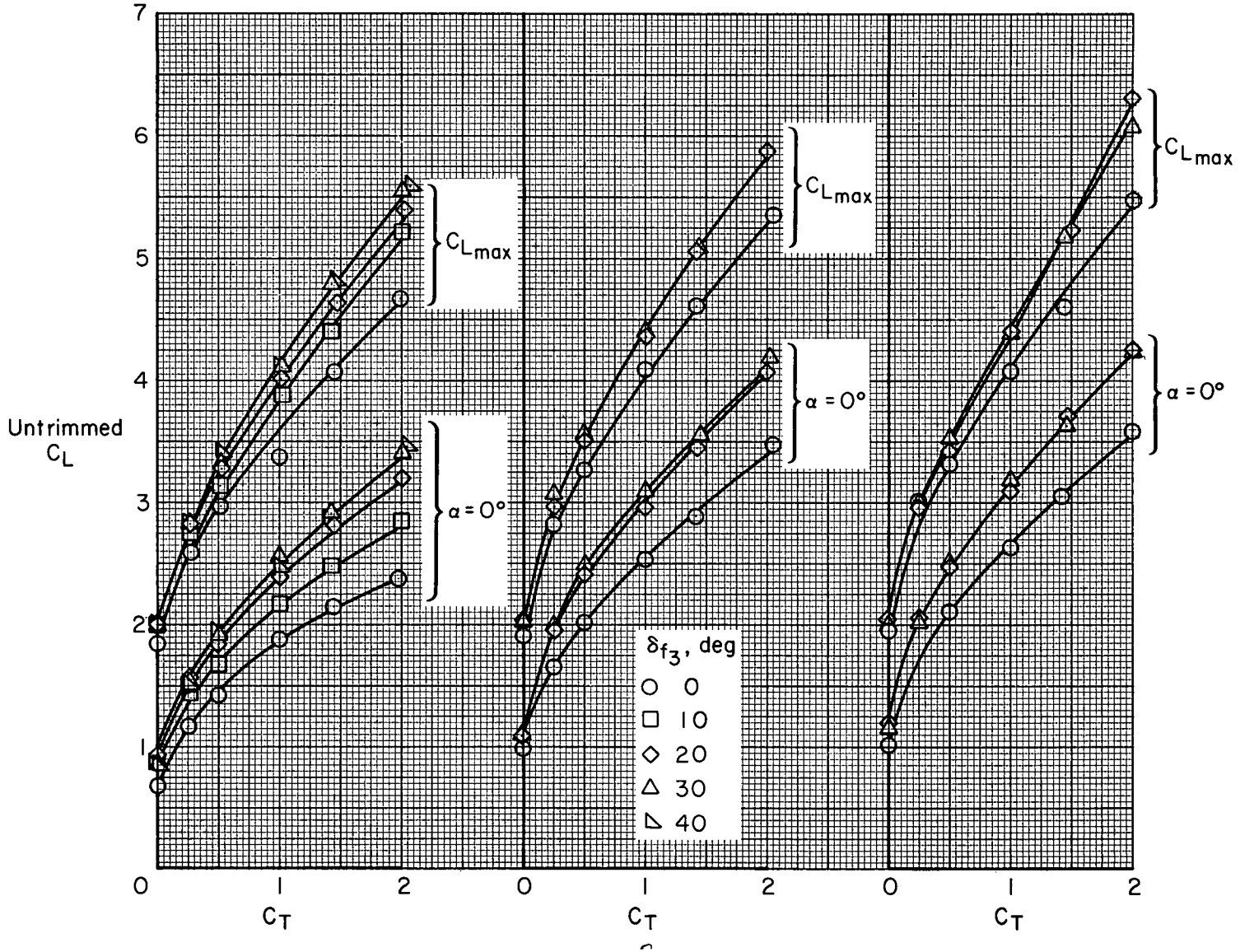

(a) $\delta_{f_1}/\delta_{f_2} = 20°/20°$ (b) $\delta_{f_1}/\delta_{f_2} = 30°/30°$ (c) $\delta_{f_1}/\delta_{f_2} = 40°/20°$

Figure 12.– Variation of lift coefficient with gross thrust coefficient at several flap deflections.

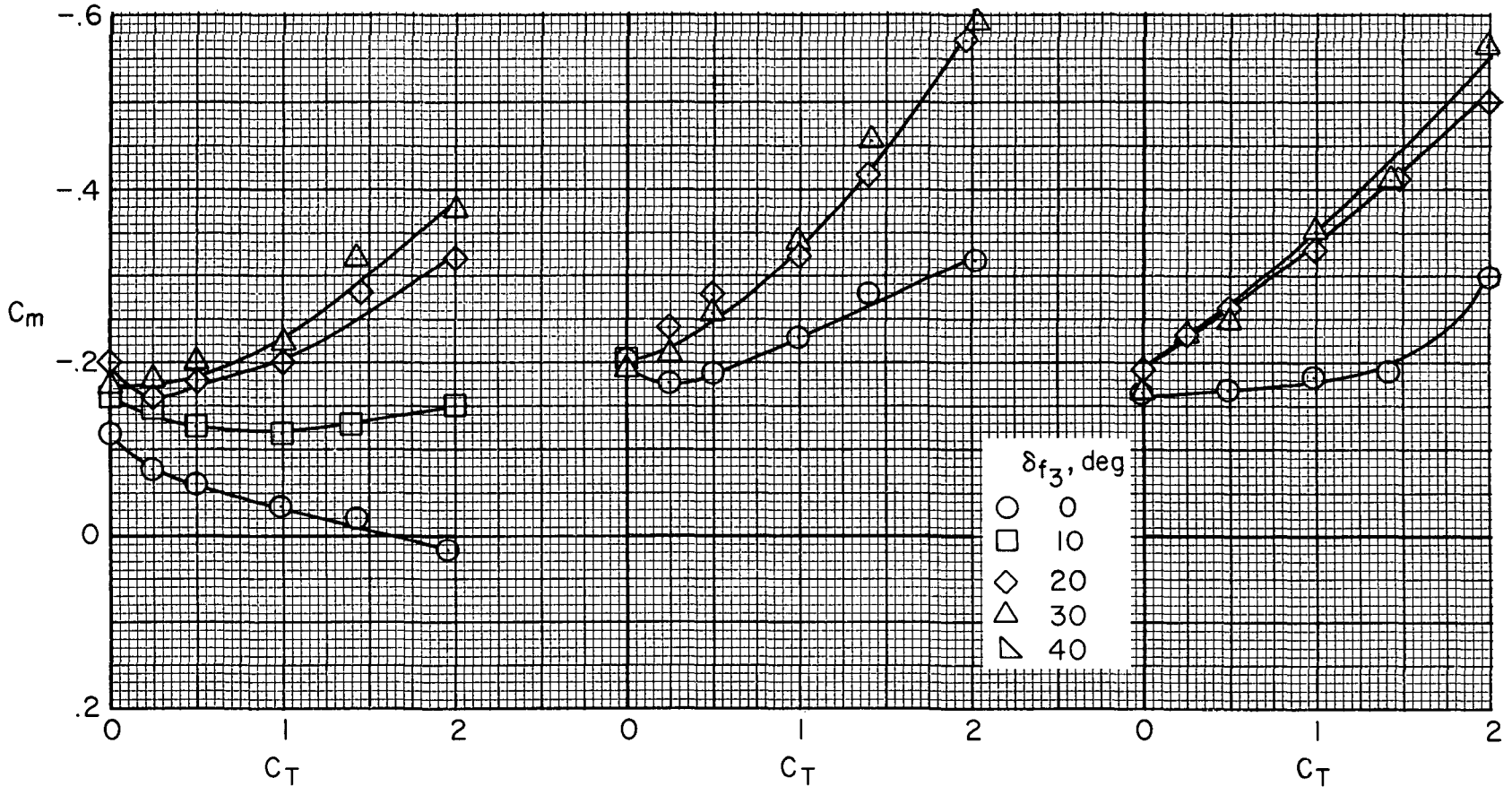

(a) $\delta_{f_1}/\delta_{f_2} = 20°/20°$ (b) $\delta_{f_1}/\delta_{f_2} = 30°/30°$ (c) $\delta_{f_1}/\delta_{f_2} = 40°/20°$

Figure 13.– Variation of pitching-moment coeffiicient with gross thrust coefficient at several flap deflections; $\alpha = 0°$.

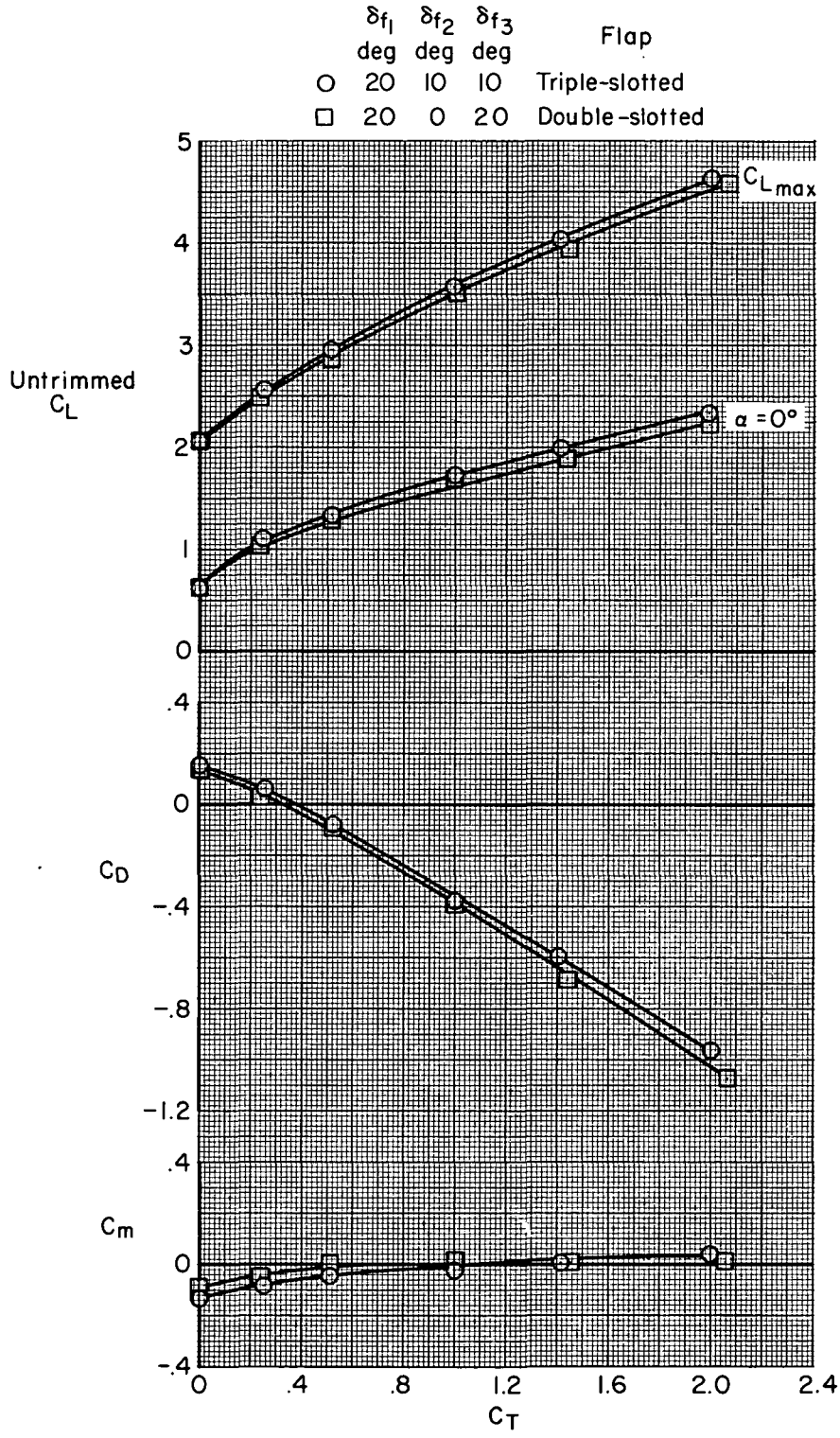

(a) $\delta_{f_{total}} = 60°$

Figure 14.– Lift, drag, and pitching-moment coefficients for triple- and double-slotted flap configuration; $\alpha = 0°$.

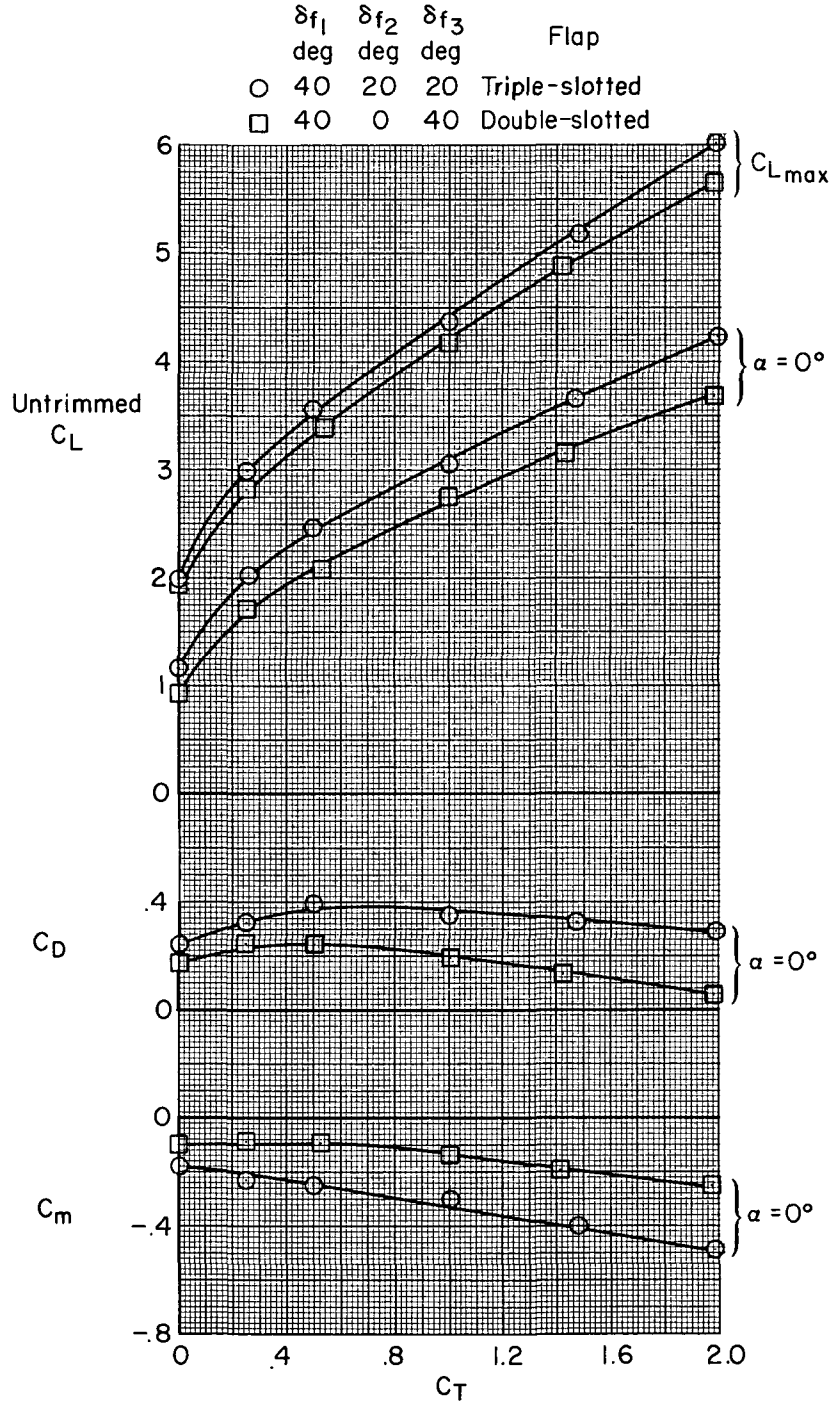

(b) $\delta_{f_{total}} = 80°$

Figure 14.– Concluded.

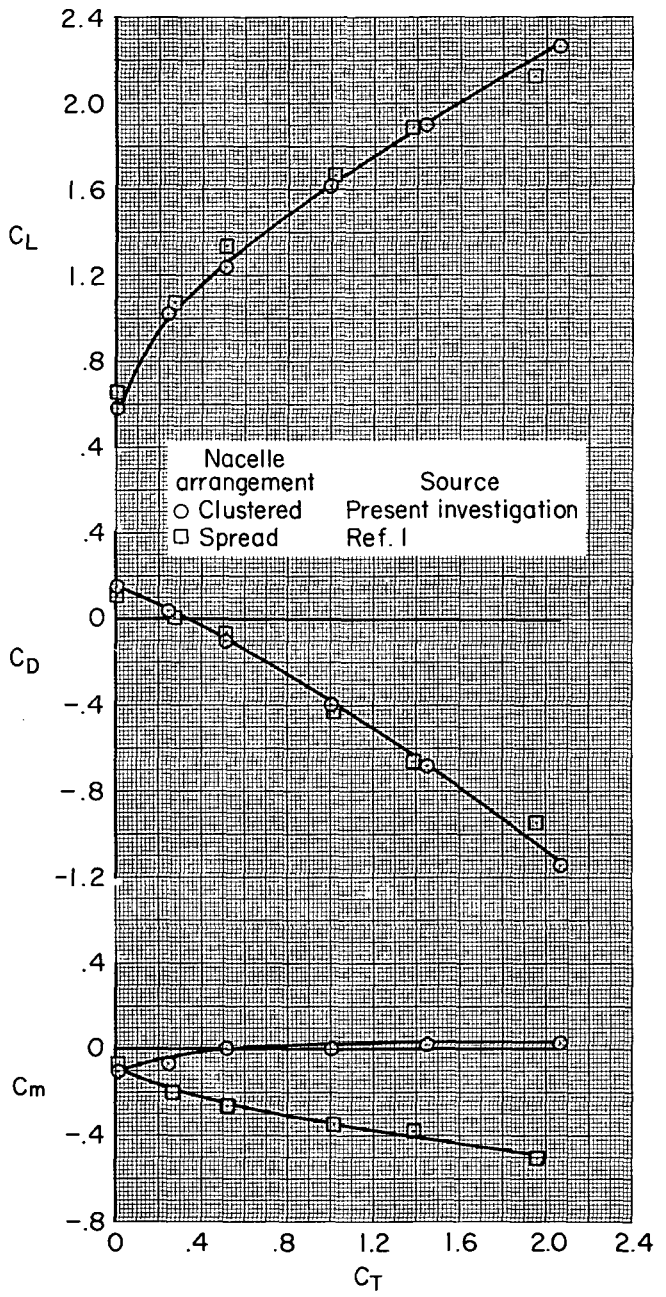

(a) $\delta_{f_1}/\delta_{f_2}/\delta_{f_3} = 20°/0°/20°$

Figure 15.– Lift, drag, and pitching-moment coefficients for spread and clustered nacelle arrangements; $\alpha = 0°$.

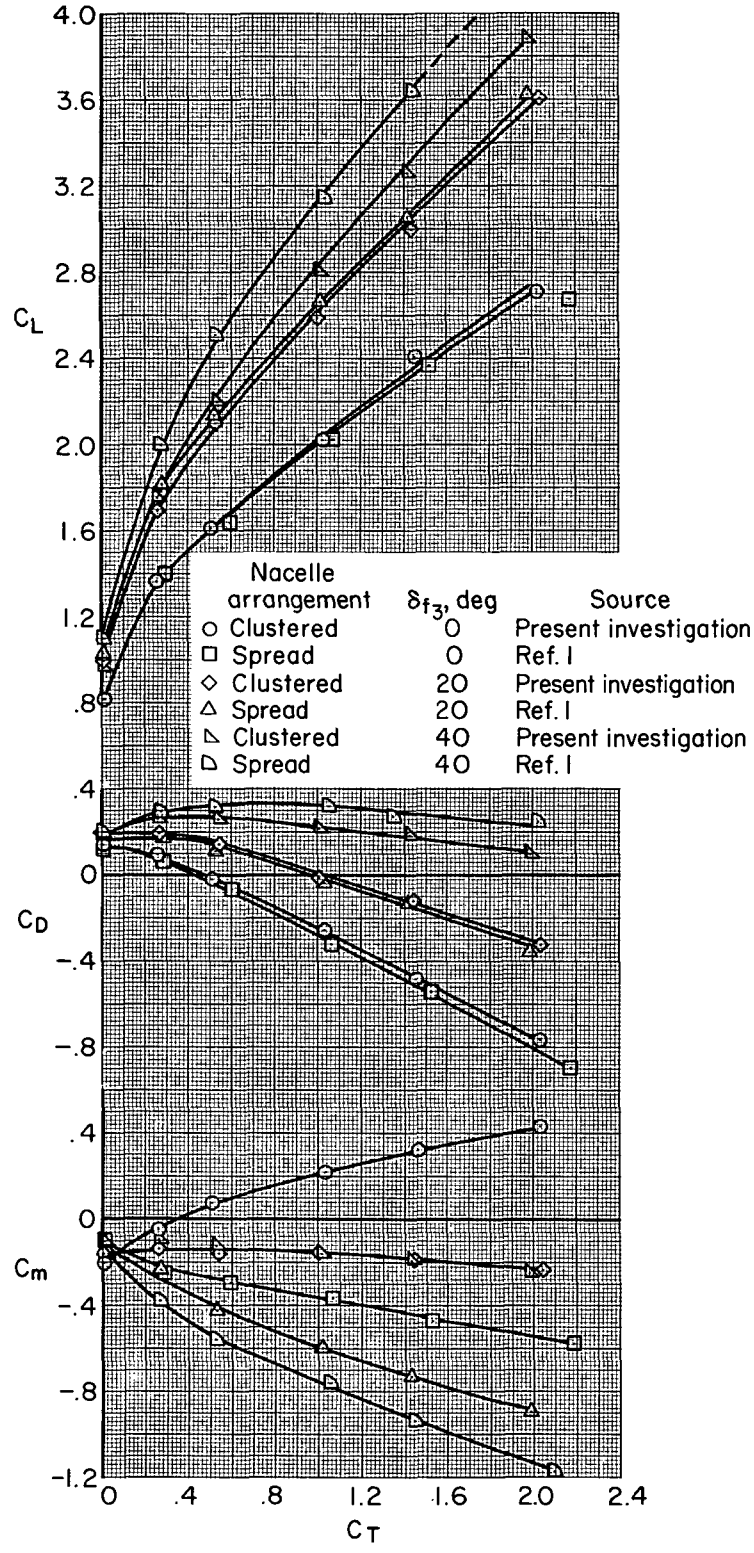

(b) $\delta_{f_1}/\delta_{f_2} = 40°/0°$

Figure 15.– Concluded.

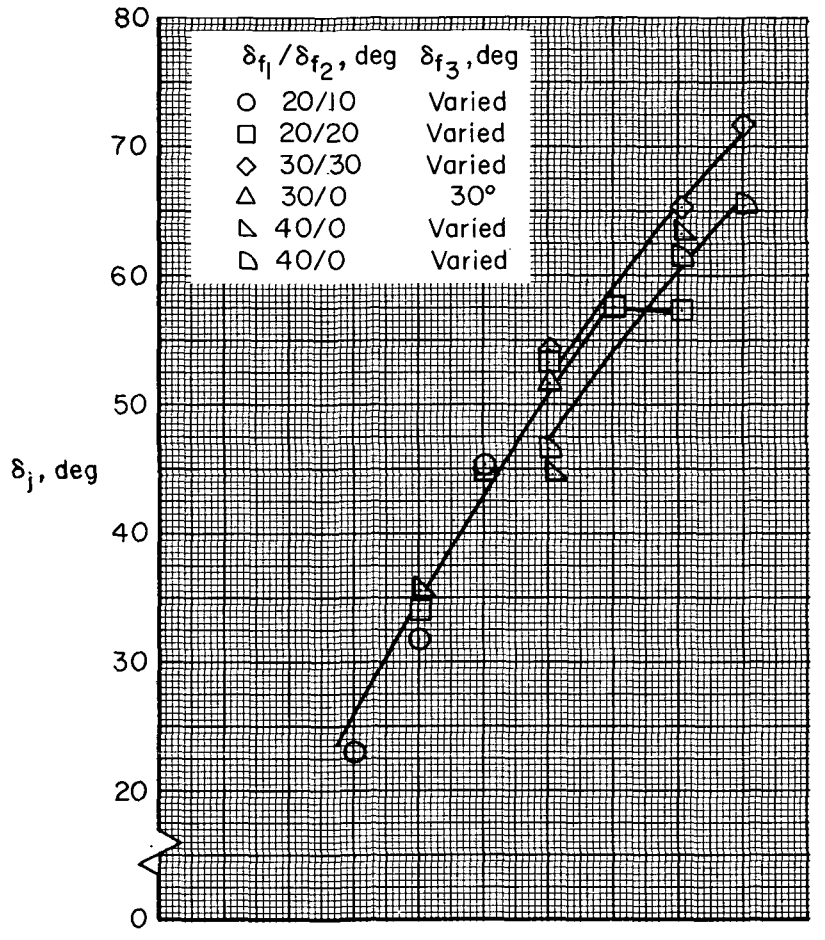

(a) Jet deflection angle.

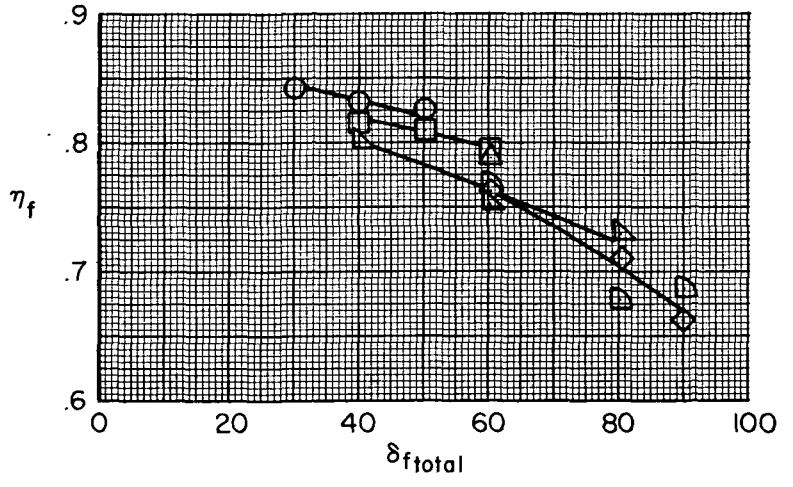

(b) Jet turning efficiency.

Figure 16.– Variation of resultant static jet deflection angle and turning efficiency; $\alpha = 0°$.

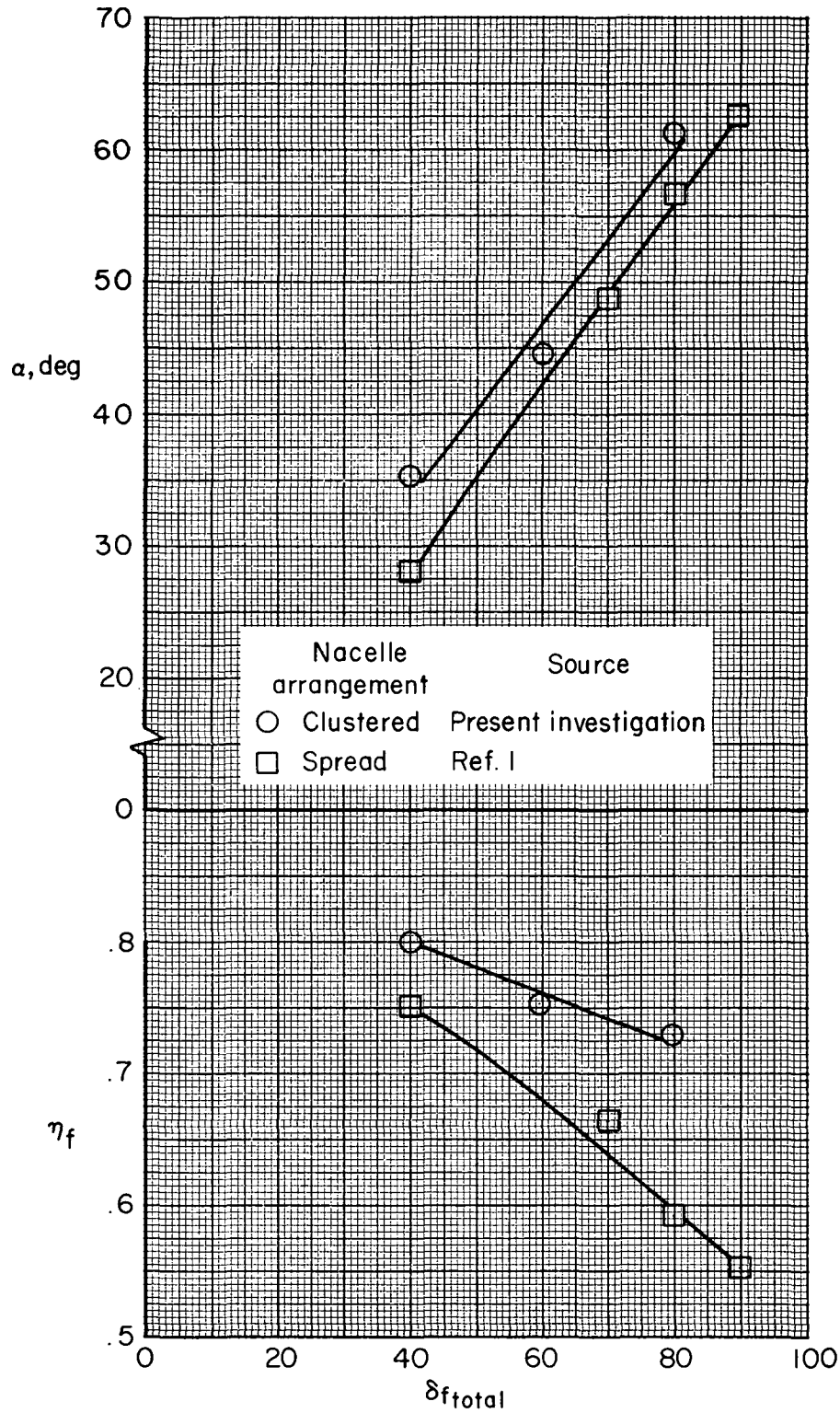

Figure 17.– Resultant static jet deflection and turning efficiency of spread and clustered nacelle arrangements; $\delta_{f_1}/\delta_{f_2} = 40°/0°, \alpha = 0°$.

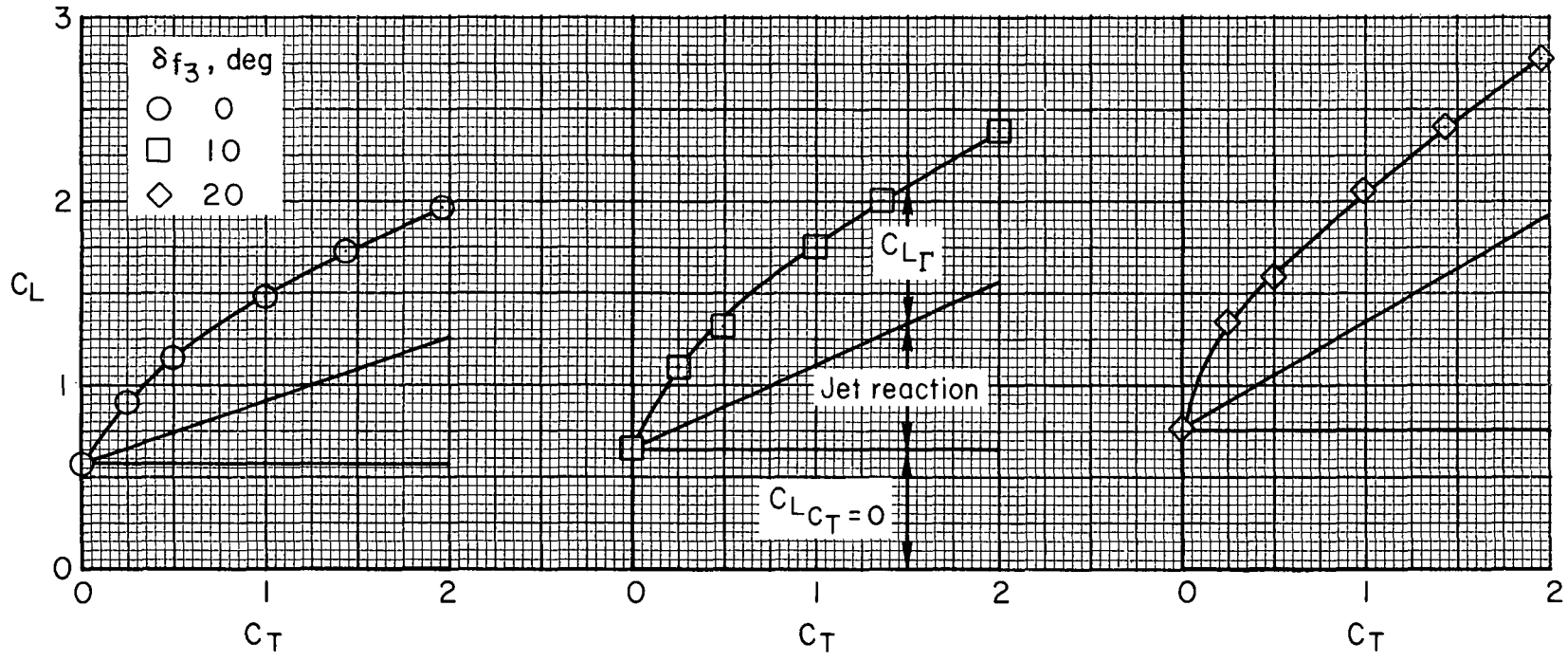

(a) $\delta_{f_1}/\delta_{f_2} = 20°/10°$

Figure 18.– Variation of lift coefficient with gross thrust coefficient; $\alpha = 0°$.

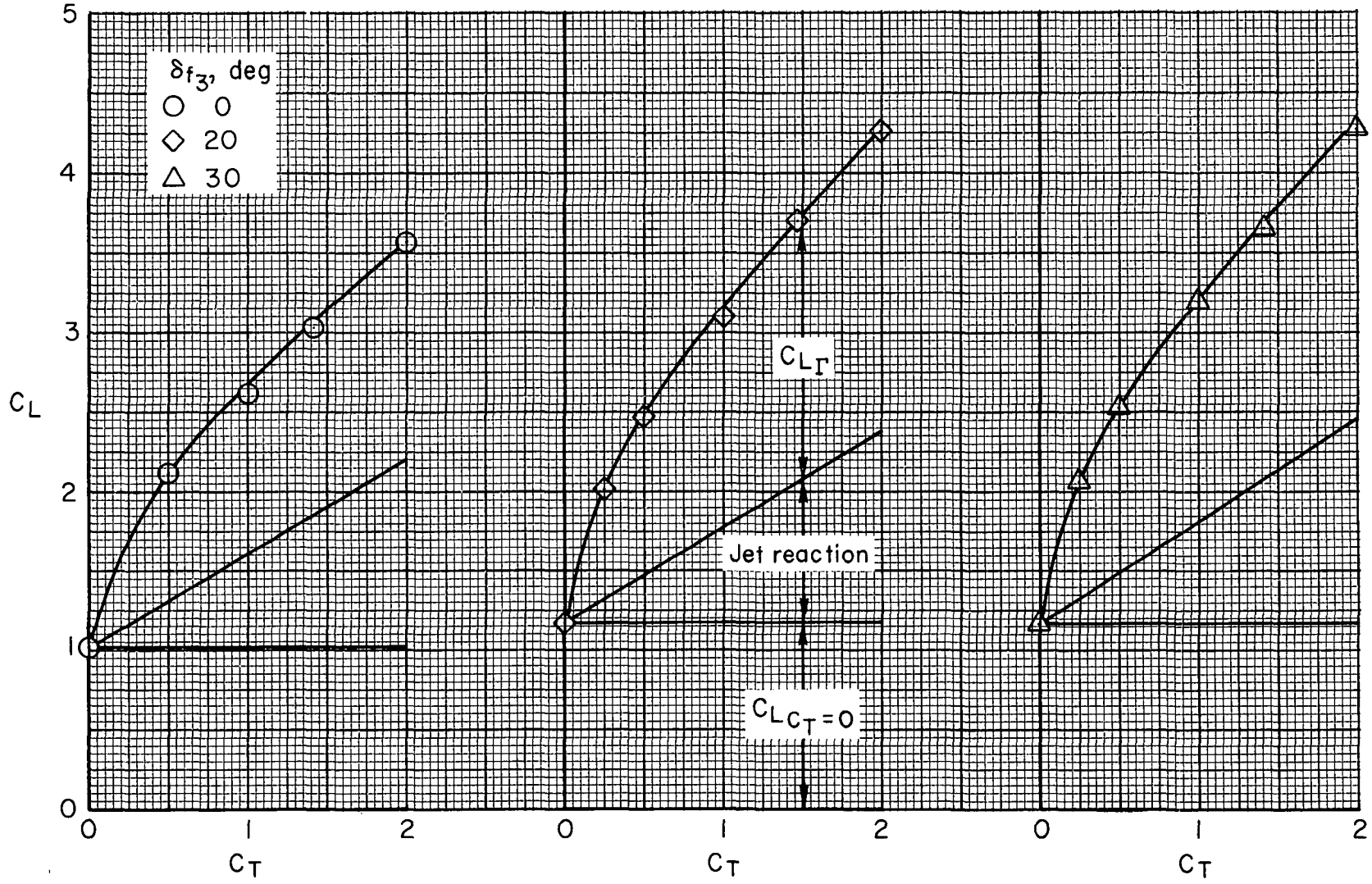

(b) $\delta_{f_1}/\delta_{f_2} = 40°/20°$

Figure 18.– Concluded.

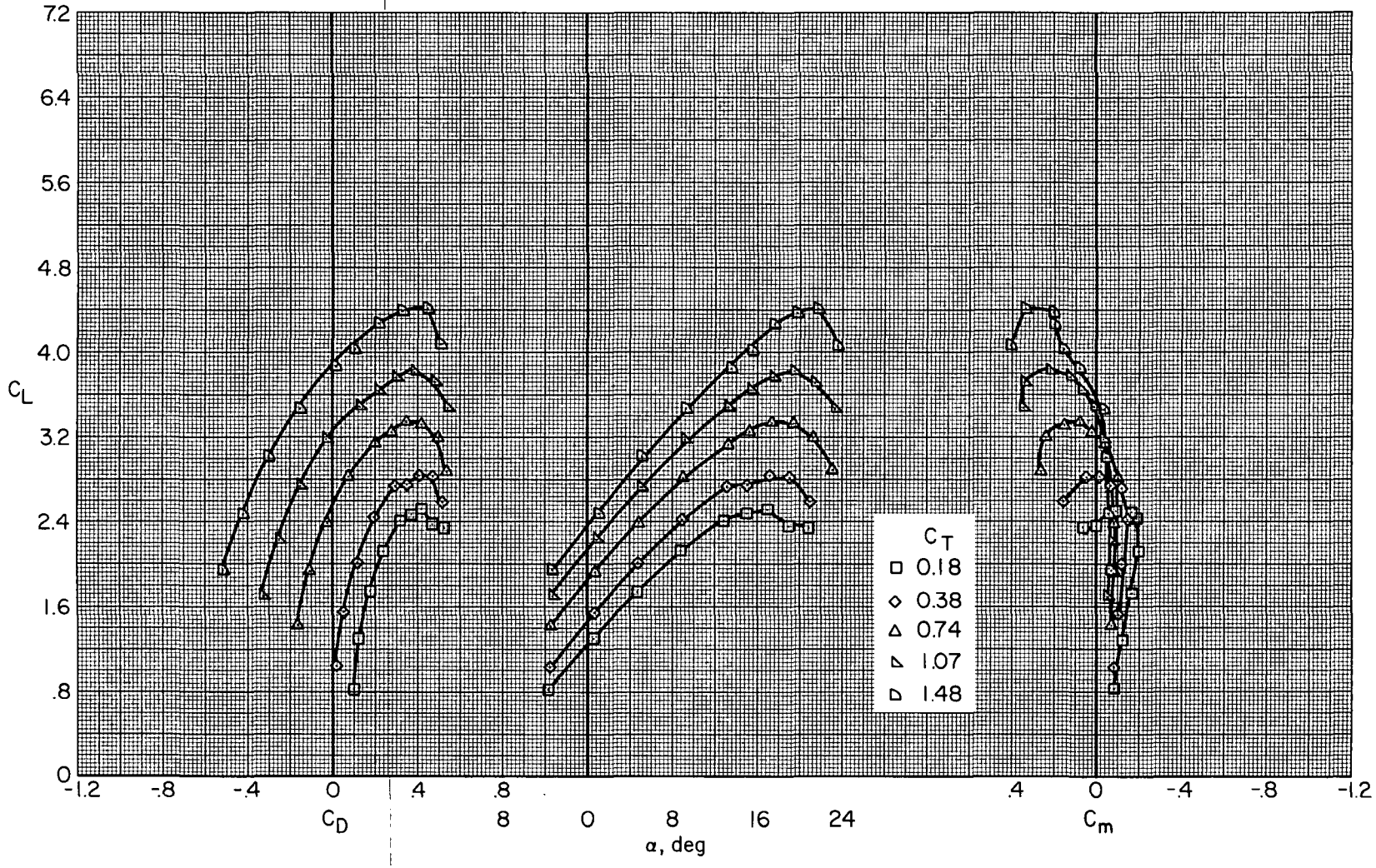

(a) Longitudinal characteristics of the model.

Figure 19.– Aerodynamic characteristics of the model with asymmetric thrust condition (left-hand outboard engine out); $\delta_{f_1}/\delta_{f_2}/\delta_{f_3} = 20°/20°/10°$.

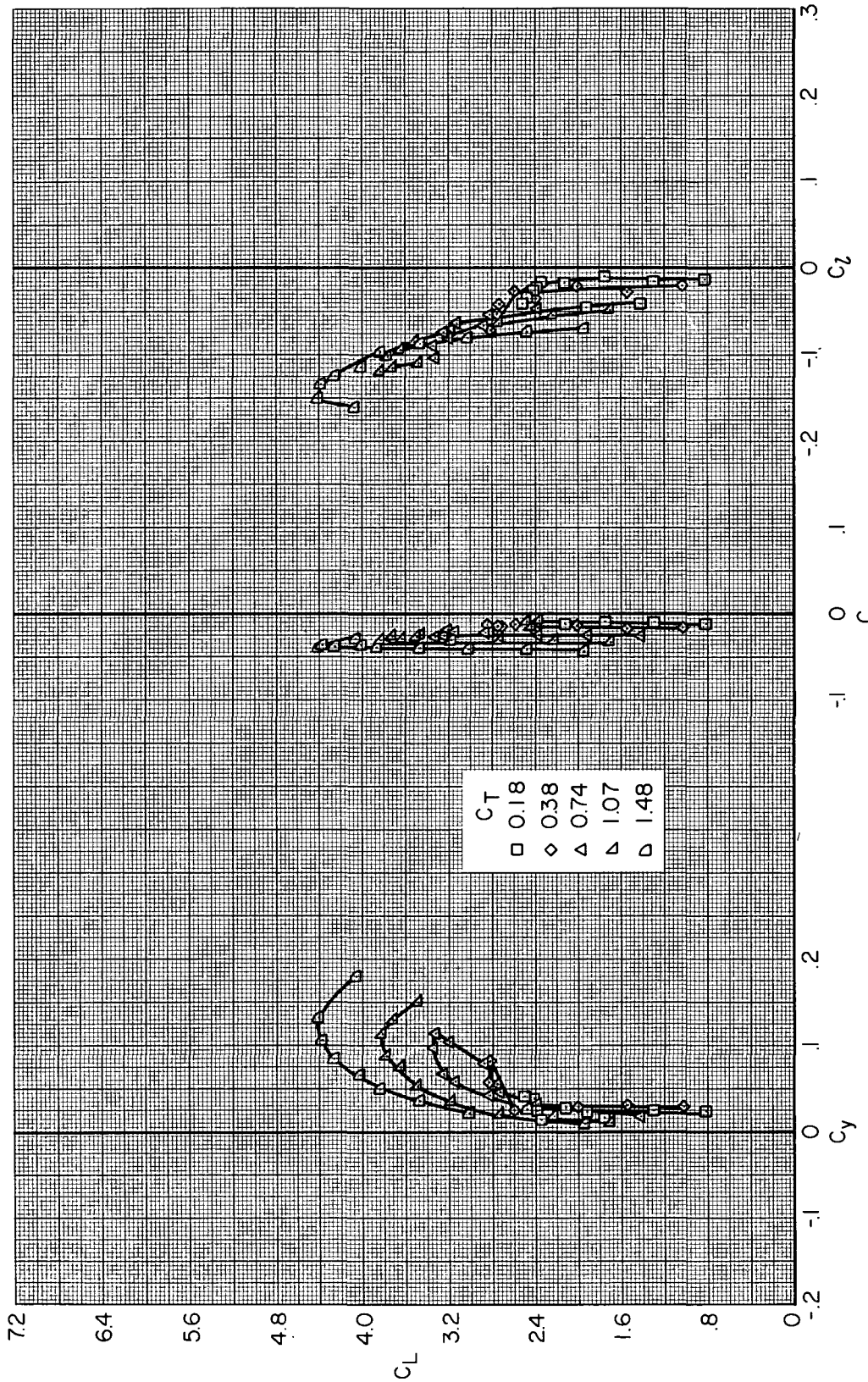

(b) Lateral characteristics of the model.

Figure 19.– Concluded.

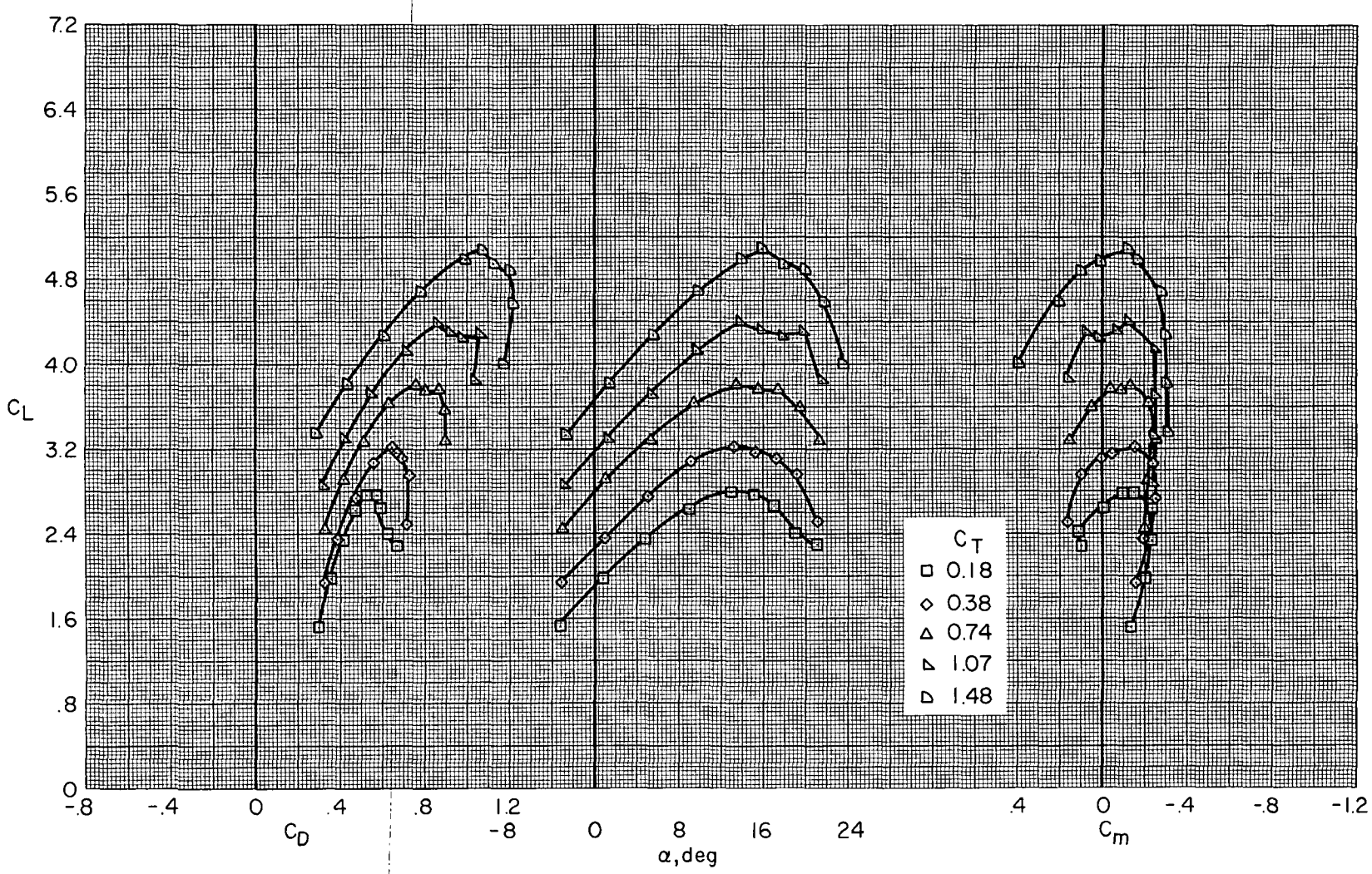

(a) Longitudinal characteristics of the model.

Figure 20.– Aerodynamic characteristics of the model with asymmetric thrust condition (left-hand outboard engine out); $\delta_{f_1}/\delta_{f_2}/\delta_{f_3} = 40°/20°/20°$.

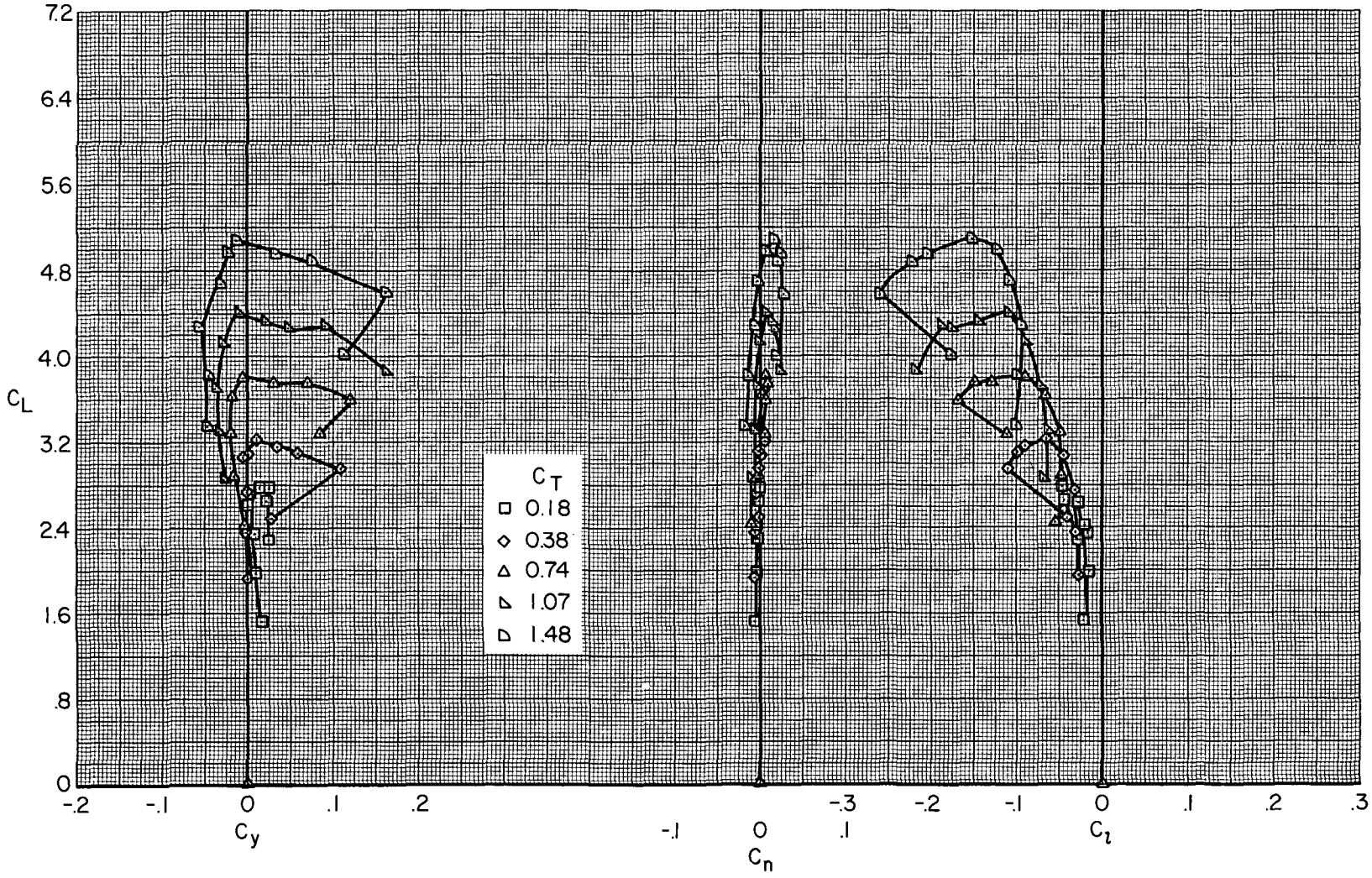

(b) Lateral characteristics of the model

Figure 20.– Concluded.

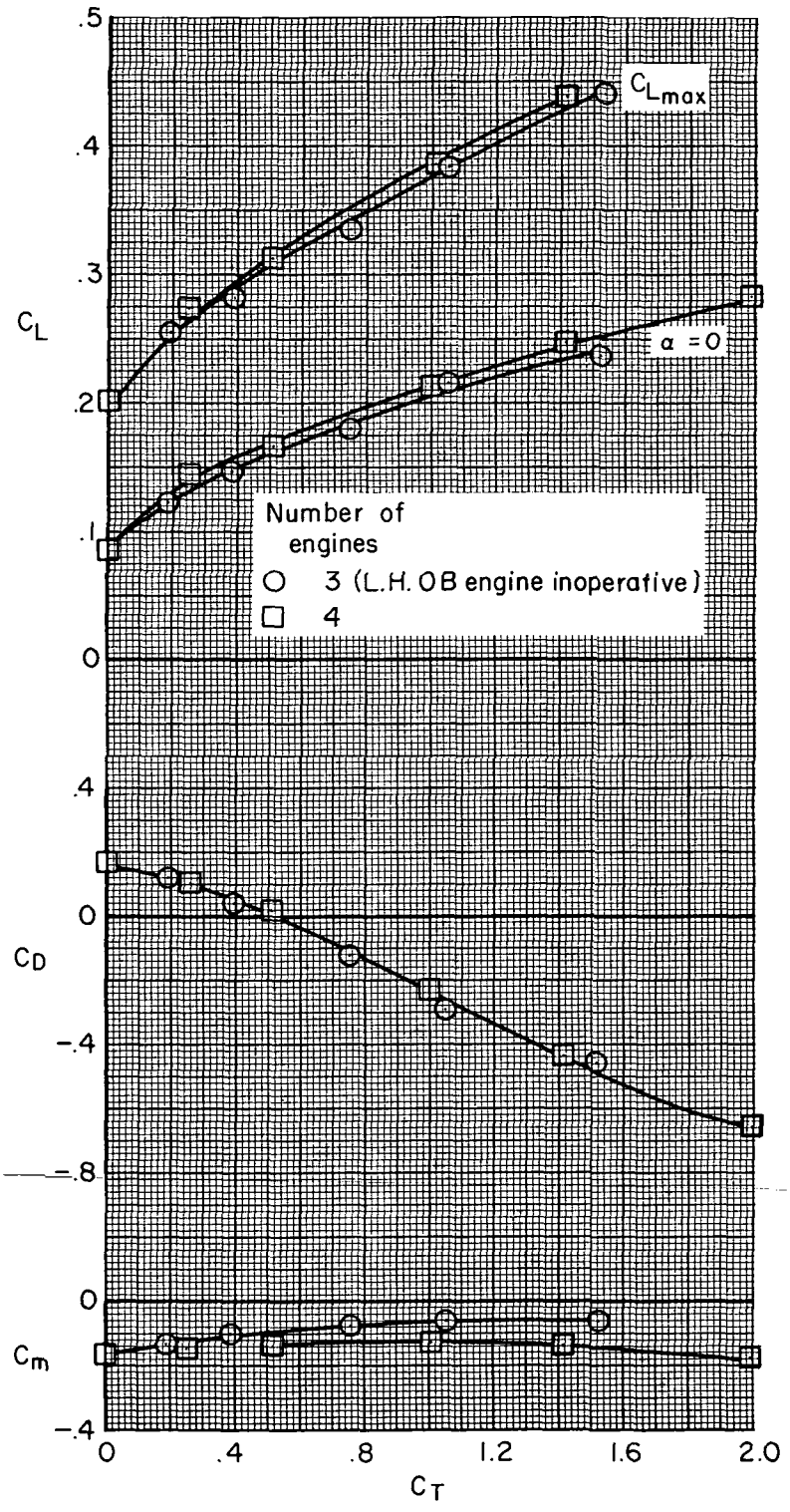

(a) $\delta_{f_1}/\delta_{f_2}/\delta_{f_3} = 20°/20°/10°$

Figure 21.– Effect of engine out condition on lift, drag, and pitching-moment coefficients; $\alpha = 0°$.

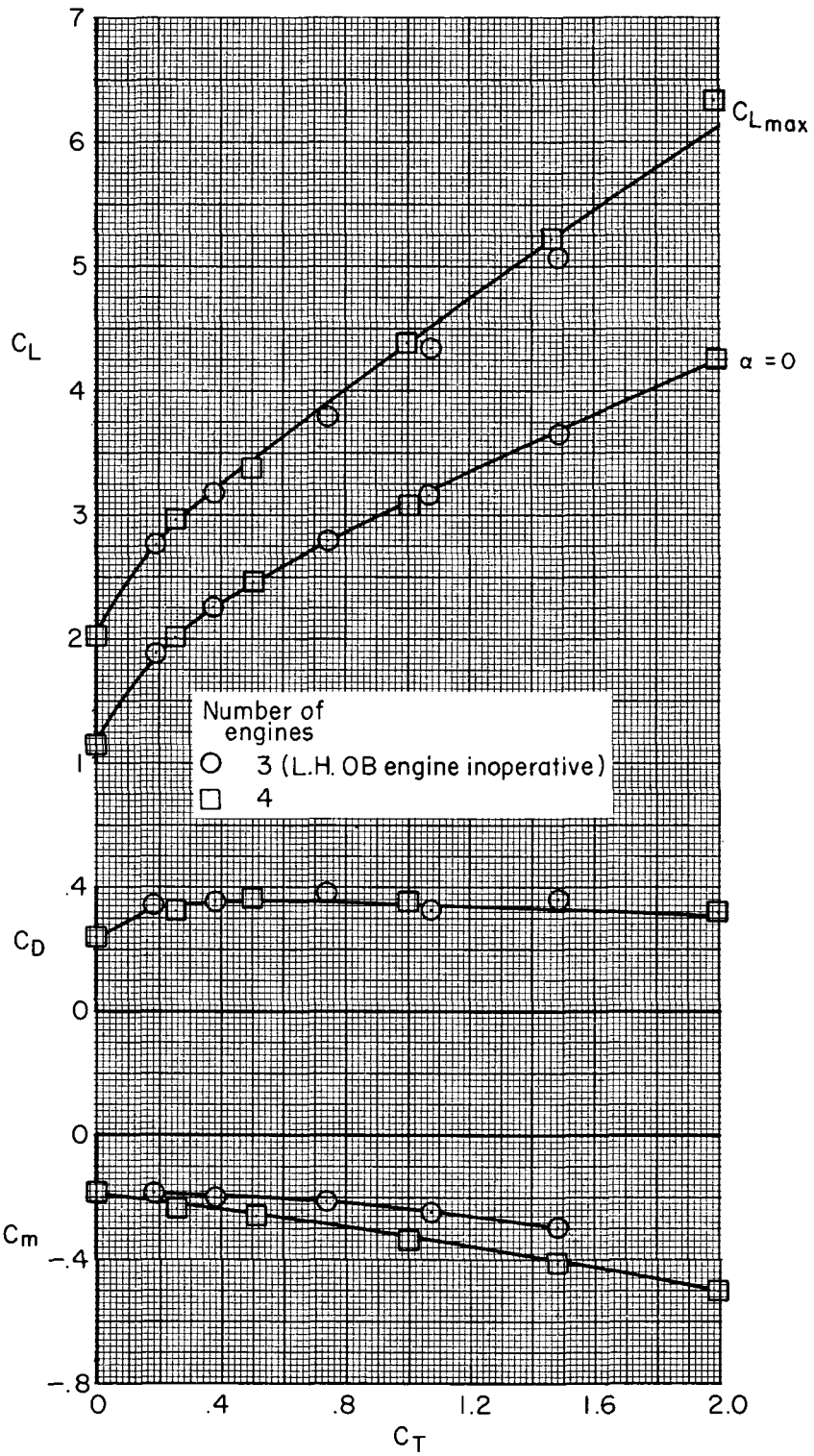

(b) $\delta_{f_1}/\delta_{f_2}/\delta_{f_3} = 40°/20°/20°$

Figure 21.– Concluded.

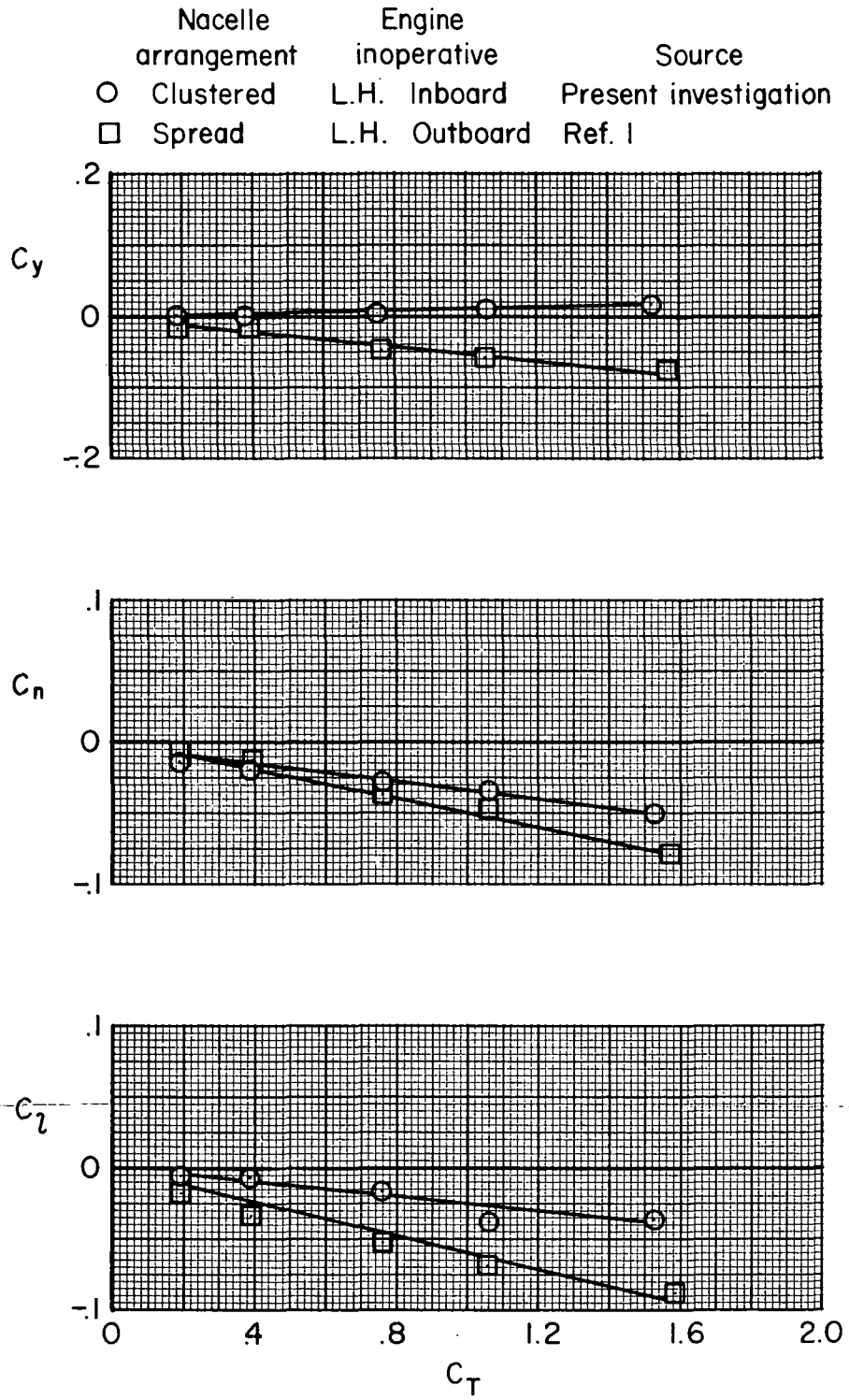

Figure 22.– Comparison of side, yawing-moment, and rolling-moment coefficients with asymmetric thrust condition between spread and clustered nacelle arrangements; $\delta_{f_1}/\delta_{f_2}/\delta_{f_3} = 20°/0°/20°, \alpha = 0°$.

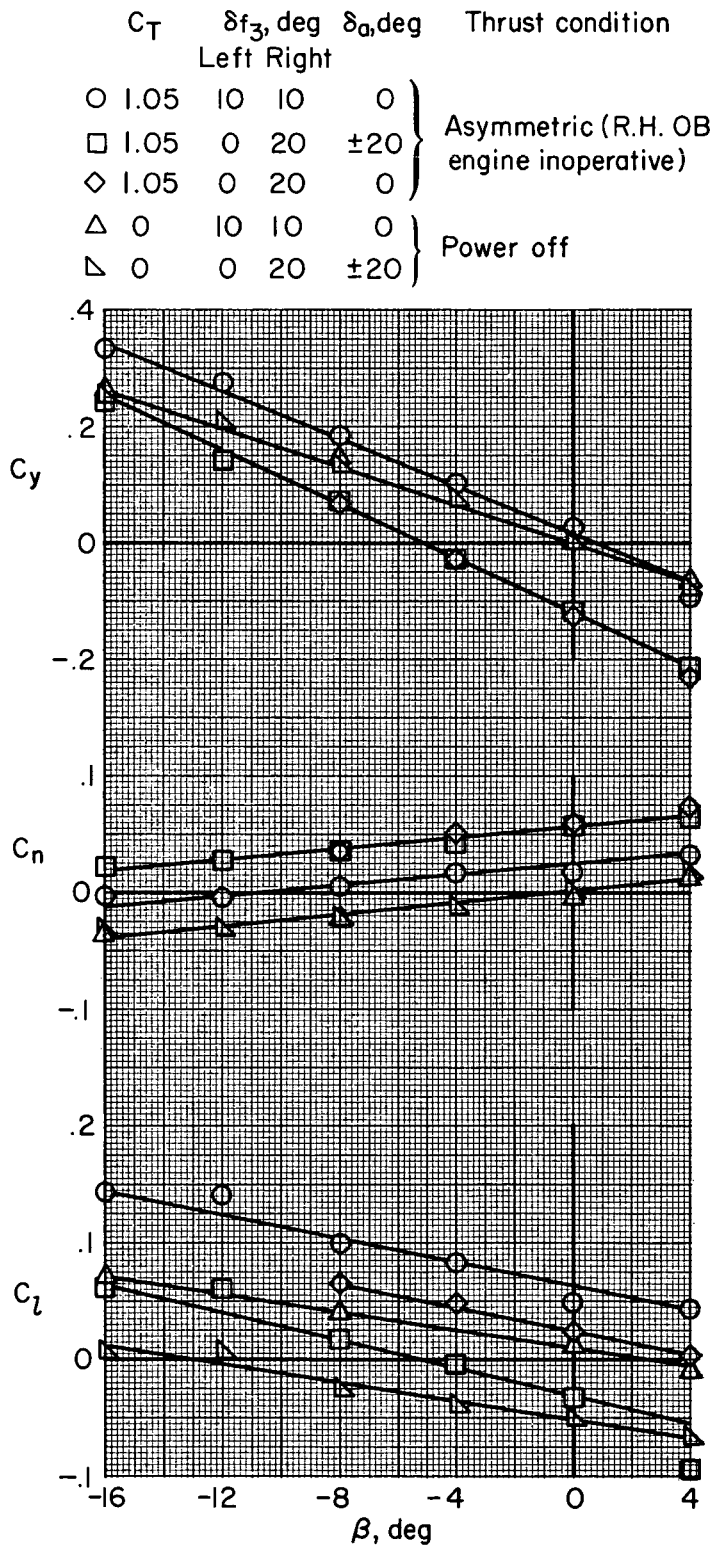

(a) $C_T = 0$ and 1.05

Figure 23.– Variation of side, yawing-moment, and rolling-moment coefficients with sideslip; $\delta_{f_1}/\delta_{f_2}/\delta_{f_3} = 20°/20°/10°$, $\alpha = 0°$

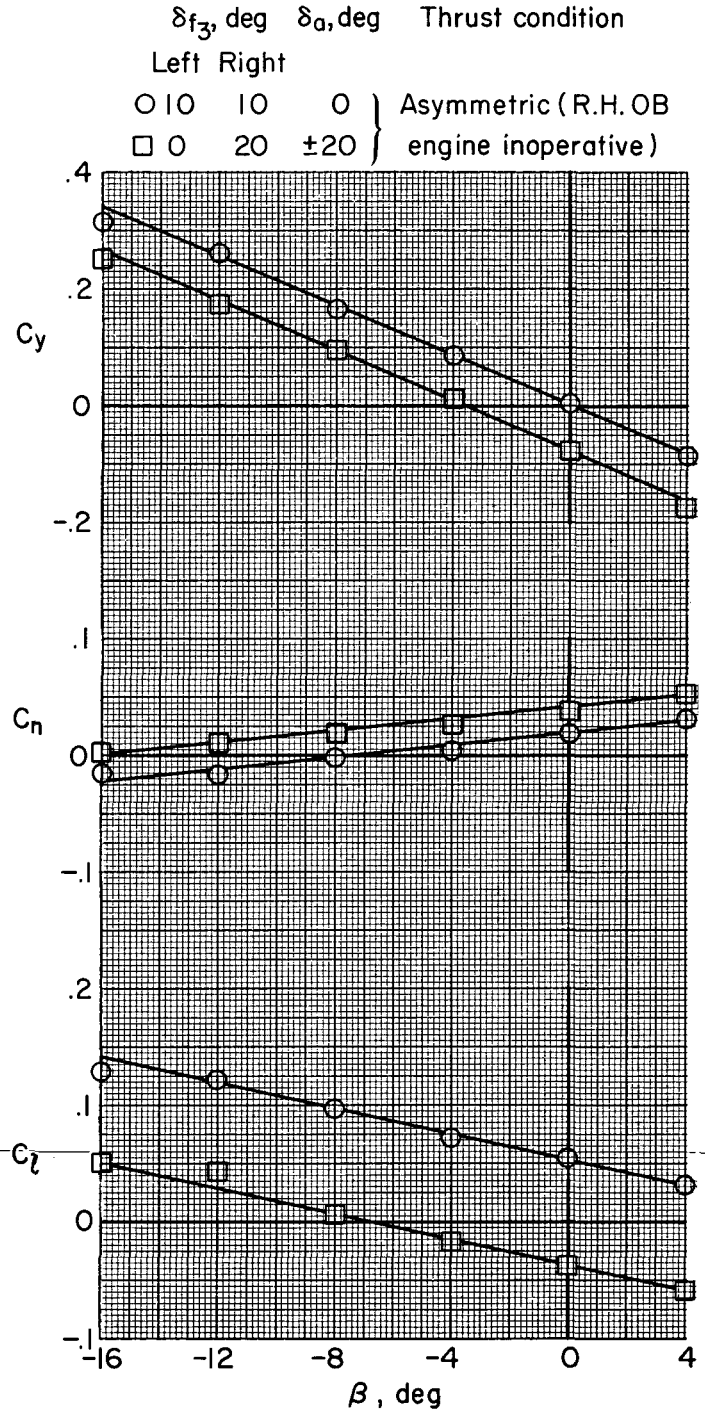

(b) $C_T = 0.75$

Figure 23.– Concluded.

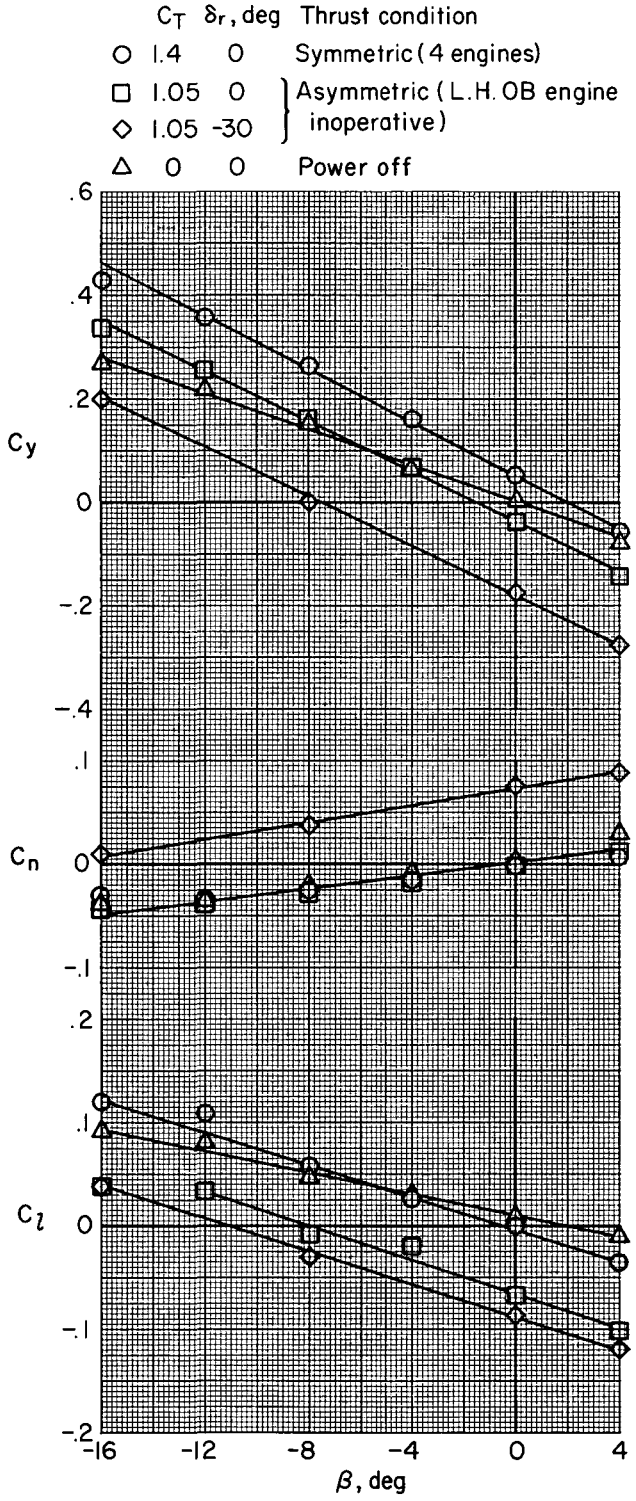

(a) $C_T = 1.4$, 1.05, and 0

Figure 24.– Variation of side, yawing-moment, and rolling-moment coefficients with sideslip; $\delta_{f_1}/\delta_{f_2}/\delta_{f_3} = 40°/20°/20°, \alpha = 0°$.
40

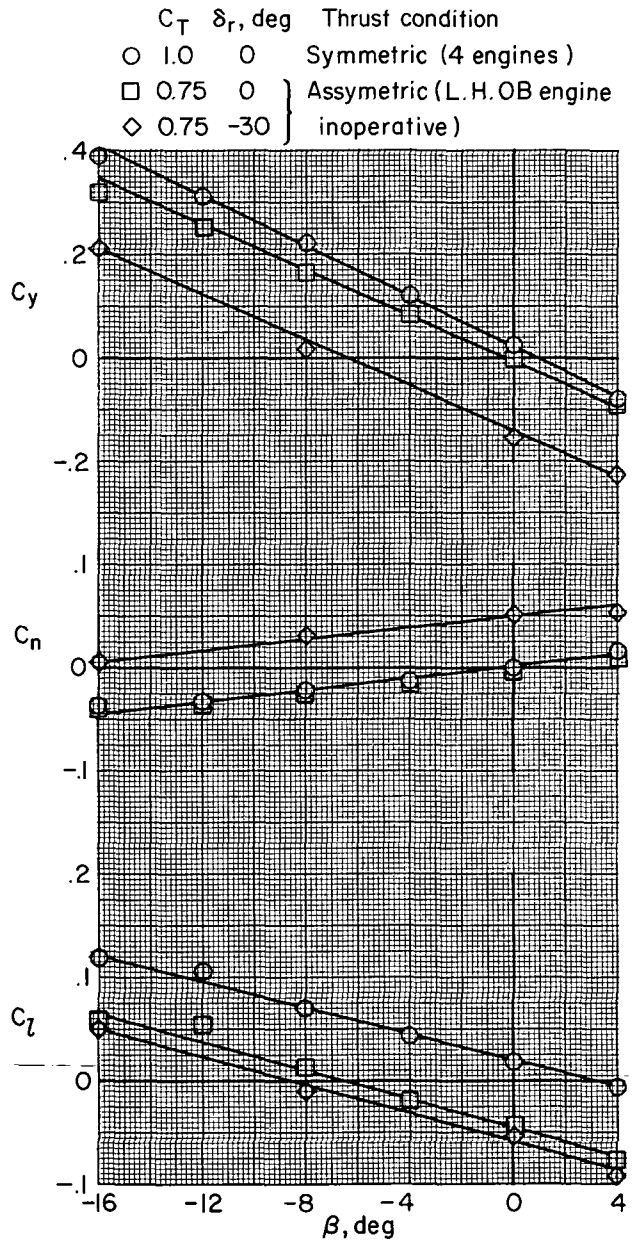

(b) $C_T = 1.00$ and 0.75

Figure 24.– Concluded.

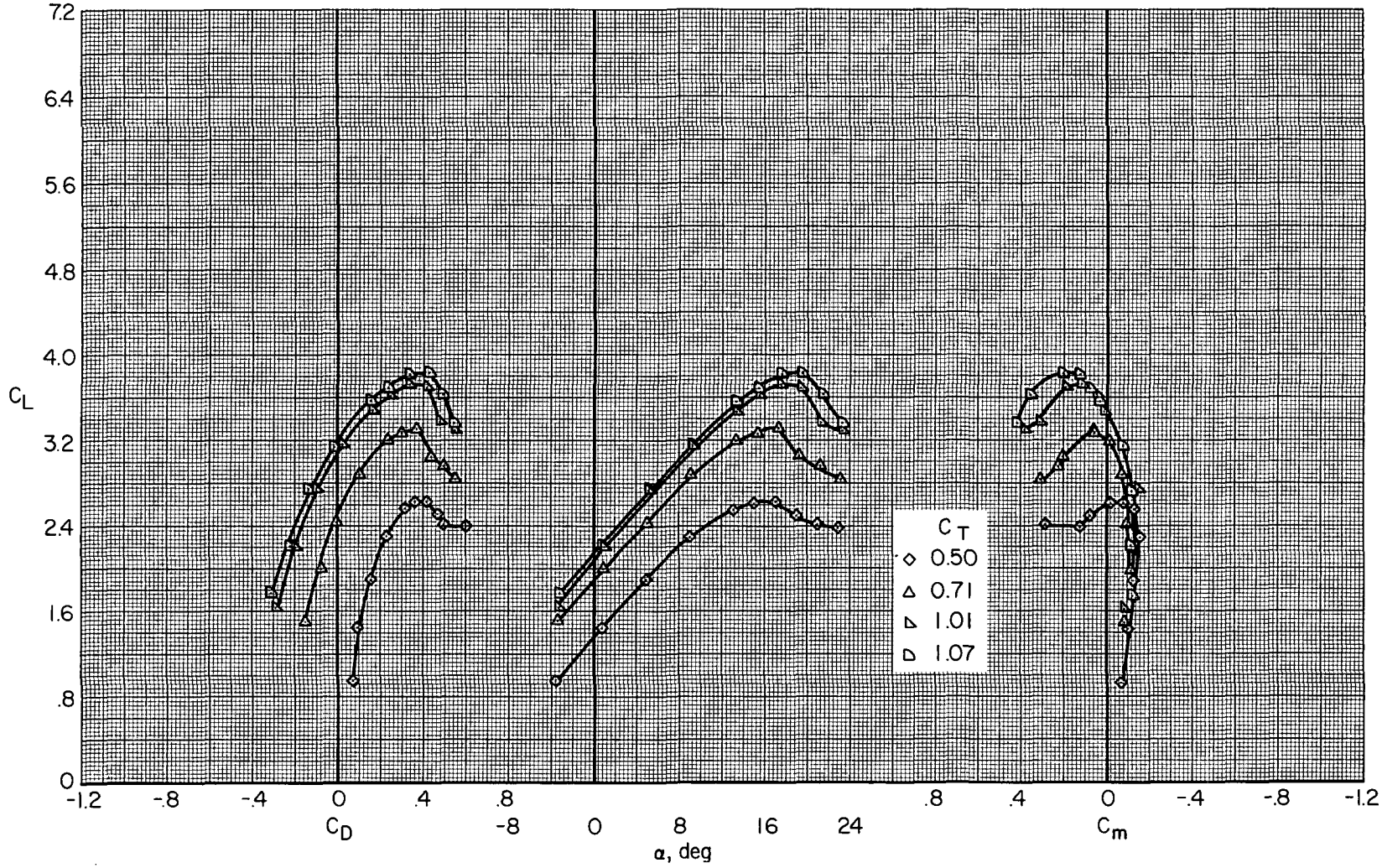

(a) Longitudinal characteristics of the model.

Figure 25.– Aerodynamic characteristics of the model with symmetric thrust condition and with three engines operating (left-hand inboard engine out); $\delta_{f_1}/\delta_{f_2}/\delta_{f_3} = 20°/20°/10°$.

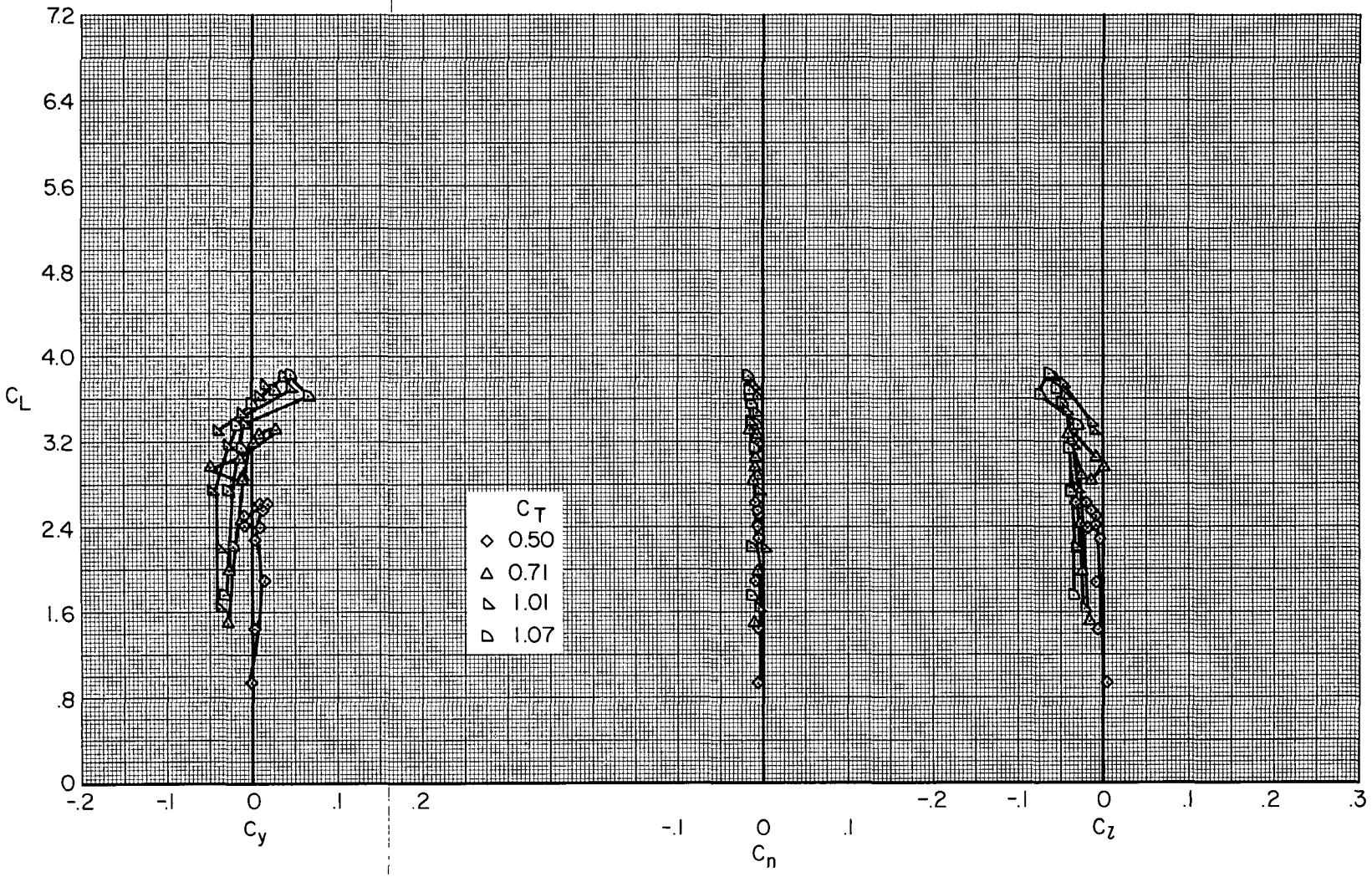

(b) Lateral characteristics of the model.

Figure 25.– Concluded.

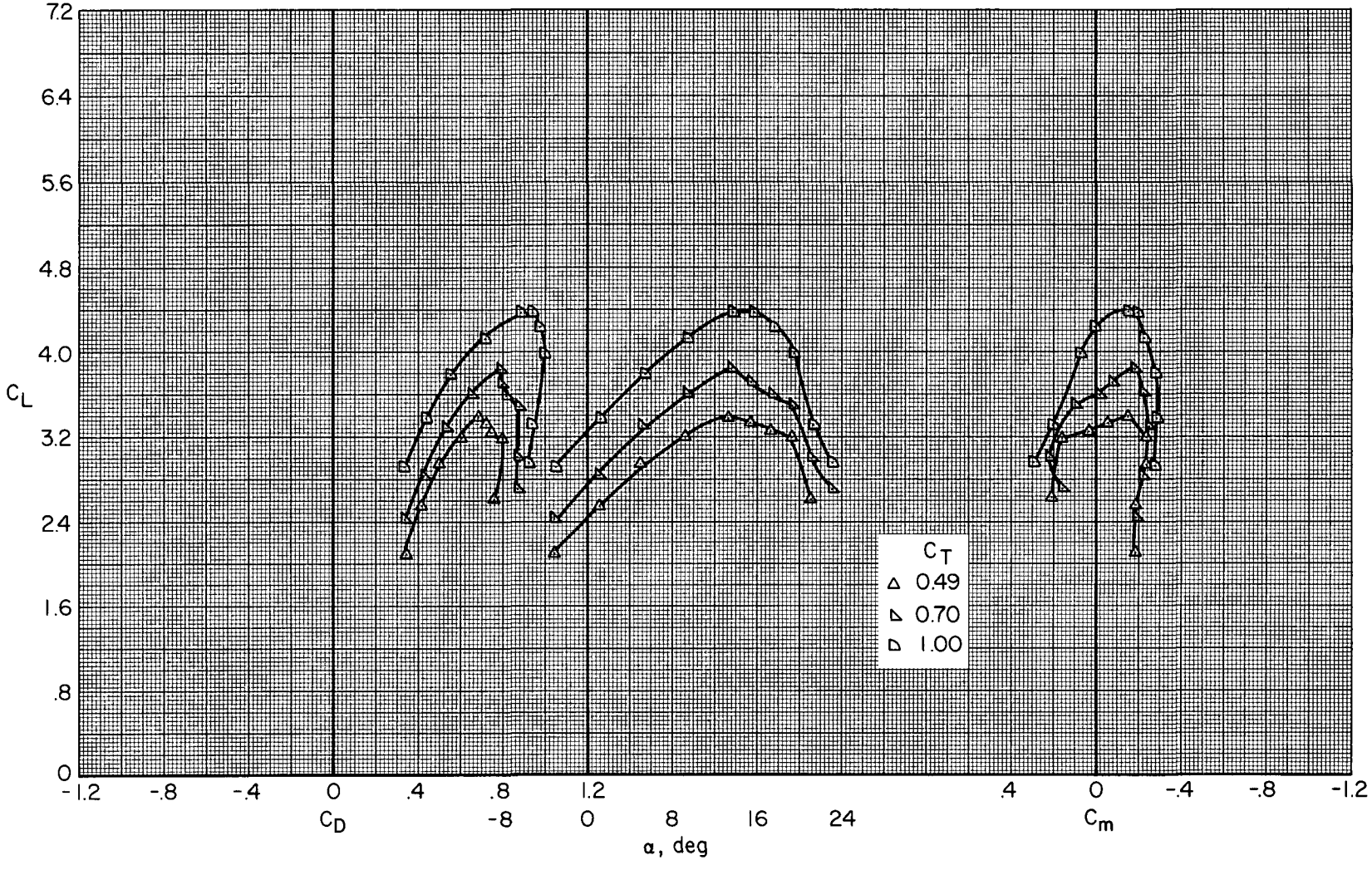

(a) Longitudinal characteristics of the model.

Figure 26.– Aerodynamic characteristics of the model with symmetric thrust condition and with three engines operating (left-hand outboard engine out); $\delta_{f_1}/\delta_{f_2}/\delta_{f_3} = 40°/20°/20°$.

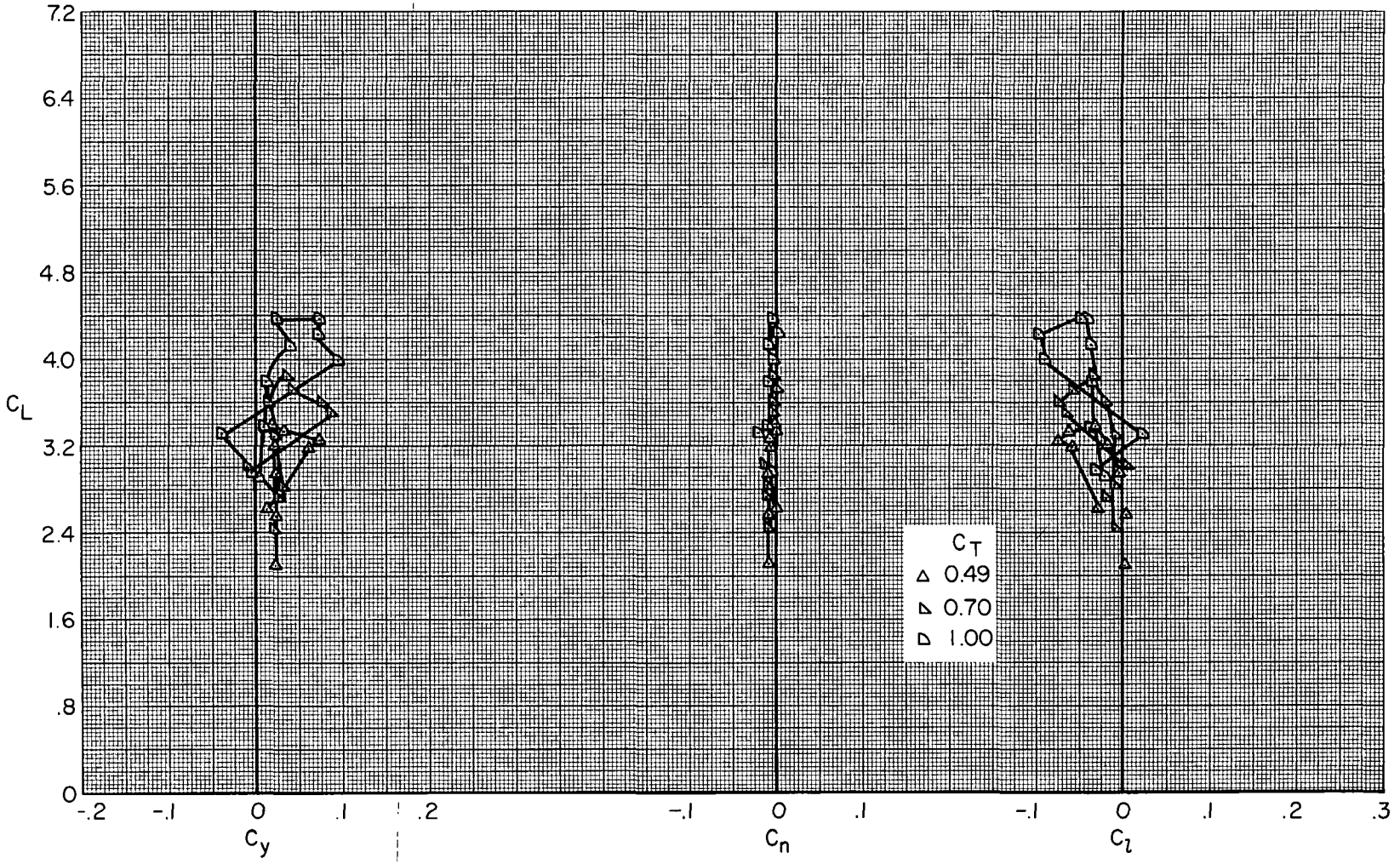

(b) Lateral characteristics of the model.

Figure 26.– Concluded.

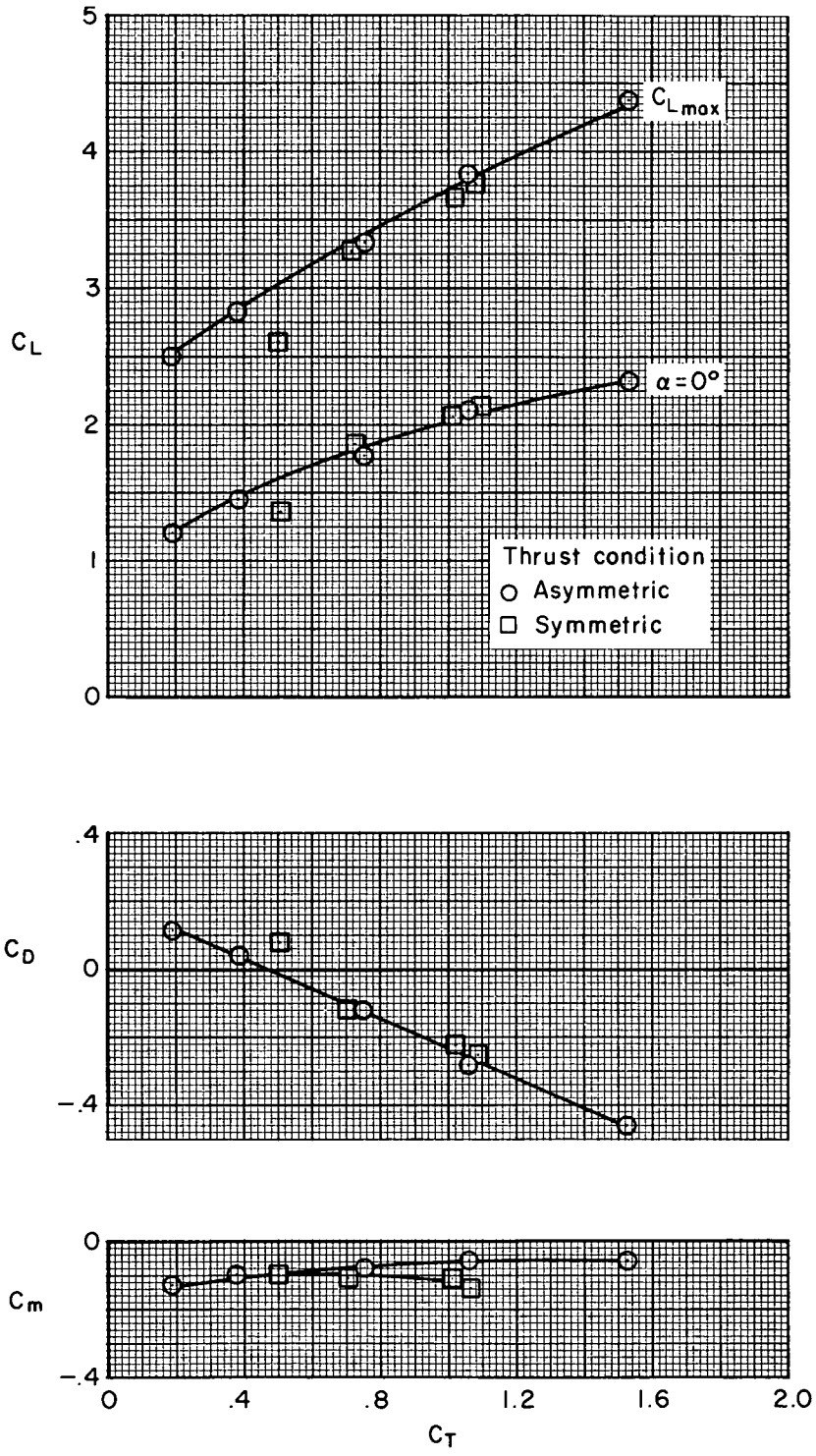

(a) Longitudinal characteristics of the model.

Figure 27.– Effect of asymmetric and symmetric thrust condition with three engines operating (left-hand outboard engine out) on the longitudinal and lateral characteristics of the model; $\delta_{f_1}/\delta_{f_2}/\delta_{f_3} = 20°/20°/10°$, $\alpha = 0°$.

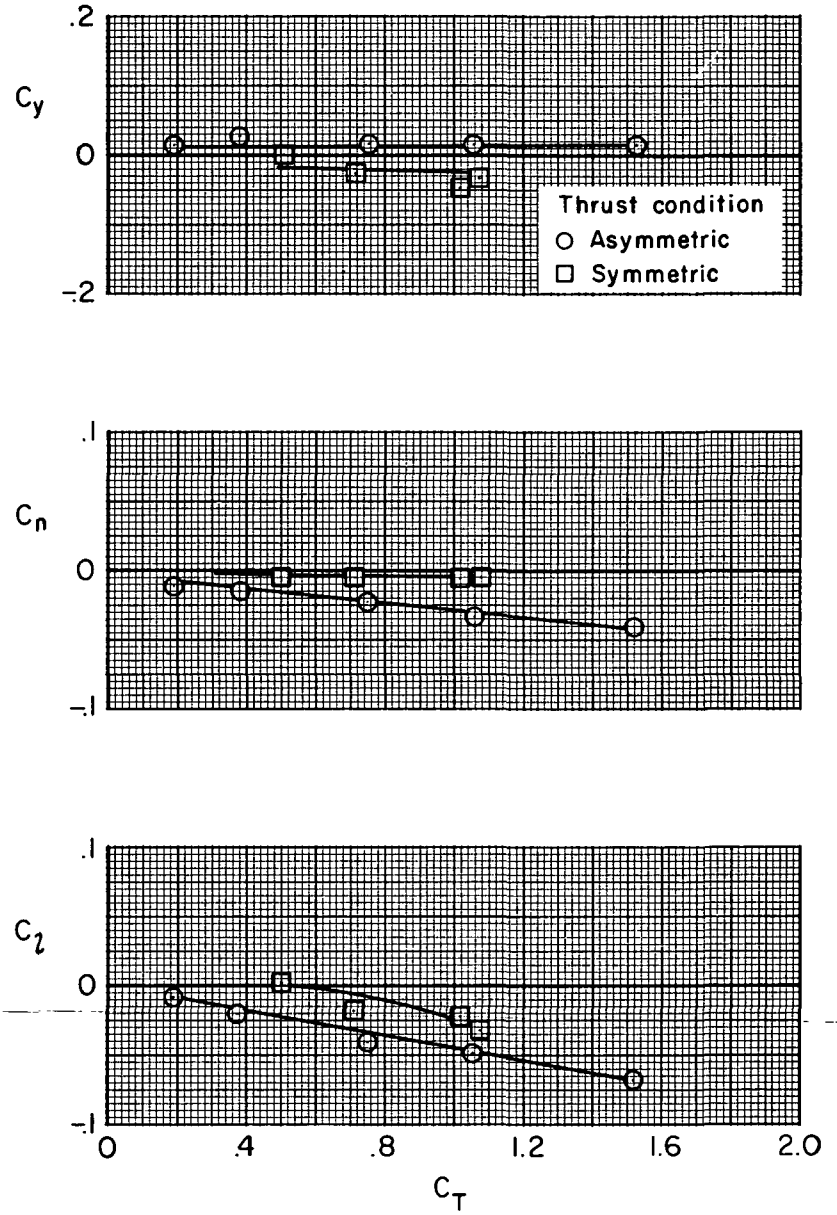

(b) Lateral characteristics of the model.

Figure 27.– Concluded.

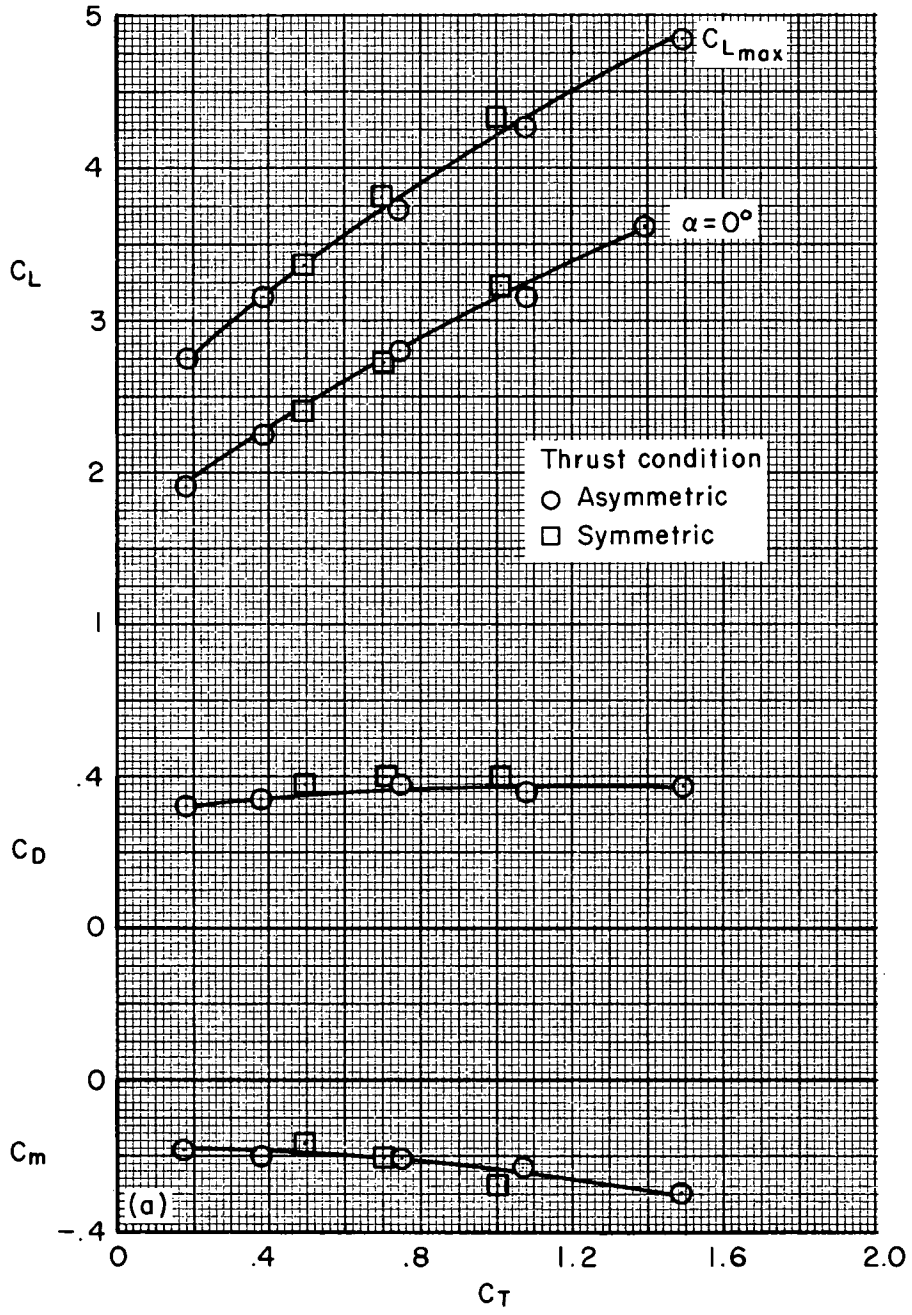

(a) Longitudinal characteristics of the model.

Figure 28.– Effect of asymmetric and symmetric thrust condition with three engines operating (left-hand outboard engine out) on the longitudinal and lateral characteristics of the model; $\delta_{f_1}/\delta_{f_2}/\delta_{f_3} = 40°/20°/20°, \alpha = 0°$.

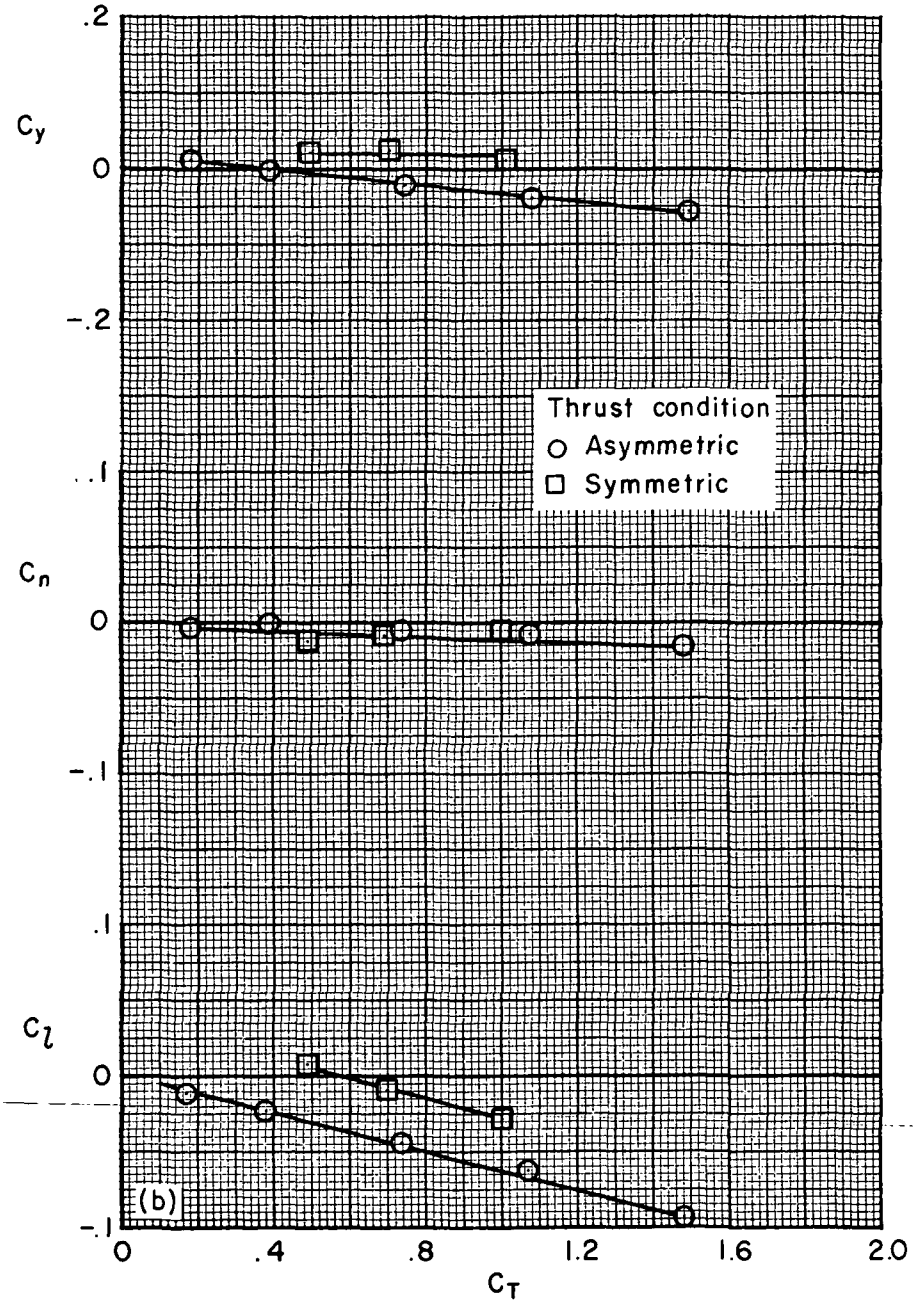

(b) Lateral characteristics of the model.

Figure 28.– Concluded.

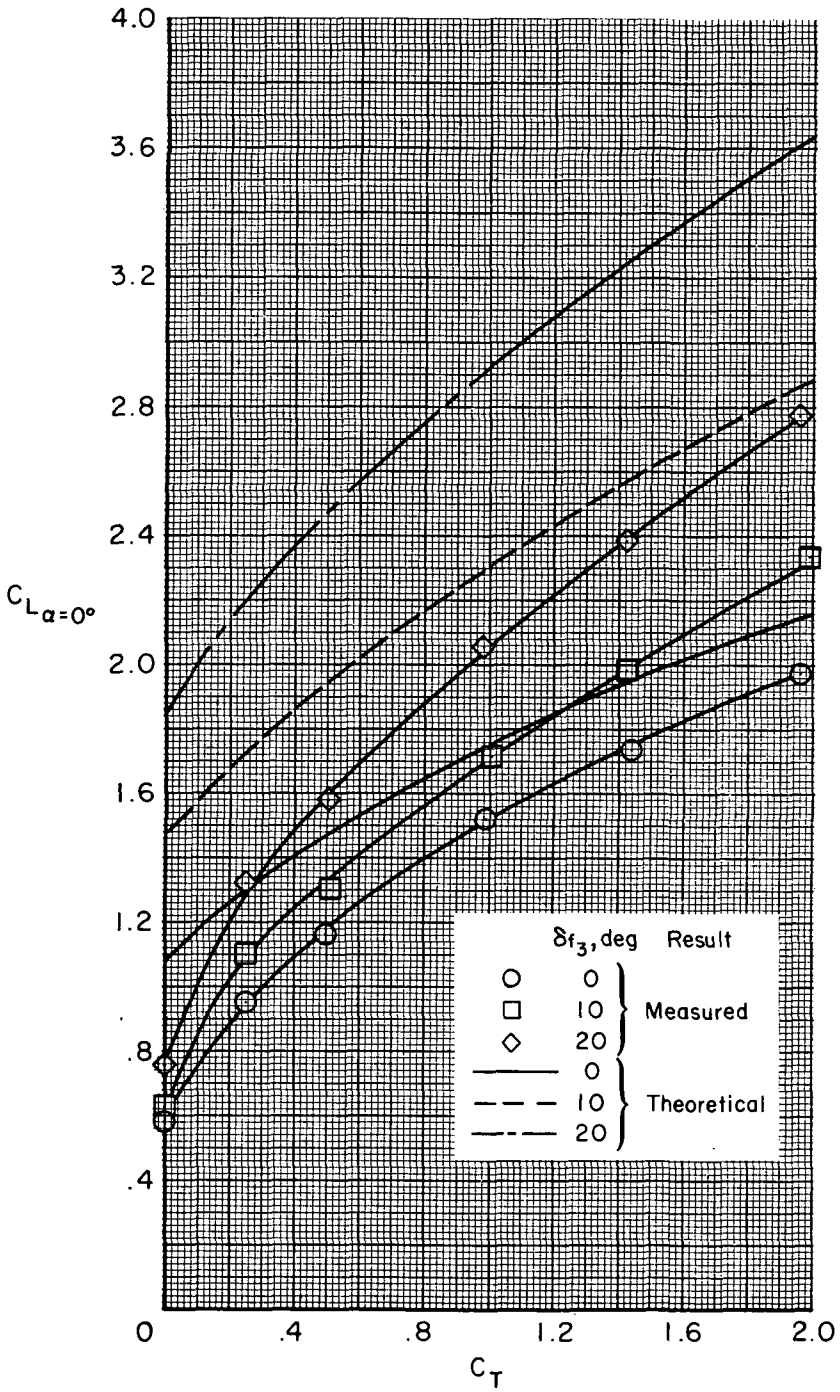

(a) $\delta_{f_1}/\delta_{f_2} = 20^\circ/10^\circ$

Figure 29.– Comparison of measured and theoretical flap lift coefficient; $\alpha = 0^\circ$.

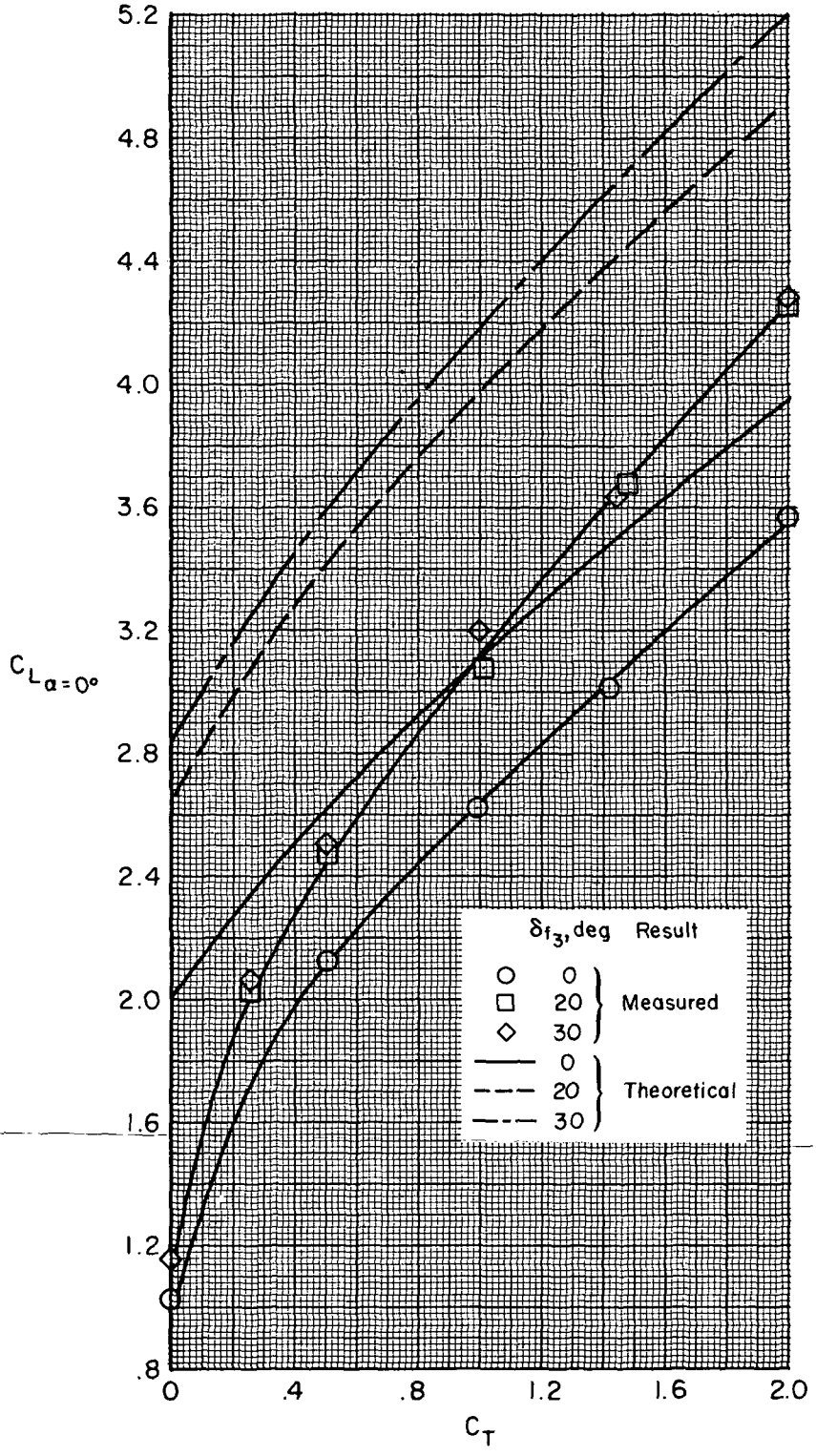

(b) $\delta_{f_1}/\delta_{f_2} = 40°/20°$

Figure 29.– Concluded.

Page Intentionally Left Blank

NATIONAL AERONAUTICS AND SPACE ADMISTRATION
WASHINGTON, D.C. 20546

OFFICIAL BUSINESS
PENALTY FOR PRIVATE USE $300

FIRST CLASS MAIL

POSTAGE AND FEES PAID
NATIONAL AERONAUTICS AND
SPACE ADMINISTRATION

U.S.MAIL

NASA 451

POSTMASTER: If Undeliverable (Section 158 Postal Manual) Do Not Return

"The aeronautical and space activities of the United States shall be conducted so as to contribute . . . to the expansion of human knowledge of phenomena in the atmosphere and space. The Administration shall provide for the widest practicable and appropriate dissemination of information concerning its activities and the results thereof."

—NATIONAL AERONAUTICS AND SPACE ACT OF 1958

NASA SCIENTIFIC AND TECHNICAL PUBLICATIONS

TECHNICAL REPORTS: Scientific and technical information considered important, complete, and a lasting contribution to existing knowledge.

TECHNICAL NOTES: Information less broad in scope but nevertheless of importance as a contribution to existing knowledge.

TECHNICAL MEMORANDUMS: Information receiving limited distribution because of preliminary data, security classification, or other reasons.

CONTRACTOR REPORTS: Scientific and technical information generated under a NASA contract or grant and considered an important contribution to existing knowledge.

TECHNICAL TRANSLATIONS: Information published in a foreign language considered to merit NASA distribution in English.

SPECIAL PUBLICATIONS: Information derived from or of value to NASA activities. Publications include conference proceedings, monographs, data compilations, handbooks, sourcebooks, and special bibliographies.

TECHNOLOGY UTILIZATION PUBLICATIONS: Information on technology used by NASA that may be of particular interest in commercial and other non-aerospace applications. Publications include Tech Briefs, Technology Utilization Reports and Technology Surveys.

Details on the availability of these publications may be obtained from:

SCIENTIFIC AND TECHNICAL INFORMATION OFFICE

NATIONAL AERONAUTICS AND SPACE ADMINISTRATION

Washington, D.C. 20546